Quantitative proteome analysis of S-nitrosylation on synaptosomal proteins in Alzheimer's disease

Dissertation

For degree of achievement

Doctor of Natural Science (PhD)

Doktor der Naturwissenschaften (Dr. rer. nat)

Faculty of Mathematics and Natural Sciences

Rheinische Friedrich-Wilhelms-Universität Bonn

by

Teodora Stella Wijasa, M.D., M.Sc.

from

Jakarta, Indonesia

Bonn 2018

Supervisors

Prof. Dr. Michael T. Heneka
Department of Neurodegenerative Diseases & Geropsychiatry
Uniklinikum Bonn

Prof. Dr. Walter Witke
Institute of Genetics
University of Bonn, Faculty of Biology

Prof. Dr. Volkmar Gieselmann
Institute of Biochemistry and Molecular Biology
University of Bonn

Prof. Dr. Sabine Tröger
Institute of Geography, Developmental Geography
University of Bonn

Date of the defense
26 April 2019

Year of publication
2019

Abstract

Alzheimer's disease (AD) is an irreversible, progressive and most common type of dementia in the aging population. AD pathophysiology starts slowly and deteriorates over time before the clinical diagnosis of dementia can be made. Neuropathologic features of AD are the presence of amyloid deposits, neurofibrillary tangles, synapse loss and neurodegeneration. Increasing evidence proposes neuroinflammation as one of the essential components of AD pathogenesis. Numerous studies have shown the involvement of protein s-nitrosylation in the development of AD pathology. The current study targeted s-nitrosylation in synaptosomal proteins, which have been isolated from mouse and human brain tissues using an isobaric mass tag (iodoTMT) method and nanocapillary high performance liquid chromatography tandem mass spectrometry (nanoHPLC MS/MS). Mice samples were collected and analyzed according to their age (3-months and 12-month-old mice) and genotype (APP/PS1 and NOS2 knockout on 12-month-old mice) effects. Data obtained from murine AD models were then compared to brain samples from Alzheimer's disease, mild cognitive impairment (MCI) and healthy elderly subjects. The results represent a candidate list of s-nitrosylated synaptic proteins isolated from mouse and human samples, which could be further evaluated as early biomarkers in AD. In addition, the iodoTMT method has been confirmed for the analyzation of S-nitrosylation instable protein modifications, particularly in studies with finite sample materials.

Table of contents

List of abbreviations

2D-DIGE	Two-dimensional difference in gel electrophoresis
Aβ	Amyloid beta
ACN	Acetonitrile
AD	Alzheimer's disease
ADAM	A disintegrin and metalloprotease family enzyme
AEBSF	4-(2-Aminoethyl)benzenesulfonyl fluoride hydrochloride
AICD	Amyloid precursor protein intracellular domain
ApoE	Apolipoprotein E
APP	Amyloid precursor protein
BACE	β-secretase
BBB	Blood brain-barrier
BCA	Bicinchoninic acid
BSA	Bovine Serum Albumin
BST	Biotin switch technique
CNS	Central nervous system
CSF	Cerebral spinal fluid
CTFα	Carboxy-terminal fragment alpha
CTFβ	Carboxy-terminal fragment beta
Cys	Cysteine
DTT	1.4-Dithiothreit
DIGE	Difference gel electrophoresis
DMF	Dimethylformide
DMSO	Dimethyl sulfoxide
EDTA	Ethylene diamine tetraacetic acid
EGTA	Ethylene glycol tetraacetic acid
EM	Electron microscope
eNOS	Endothelial nitric oxide synthase
EOAD	Early-onset AD
FA	Formic acid
FAD	Familial Alzheimer's Disease
GSNOR	S-nitrosoglutathione reductase
HCD	Higher energy collision induced dissociation

HENS	HEPES EDTA Necuproine SDS
HPLC	High performance liquid chromatography
IAM	Iodoacetamide
IFN-g	Interferon gamma
iNOS	Inducible nitric oxide synthase
IL-1	Interleukin-1
IodoTMT	Iodoacetyl tandem mass tag
ko	Knock out
LC	Liquid chromatography
LOAD	Late-onset AD
MCI	Mild cognitive impairment
MES	2-(*N*-morpholino)ethanesulfonic acid
MMSE	Mini mental stage examination
MMTS	Methyl methanethiosulfonate
MS	Mass spectrometry
MS/MS	Tandem mass spectrometry
NaCl	Sodium chloride
NaDOC	Sodium deoxycholate
NaF	Sodium fluoride
$Na_2H_2P_2O_7$	Sodium pyrophosphate dibasic
nanoHPLC	Nanocapillary high performance liquid chromatography
NaVO3	Sodium metavanadate
NFT	Neurofibrillary tangles
NitroDIGE	modification of BST and 2D-DIGE
nNOS	Neuronal nitric oxide synthase
NOS	Nitric oxide synthase
NP-40	Nonidet-P-40
PAGE	Polyacrylamide gel electrophoresis
PBS	Dulbecco’s Phosphate Buffered Saline
PDI	protein disulfide isomerase
PIC	Protein Inhibitor Cocktail
PMI	Post mortem interval
PRR	Pattern recognition receptors
PSD	Postsynaptic density

PSEN1	Presenilin 1
PSEN2	Presenilin 2
PTM	Post-translational modifications
RNS	Reactive nitrogen species
ROS	Reactive oxygen species
RT	Room temperature
SAD	Sporadic alzheimer’s disease
sAPPα	Secreted amyloid precursor protein-α
sAPPβ	Secreted amyloid precursor protein-β
SDS	Sodium Dodecyl Sulfate
SDS-PAGE	SDS-polyacrylamide gel electrophoresis
SNO	S-nitrosylation
SNO-Cys	S-nitrosylated cysteine
SNOSID	S-nitrosylation site identification
SWR	Standard working reagent
TBS	Tris-buffered saline
TBS-T	Tris-buffered saline with tween 20
TFA	Trifluoroacetic acid
TMT	Tandem mass tag
TNF-α	Tumor necrosis factor alpha
TrxR	Thioredoxin reductase
WB	Western blot

1. Introduction

1.1. General Introduction

Alzheimer's disease is an irreversible, progressive and most common type of dementia in the aging population (Crous-Bou et al., 2017). The disease is named after the German psychiatrist and neuropathologist Dr. Alois Alzheimer. In 1906, Dr. Alzheimer described the case of his 51-year-old patient Auguste Deter (Hippius, 2003). In the period of 5 years she developed progressive cognitive impairment, impaired social functioning, delusions, and hallucinations. In her brain autopsy, Dr. Alzheimer examined many abnormal clumps (now known as amyloid deposits) and tangled bundles of fibers (now known as neurofibrillary tangles) (Graeber and Möller, 1998; Hippius, 2003).

The world Alzheimer's report 2016 estimates approximately 46.8 million people worldwide suffered from dementia in 2015 and this number will reach 131.5 million in 2050 (Hebert et al., 2013). In principle, AD is an advanced stage of dementia, which gets progressively worse over time. AD accounts for around 50-70% of all dementia cases in the EU (reported by European commission on Health and Food Safety) (Europa.eu, 2017). Currently, there is no cure for AD but there is a worldwide attempt to find better ways to delay its onset, treat the disease and hamper it from developing (Yiannopoulou and Papageorgiou, 2013).

One known major risk factor for AD is advanced age: the majority of people who are affected by Alzheimer's are age 65 and older (Gleason, 2003; Qiu et al., 2009). There is strong evidence that cardiovascular risk factors such as hypertension, stroke, high cholesterol, and diabetes are also associated with AD. In a minority of cases, there is a familiar background with mutations in disease-associated genes that can result in higher risk or earlier onset of the disease (Bruijn and Ikram, 2014). The origin of AD is not entirely known. Its pathophysiological process probably begins years, if not decades before the clinical diagnosis of dementia is made (Sperling et al., 2014). This "preclinical" stage of AD might provide the chance for early diagnosis and therapeutic intervention (Fiandaca et al., 2014). The definite clinical onset of AD is difficult to conclude and once dementia is present, disease-modifying interventions may be no longer successful. Therefore, biomarkers are essential to anticipate the

disease progression from preclinical AD phase to AD (Fiandaca et al., 2014; Sperling et al., 2011).

1.2. Alzheimer's disease pathology

1.2.1. Clinical features

People with AD start to forget and often show changes in their abilities and personality. Over time, short-term memory failure gradually turns into confusion about time and place that may turn to depression or even aggressive behavior in later stages. Currently, the AD diagnosis is based on the clinical history, neurological examination, and neuropsychological tests. Clinically, AD is characterized by gradual memory loss, progressive cognitive function, loss of language function, impaired executive functioning (difficulties with everyday decision making), problems with complex movement (apraxia), and personality changes. The first clinical diagnosis was established in 1984 and revised by the National Institute on Aging-Alzheimer's Association (NIA-AA) workgroup in 2011 for a better understanding of the disease (Montine et al., 2012). There is no single test that confirms a person has Alzheimer's or not. The diagnosis is made through a comprehensive evaluation that analyzes all possible causes of the observed dementia. AD generally starts as a condition referred to as mild cognitive impairment (MCI due to AD). Flicker et al. first used this term in 1991; it refers to patients with mild cognitive dysfunction but has not yet affected daily life. MCI due to AD is often noted as a precursor or a transition stage between healthy cognitive aging and dementia. Research has demonstrated that persons with MCI due to AD have a higher chance of developing Alzheimer's disease in a few years in contrast to people with normal cognitive function (Flicker et al., 1991; Korolev, 2014). However, MCI does not always lead to AD. There are two types of MCI: amnestic and non-amnestic. A person with amnestic MCI (mainly affects the memory) has a higher risk of developing AD than non-amnestic MCI (affects thinking skills) (Petersen, Ronald C., 2009), who may suffer from AD from various other causes.

1.2.2. Neuropathological features

The classic neuropathological hallmarks of AD are the presence of extracellular amyloid deposits, intracellular neurofibrillary tangles and early synapse loss (de Paula et al., 2009; Serrano-pozo et al., 2011). The gold standard for AD diagnosis is an autopsy-based (post mortem) pathology evaluation. Neuropathologically AD is characterized by the presence of extracellular deposition of amyloid beta (Aβ), intracellular accumulation of neurofibrillary tangles, synapse loss and neurodegeneration (Boyd-Kimball et al., 2005). Aβ is the main component of senile plaque deposits and tau is the component of neurofibrillary tangles (NFTs) (Heneka et al., 2010; Swomley et al., 2014). The National Institute on Aging/Reagan Institute of the Alzheimer Association (NIA-Reagan) Consensus published AD neuropathologic change in three parameters also known as "ABC score" (Hyman et al., 2012). Moreover, cognitive impairment in AD cases is strongly associated with synaptic dysfunction (Terry et al., 1991).

"ABC score" (Aβ deposit score from Thal, NFT stage from Braak, Neuritic plaque score from CERAD):

A. Aβ deposit score by Thal (Thal et al., 2002):
   A0: no amyloid deposit (Aβ)
   A1: phases 1 or 2
   A2: phase 3
   A3: phases 4 or 5
B. NFT stage by Braak (Braak et al., 2011)
   B0: no neurofibrillary tangle (NFT)
   B1: stage I or II
   B2: stage III or IV
   B3: stage V or VI
C. Neuritic plaque score by CERAD (Mirra et al., 1991)
   C0: no neuritic plaques
   C1: score sparse
   C2: score moderate
   C3: score frequent

Plaque deposits

One of the main pathological lesions in AD patients is the senile or neuritic plaque. Senile plaques are abnormal extracellular accumulations of dystrophic neurites (abnormal neuronal processes) around a deposition of amyloid beta peptide in the gray matter of the brain (Baumann et al., 2017). Whereas diffuse deposit is not surrounded by dystrophic neuritis and has been called “preamyloid deposits” (Serrano-Pozo et al., 2011). In 1986, the Consortium to Establish a Registry for Alzheimer’s Disease (CERAD) generated a neuritic plaque scoring system for a standardized and validated measure of AD assessment, which was then used as a parameter in ABC score (Fillenbaum et al., 2008). This scoring ranks neuritic plaque density that histochemically identified in neocortex regions (Hyman et al., 2012).

It was discovered in the mid-1980s that the deposits consist of Aβ aggregates (Laferla et al., 2007). The most common isoforms are Aβ40 and Aβ42 that are part of the Amyloid Precursor Protein (APP), generated by sequential cleavage of β- and γ-secretases (Heneka et al., 2010;Serrano-Pozo et al., 2011). Aβ is chemically “sticky”, which gradually forms into deposits that are hallmarks of Alzheimer’s. Aβ monomers can spontaneously assemble into soluble Aβ oligomers and insoluble fibrils. It has been widely reported that soluble oligomers are the most toxic form of Aβ to neurons (Heneka et al., 2015; Sakono and Zako, 2010; Sengupta et al., 2016). The human body has a break-down system to clear amyloid from the brain. However, the Aβ accumulation in AD cases is thought to be an imbalance in the production and clearance of this peptide causing the formation of amyloid deposits in specific brain regions (Kummer and Heneka, 2014).

Braak and Braak in 1991 categorized gradual development of cortical amyloid deposits in three stages (Figure 1A) (Braak and Braak, 1991):

Stage A: Low densities of amyloid deposits are found first in the isocortex (frontal, temporal, and occipital lobe).

Stage B: Medium density of amyloid deposits in almost all of the isocortical association areas.

Stage C: Essentially all isocortical areas (belt field and primary areas) show densely packed amyloid deposits.

Later in 2002, Thal et al. recommended the severity of Aβ deposits in 5 phases (Figure 1B), which then used as Aβ deposit score on ABC scoring (Thal et al., 2002). The main analysis of Thal's phase model is that in the brain, Aβ spreads systematically (Hyman et al., 2012).

Phase 1: Aβ deposits start to develop in the neocortex.

Phase 2: Continued to the allocortical regions.

Phase 3: Spread to diencephalon, basal forebrain and striatum.

Phase 4: Then midbrain and medulla oblongata.

Phase 5: Finally, into the pons and the cerebellum.

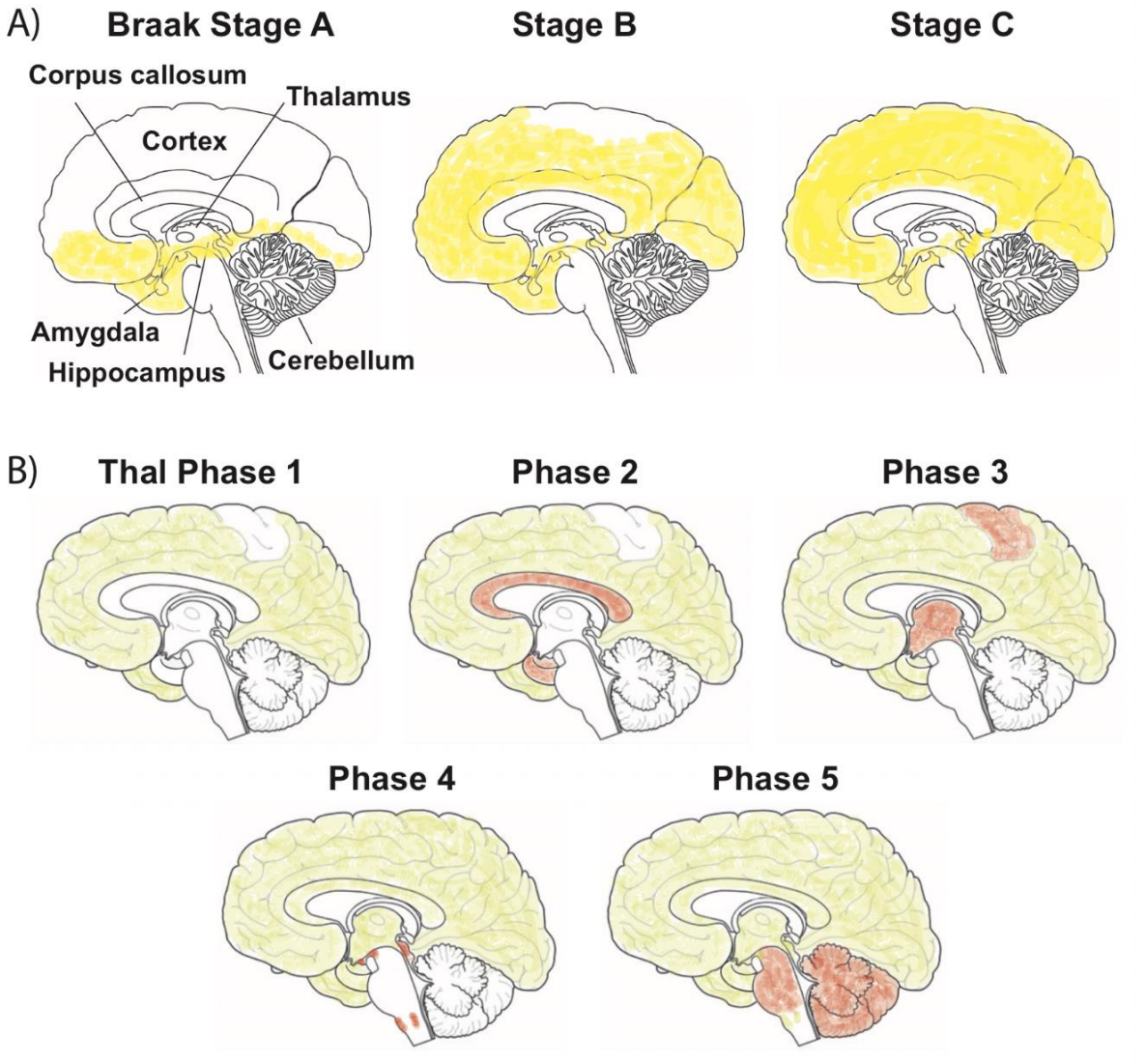

Figure 1. The pathological evolution of amyloid deposits in AD. (A) The severity of Aβ deposits adapted from Braak and Braak (Braak and Braak, 1991). Amyloid deposits spread through the brain as the disease progresses. Aβ deposits develop first in one

or more sites in the frontal, temporal, and occipital lobe (Stage A). They are observed later in almost all of the isocortical association areas. (Stage B). In severe cases of AD, Aβ deposits are found densely packed in all isocortical areas (Stage C). (B) The anatomical distribution of Aβ taken from Thal et al (Thal et al., 2002). Thal's first phase shows Aβ deposits only in the neocortex (green). The second phase is defined by additional spreading in allocortical brain regions (red). Phase 3 shows Aβ deposits in the striatum and the interbrain. Several nuclei in the brainstem become affected in phase 4, and phase 5 is described by the presence of Aβ deposits in the cerebellum and other brain areas.

Neurofibrillary Tangles

Another common primary marker of AD is neurofibrillary tangle. NFTs are characterized by intra-neuronal aggregates of insoluble hyperphosphorylated microtubule associated protein tau, which become extra-neuronal after tangle-bearing neurons die (Braak and Braak, 1991; Serrano-pozo et al., 2011). Tau proteins are proteins that function as microtubules stabilisators and a cellular transport system. The loss of normal tau function, combined with a toxic gain of function (the aggregation) could compromise transport along the long nerve cell projections, the axons, and contribute to degeneration beginning with the important signaling synapses at the end of the axon. Furthermore, formation of large NFTs inside the cell can result in cell death and the number of neurofibrillary tangles is linked with the severity of AD. There is speculation that the formation of NFTs and amyloid aggregation are interlinked for example by toxic amyloid oligomers. The exact mechanism however is not finally resolved (Castellani et al., 2010; Gendron and Petrucelli, 2009).

Figure 2 shows Braak stages of NFTs (on ABC score). The locus coeruleus is one of the earliest places to develop NFTs, which may act as a seed for spreading of the pathology throughout the brain before Aβ accumulation (Braak and Del Tredici, 2011; Braak et al., 2011; Satoh and Lijima, 2017). Locus coeruleus is a nucleus in the brainstem, which has roles in attention, emotion, memory and cognition (Sara, 2009; Satoh and Lijima, 2017).

a) Early stage: NFTs first appear in the transentorhinal region (stage I), followed by the entorhinal region and hippocampus (stage II).

b) Middle stage: NFTs accumulate in the basal neocortical areas of the temporal lobe (stage III) then insular and basal frontal areas (stage IV).

c) Late stage: NFTs spread to all prefrontal cortex and neocortical areas (stage V) than the primary sensory, motor, and visual areas (stage VI).

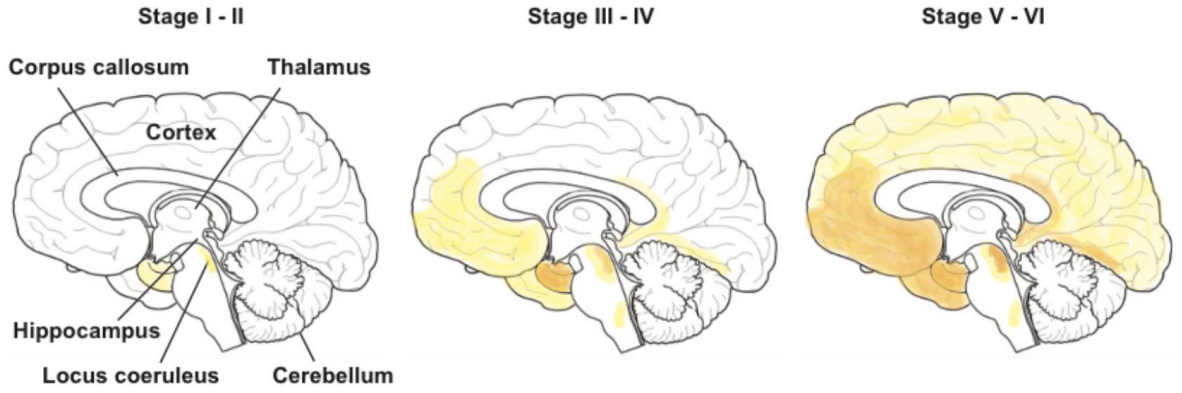

Figure 2. The pathological evolution of neurofibrillary tangle in AD, adapted from Braak and Braak (Braak et al., 2011). NFTs first develop in the locus coeruleus, as well as in the transentorhinal and entorhinal regions (stages I and II). Then spread through the neocortex (stages III and IV), followed by large parts of the neocortex (stages V and VI).

Synaptic loss and neurodegeneration

The loss of synapses is also considered a hallmark of AD. Whittaker's group first mentioned the concept of "Synaptosome" in their article in 1964, which considered as isolated nerve terminals (Whittaker et al., 1964). The synapses consist of three major components: the presynaptic membrane (also known as axon terminal), a synaptic cleft, and a postsynaptic membrane (also known as dendritic spine) (Whittaker et al., 1964). The pre- and the postsynaptic membranes are exclusively noticeable by visible densities along their plasma membranes. Their function is for neurons communication (electrical or chemical). The synaptic proteins interaction

controls functions of learning and memory (Bai and Witzmann, 2007; Swomley et al., 2014).

Diverse studies have shown the connection between cognitive impairment and synaptic dysfunction as a start of AD pathogenesis. Synapses dysfunction is considered to take place before the neuronal degeneration and death, which make the synapses as an essential therapeutic target (Boyd-Kimball et al., 2005; Chang et al., 2013). Prior studies have demonstrated significant decreases in synaptic density, which are area-specific in AD brain (Terry et al., 1991). Davies et al. showed 14% to 38% lesser number of synapses per surviving neuron in the frontal and temporal cortex and around 25% to 36% deficit in synaptic density (Davies et al., 1987). In AD patients, the remaining synapses are impaired functionally. Though they appear to be intact structurally, they may be dysfunctional (Yao et al., 2003).

1.3. Generation of amyloid beta

The Aβ is derived from proteolysis of APP, which encode gene is located on chromosome 21 in humans (Goate et al., 1991). APP is a transmembrane glycoprotein that is expressed by neurons, astrocytes and microglia**.** APP can be processed by one of two pathways (Figure 3). Around 90% is processed through the non-amyloidogenic pathway, and 10% the amyloidogenic pathway, however these ratios can change as a result of environmental factors, mutations and the age of the individual. The cleavage products from both pathways may have crucial roles in neural function and development (Plácido et al., 2014).

In non-amyloidogenic pathway, APP is first enzymatically cleaved by α-secretase, of which three enzymes have been identified, belonging to the ADAM family: ADAM9, ADAM10 and ADAM17 (a disintegrin and metalloprotease family enzyme). The two yield fragments are the soluble secreted amyloid precursor protein-α or N-terminal fragment (sAPPα) and carboxy-terminal fragment (CTFα). This cleavage by α-secretase occurs within the Aβ domain, hence preventing the generation of the Aβ peptide. While Aβ is neurotoxic, studies suggest that sAPPα may be involved in neuronal survival and has a neuroprotective role. Furthermore, CTFα undergoes an additional cleavage by γ-secretase to generate a soluble N-terminal

fragment (P3) and a membrane-bound C-terminal fragment or amyloid precursor protein intracellular domain (AICD or APP intracellular domain) (Furukawa et al., 1996; Laferla et al., 2007; Mattson, 1997).

In the amyloidogenic pathway, APP is initially cleaved by β-secretase (BACE; β-site APPcleaving enzyme), generating a soluble N-terminal fragment (sAPPβ), and C-terminal fragment (CTFβ) within the membrane. CTFβ is then cleaved by the γ-secretase, yielding AICD (the same as non-amyloidogenic pathway) and soluble Aβ (Furukawa et al., 1996; Laferla et al., 2007; Mattson, 1997). This cleavage generates two mainly toxic species, $A\beta_{1-40}$, and $A\beta_{1-42}$ (more amyloidogenic) at a ratio of 10:1. Aβs rapidly aggregate to form oligomers and the insoluble amyloid fibrils, which disrupt neuronal function (Chow et al., 2011; Qu et al., 2016).

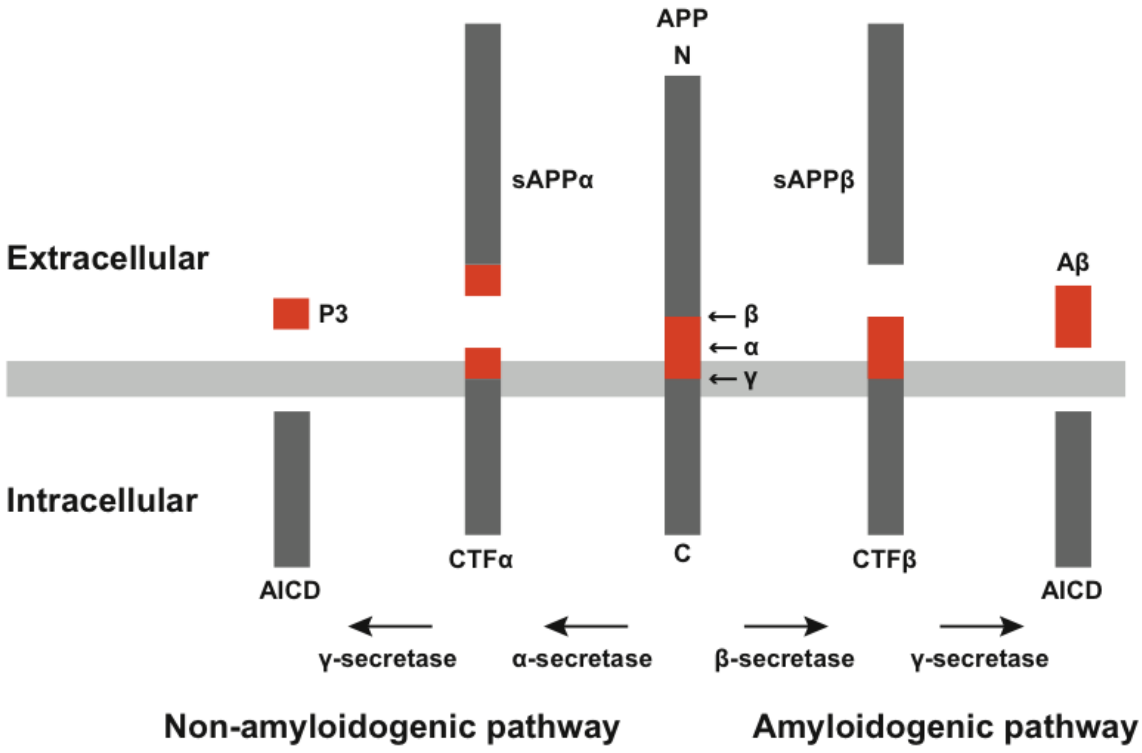

Figure 3. The processing of amyloid precursor protein (APP). APP can be cleaved by α-, β-, and γ-secretases, which undergo non-amyloidogenic (left) or amyloidogenic (right) processing. The non-amyloidogenic pathway, cleaved by α-secretase yields in fragments of the soluble secreted amyloid precursor protein-α (sAPPα) and carboxy-terminal fragment α (CTFα). Furthermore, CTFα undergoes an additional cleavage by

γ-secretase resulting P3 and amyloid precursor protein intracellular domain (AICD). In the amyloidogenic pathway, APP is first cleaved by β-secretase generating a soluble secreted amyloid precursor protein-β (sAPPβ), and carboxy-terminal fragment β (CTFβ). CTFβ is then cleaved by the γ-secretase, yielding AICD and Aβ.

1.4. Genetics of Alzheimer's disease

Ageing is the most influential known risk factor of AD. Family history is the second greatest risk factor for the development of AD. Based on the age of onset, AD is divided into 2 types: early-onset AD (EOAD) and late-onset AD (LOAD). EOAD or also called Familial Alzheimer's Disease (FAD) represents the minority of all AD cases and affects people before the age of 65. Three genes are considered as the main risk factors of EOAD: amyloid precursor protein (APP) on chromosome 21, presenilin 1 (PSEN1) on chromosome 14, and presenilin 2 (PSEN2) on chromosome 1. Each of these mutations plays a role in APP breakdown and can form abnormal proteins. This breakdown generates harmful forms of amyloid deposit in the brain (Bertram and Tanzi, 2005; Goate et al., 1991; Tanzi and Bertram, 2005).

The majority of people with AD have LOAD or Sporadic Alzheimer's Disease (SAD), which symptoms become visible at the age of 65 and over. The causes of LOAD are not fully understood though it is predicted as a combination of factors of genetic, lifestyle and environmental, which may affect a person's risk to develop the disease. The important genetic risk factor for LOAD is *APOE* gene, located on chromosome 19. APOE comes in different forms: APOE ε2, APOE ε3, and APOE ε4. Both EOAD and LOAD can happen in people with a positive family history of AD (Bertram and Tanzi, 2005; Goate et al., 1991; Tanzi and Bertram, 2005).

1.5. Inflammatory process

Another important sign of AD is neuroinflammation; it is a complex process that has both beneficial aspects in maintenance of brain homeostasis and facilitates injury resolution (degenerative, infection and tissue damage); but also can be detrimental if sustained chronically, over years and decades (Schwartz et al., 2013; Sochocka et al., 2017). Increasing proof proposes neuroinflammation as an essential contributor in AD

pathogenesis (Heneka et al., 2010, 2015). Though the exact disease stage at which neuroinflammation begins in AD is unknown, it may be one of the earliest events associated with the disease process (Qu et al., 2014a; Wyss-coray and Rogers, 2012). The term “neuroinflammation” describes the inflammatory response in the central nervous system (CNS) triggered by autoimmunity, infection, or toxins that causes glial cells to accumulate (Glass et al., 2010).

Under pathological conditions such as inflammation, altered neuronal function, infection, injury and ischemia, microglia are activated (physiologically in inactive state), which change the morphology of microglia, from ramified (resting) to ameboid (active) (Wang et al., 2015). Microglia detects pathogens via pattern recognition receptors (PRRs) that include specific toll-like receptors (TLRs), nucleotide-oligomerization binding, C-type lectin receptors and domain (NOD) proteins (Sterka and Marriott, 2006). These receptors recognize pathogen-associated molecular patterns (PAMPs) or damage-associated molecular patterns (DAMPs) and initiate the cellular defense mechanisms (Heneka et al., 2015). Astrogliosis, which demonstrated by an increase in the size, number and motility of astrocytes is also seen in AD. Once activated, microglia and astrocytes produce several proinflammatory signal molecules, including cytokines, chemokines, complement molecules, growth factors and cell adhesion molecules (Bai and Witzmann, 2007; Heneka et al., 2015).

Microglia activation also contributes to the release of reactive oxygen species (ROS) and nitric oxide (NO) through the activation of myeloperoxidase, NADPH oxidise and inducible NO synthase (iNOS or NOS2) (Heneka et al., 2014). Previous studies reported increased levels of nitrosylated proteins in AD brain and cerebral spinal fluid (CSF). The increase of oxidative stress modification indicates inflammation as an important source in the pathogenesis of neurodegenerative disease (Galasko and Montine, 2010; Zahid et al., 2014). Activated microglia and astrocytes are characteristically found surrounding and engulfing the Aβ senile deposits (Glass et al., 2010).

1.5.1. Mechanisms of nitric oxide synthesis

Reactive oxygen/nitrogen species (ROS/RNS) are commonly produced at relatively low concentrations by all cell types (such as macrophages, monocytes) and have a role as physiological messengers of intracellular signaling pathway required for immune response and cell growth (Finkel, 2011; Nakamura et al., 2012). Nonetheless, exposure to environmental toxins, neuroinflammatory stimuli (pathogens, irritants or damaged cells), Aβ oligomers and also the normal process of aging can provoke redox imbalance, leading to nitrosative/oxidative stress (Nakamura et al., 2012). An imbalance of this system by increased oxidant production and reduction of antioxidants contributes to neuronal cell damage and results in neurodegeneration (Martínez-Ruiz et al., 2011). Additionally, peripheral inflammation also contributes to neuroinflammation by increasing the blood brain-barrier (BBB) permeability and brain inflammatory responses such as glial cells activation, which release ROS, chemokines and pro-inflammatory cytokines (Takeda et al., 2013).

RNS are derived mainly from O_2^- and nitric oxide (NO), a small, diffusible messenger (Mangialasche et al., 2009). NO is a free radical that is synthesized through the conversion of L-arginine to L-citrulline and NO via nitric oxide synthase (NOS) enzymes (Chung, 2007; Habib and Ali, 2011). NO contributes to numerous physiologic responses such as neurogenesis, vasculature vasodilation, synaptic neurotransmission, inflammation, and apoptosis (Forstermann et al., 1994; Mannick and Schonhoff, 2002). NO is a signaling molecule or intracellular messenger that coordinates the communication between endothelial cells and immune cells. It is involved in both central and peripheral nervous system as a host protection from infectious organisms (bacteria, viruses and other microorganisms), which can induce the death of host immune cells (Bogdan et al., 2000).

There are three isoforms of the NOS enzyme: neuronal (also known as nNOS or NOS1), inducible (also known as iNOS or NOS2), and endothelial (also known as eNOS or NOS3). nNOS and eNOS are expressed constitutively and Ca^{2+} dependent, while iNOS is inactive under non-pathological conditions and is Ca^{2+} independent. Each isoform has specific functions (Förstermann and Sessa, 2012): The human nNOS gene is located in chromosome 12 and expresses NO mainly in neurons (Knowles and Moncada, 1994; Viaro et al., 2000). Its functions are synaptic plasticity,

cell communication, relaxation of smooth muscle and blood pressure regulation (Viaro et al., 2000). eNOS produces NO in endothelial, blood vessels and is involved in vascular tone regulation (vasodilatation) and platelet function (adhesion and aggregation) (Knowles and Moncada, 1994; Viaro et al., 2000). The expression of the inducible nitric oxide synthase (also known as inflammatory NOS) has been defined as a result of the inflammatory processes, which come with tissue damage, infection, or disease (Colton et al., 2008; Heneka and Feinstein, 2001). In the brain, iNOS is produced in microglia cells, astrocytes and in lesser amount in endothelial cells (Heneka and Feinstein, 2001). The iNOS gene coding is located in chromosome 17 (Knowles and Moncada, 1994). iNOS is not usually expressed in cells and it is induced upon stimulation by proinflammatory cytokines (such as tumor necrosis factor alpha/TNF-α, interleukin-1/IL-1 and interferon gamma/IFN-g) and lipopolysaccharide (LPS) (Green et al., 1994).

1.5.2. Protein S-Nitrosylation and denitrosylation

S-nitrosylation of cysteine (SNO) is one of the most important post-translational modifications (PTM) induced by NO (Nakamura et al., 2013). SNO is a reversible PTM with covalent addition of a nitrosyl group (NO) to the cysteine (Cys) thiol group (Anand and Stamler, 2012). It is observed as an essential redox signaling mechanism in the regulation of many cellular and physiological functions. In normal physiological conditions, SNO can influence protein-protein interaction, regulate (by activation or inhibition) protein activity, affect protein localization, alter protein aggregation, promote conformational changes and regulate cell signal transduction pathways (Choi et al., 2000; Qu et al., 2011; Uehara et al., 2006). In contrast, under pathological conditions, excess SNO can trigger protein misfolding, mitochondrial dysfunction, and ER stress, which leads to synaptic degeneration and cell death (Nakamura and Lipton, 2007).

Due to an increasing number of PTM protein identifications, a central database (dbSNO 2.0) is made to collect all datasets for S-nitrosylated proteins from different sources, which is available at http://dbSNO.mbc.nctu.edu.tw (Lee et al., 2012b). The scope of SNO proteins depends on the level of both nitrosylation and denitrosylation (Benhar et al., 2009). S-nitrosylated protein formation could be counterbalanced by denitrosylation, which is involved in the NO removal from S-nitrosylated cysteine,

through non-enzymatic and enzymatic mechanism (Zhao et al., 2015). Non-enzymatic mechanism is mediated by free metal ions of iron or copper. Enzymatic mechanism is mediated by enzymes such as S-nitrosoglutathione reductase (GSNOR), protein disulfide isomerase (PDI) and thioredoxin reductase (TrxR) (Benhar et al., 2009; Nakamura et al., 2012).

1.5.3. S-nitrosylation (SNO) in neurodegenerative disorder

During aging, there is an increase of free radical and a decrease of antioxidant, which may contribute to the neurodegenerative development such as AD (Sayre et al., 2008). It has been shown in previous publications that nitric oxide (NO) has an important part in neurodegeneration process (Nakamura and Lipton, 2016; Reczek et al., 2006). In neurodegenerative disorders, aberrant SNO can propagate synaptic injury, mitochondrial dysfunction, protein misfolding, and neuronal death (Nakamura et al., 2013). In AD, studies have shown that neuroinflammatory stimuli such as Aβ oligomers can stimulate microglia cells. Once activated, microglia cells recruit astrocytes, which boost the inflammatory response on the extracellular Aβ deposits (Zhao et al., 2015). This AD neuroinflammatory component is then characterized by acute-phase response of cytokine, complement cascade activation and induction of iNOS (Heneka et al., 2010; Wallace et al., 1997).

1.5.4. Detection and analysis of SNO-proteins

The detection and quantification of S-nitrosylation has been a difficult task due to the low abundant and labile nature of the modification (sulfur-nitrogen bond in S-nitrosothiol) (Qu et al., 2014a). Nitrosothiols can be detected using several ways such as chemiluminescence, colorimetric, fluorometric, S-nitrosylated cysteine antibody, and mass spectrometry (MS) analysis (Chen et al., 2013; Ju et al., 2015).

The first and frequently used method for SNO detection is the biotin switch technique (BST) developed by Jaffrey and Snyder in 2001. This method utilizes a replacement strategy by adding a stable biotin-label on the SNO modification, allowing their detection and identification by anti-biotin antibodies or mass spectrometry (Jaffrey and Snyder, 2001). General approaches for quantitative SNO proteomics are

two-dimensional difference gel electrophoresis (2D-DIGE) or liquid chromatography (LC) followed by mass spectrometry. To achieve an optimal result, a combination of protein enrichment and/or fractionation (one- or 2D-DIGE, liquid chromatography) and identification technique (Western blotting, tandem mass spectrometry) is needed (Bai and Witzmann, 2007). One of the recent SNO detection is NitroDIGE, which combined 2D-DIGE with modified BST using fluorescence dye CyDye™ (Qu et al., 2014b).

One of the fractionation procedures is HPLC (high performance liquid chromatography) (Issaq et al., 2002). It depends on their pumps to undergo a liquid solvent containing the sample mixture via a column loaded with a solid adsorbent material (Issaq et al., 2002). Each sample component reacts slightly different with the adsorbent material, generating different flow rates for the each component and causing the segregation of the components when they flow out of the column (Issaq et al., 2002; Mitulovic and Mechtler, 2006).

Most of the methods address high amounts of starting materials that range around 100 to 500 µg of protein lysate (Wojdyla and Rogowska-Wrzesinska, 2015). Moreover, it is a common procedure to use NO-donors as an induction to analyze SNO modification sites. Making it difficult for results comparison of studies using NO donors with the in vivo situation, where cysteine S-nitrosylation depends on the unknown concentrations of nitrosylating compounds (Zareba-Koziol et al., 2014). Therefore, endogenous SNO level identification that is produced from sub-fractionated compartments such as synaptosomes need high sensitivity and specificity of the detection (Wijasa et al., 2017).

In the current approach, an MS-based, isobaric tag labeling strategy was proposed, where peptides are linked with various tags with the same mass and fragmented to generate reporter ions of different mass (Dayon and Sanchez, 2012). In a classic bottom-up proteomics workflow, proteins are enzymatically digested by proteolytic digestion to generate peptides, which are then labeled with various isobaric tags (Zhang et al., 2013). Analogous with BST, the iodoTMT™ 126-131 labeling reagents are used as a substitute chemistry of SNO modifications (Qu et al., 2014a). This approach has been rarely described with low amounts of starting material and under basal condition (with NO donor treatment) (Wijasa et al., 2017). Despite

introduced in 2012, this approach has been barely described in the literature utilizing endogenous condition samples (without NO donor treatment) and low amounts of starting material.

1.6. Synaptosomes preparations for proteomic analysis

Various techniques have been established for synaptosome isolation using different centrifugation and buffer reagents, such as sucrose, Ficoll/sucrose or Percoll density gradient centrifugation, all of which result in purifying a crude synaptosome fraction from the contamination (Jaffrey and Snyder, 2001; Scheff et al., 2014). Density gradient centrifugation is a common procedure used for subcellular fractionation such as synaptosome for further analysis (Kiss et al., 2016). Sucrose solution is the most common used solution for density manipulation (Clayton and Shadel, 2014). In the process, the sample is first lysed to break the cell membrane then layered on a discontinuous sucrose density gradient (Wijasa et al., 2017). After repeated centrifugations using swinging bucket rotors, the density separation generates sediment called pellet (the full protocol is described on the material and methods section).

The purity of synaptosome isolation can be confirmed by western blotting analysis or examined under an electron microscope (EM) (Bai and Witzmann, 2007). Western blotting is a widely used analytical technique to detect specific proteins in a sample using certain markers (Jensen, 2012). In a western blot, gel electrophoresis is used for separation of the native proteins and their fragments based on their size and charge. Polyacrylamide gel is usually utilized for the electrophoretic separation of proteins, and SDS is mainly used as a buffer (also in the gel) thus all proteins will be in a uniform negative charge (proteins can be charged positively, negatively, or neutrally) (Towbin et al., 1979). This is known as SDS-polyacrylamide gel electrophoresis (SDS-PAGE). After the electrophoretic separation, the proteins are transferred to a membrane (nitrocellulose or PVDF), which are then blocked with Bovine Serum Albumin (BSA) or milk to prevent non-specific binding of the antibody. The membrane then stained with antibodies specific to the target protein (first antibody) and a secondary antibody that recognizes the first antibody staining for the detection (Towbin et al., 1979). There are many technical approaches used for

synaptosomal proteome analysis; each has its own advantages and disadvantages (Nesvizhskii, 2007). Consequently, the chosen approach can affect the study outcome and therefore has to be done carefully (Bai and Witzmann, 2007).

1.7. Quantitative proteomic

Mass spectrometry-based proteomics facilitates large-scale analysis of biological systems, as it allows sensitive and unbiased detection of proteins/peptides and PTM such as s-nitrosylation (Ong, 2010). Proteomic studies can be performed using various biological samples such as whole tissue samples, isolated cells and body fluids. Quantitative proteomics comprises analytical techniques to determine not only the identity but also relative or absolute concentrations of protein components in a sample. For mass spectrometry, proteins are typically digested with specific proteases, for example trypsin, which generates specific sets of peptides, following ionization and analysis by MS instruments (Kito and Ito, 2008).

Tandem mass spectrometry (MS/MS) has been broadly used in proteome analysis, where an ion peptide is then selectively isolated and fragmented to generate an MS/MS spectrum. The pattern of these fragment ions is comparable with theoretical ones calculated from protein sequences in databases. If the MS/MS spectrum calculated for a peptide shows a reliable match with one of the theoretical spectra, the peptide is then selected for the theoretical spectrum calculation (Kito and Ito, 2008; Tuli and Ressom, 2009). MS-based proteomics enables quantitative analysis of post-translational modifications and protein abundance in cell, tissue and whole organism (Ren et al., 2014).

In order to generate reliable and consistent data sets, an extensive internal quality control of the procedure is required. The use of an internal standard can aid to control the variability in a quantitative analysis. It should be added in the analytical procedure as early as possible and treated equally to other samples (Ong, 2010).

1.8. Data analysis and protein identification

One of the ways to visualize the significant differential abundance (between two conditions or more) from proteomic data is by significant fold change assessed by statistical analysis such as Limma, RankProduct (RP) and bootstrap analysis (Mukherjee et al., 2003a; Pursiheimo et al., 2015). Limma, RankProduct and bootstrap analysis were first developed for microarray data which also work well for proteomics data (Breitling et al., 2004; Schwammle et al., 2013). One of the well-known problems of proteomics data analysis is missing values. This problem became worse when the detection of significant changes on the peptide level is wanted (Schwammle et al., 2013; Webb-Robertson et al., 2015). In order to solve this problem, Schwammle et al in 2013 investigated and optimized the performance of three statistical approaches (standard t-test, Limma and RankPrduct) using experimental data sets with varying missing values (Schwammle et al., 2013).

Schwammle et al. recommended the combined use of Limma and RankProduct as a new and excellent way to detect significant changes in large quantitative data sets from mass spectrometry experiments (Schwammle et al., 2013). Limma or short for “linear models for microarray data” is a modified version of standard t-test, which fit the statistic model of linear model (Pursiheimo et al., 2015). While RP is based on the statistic model of rank statistic (ranks of fold changes) for the analysis (Breitling et al., 2004). Limma and RankProduct are well-established methods for statistical analysis of large data sets with missing values. The tests provide more sensitive and reliable results than standard t-test (Schwammle et al., 2013). Nonetheless, both tests perform optimally on different types of data sets. In general, LM performs better for high variation samples with low amounts of missing values. While RP is a more suitable test for data sets with more missing values and low variation of regulated values. The requirement to achieve high-confident results using this combination is a large data set (more than 1000 features) (Schwammle et al., 2013).

Another statistical analysis for handling the proteomics data is the bootstrap method/bootstraping (Mukherjee et al., 2003a). This method was first introduced in 1979 by Bradley Efron (Efron and Tibshirani, 1993). Bootstrapping is a random resampling method with replacement from the sample data (from a population) to calculate confidence intervals on interest parameters (Mukherjee et al., 2003a).

Bootstrapping can be used for insufficient/small samples of the same size which then repeatedly drawn in a large number of times. So the same replicate can occur more than once in the data table with the same or different condition (Efron and Tibshirani, 1993; Mukherjee et al., 2003a).

1.9. Aim of the thesis

Aim of this study was to characterize NOS2-dependent S-nitrosylation on synaptic proteins to discover new potential biomarker candidates of neuroinflammation in early AD stages. In order to achieve that, synaptosomes were isolated from transgenic mice and human post mortem brain tissues.

A biomarker refers to a material used as a measurable indicator of some biological state (normal and pathogenic biological process) (Liu et al., 2014). Changes in the brain begin years prior to clinical onset and diagnosis of AD. Until now, diagnosing AD in early stage can be difficult and challenging (Fiandaca et al., 2014). Thus the biomarker development for AD is important to enhance early diagnosis and stimulate the development of new therapies (Chintamaneni and Bhaskar, 2012). It has been known for some years that synapses are the important target because synapse degeneration occurs early during AD pathogenesis. To identify potential candidate biomarkers in synaptic proteins and determine the effect of inflammation on AD pathogenesis, mass spectrometry (MS)-based proteomic was used on AD synaptosomal samples from mouse and human groups.

To analyze the mouse data thoroughly, the age effect of each genotype (comparing 12-month to 3-month-old mice) and the genotype effect on old mice (APP/PS1 and NOS2 knockout effect) were analyzed. The age effect on WT mice was used as a control, which shows the differentially regulated proteins during healthy aging. While the age effect on APP/P1 mice was used as a pathological aging. AD progression was analyzed in human samples by comparing the disease stages (MCI-Control, AD-MCI, and AD-Control) (Figure 4).

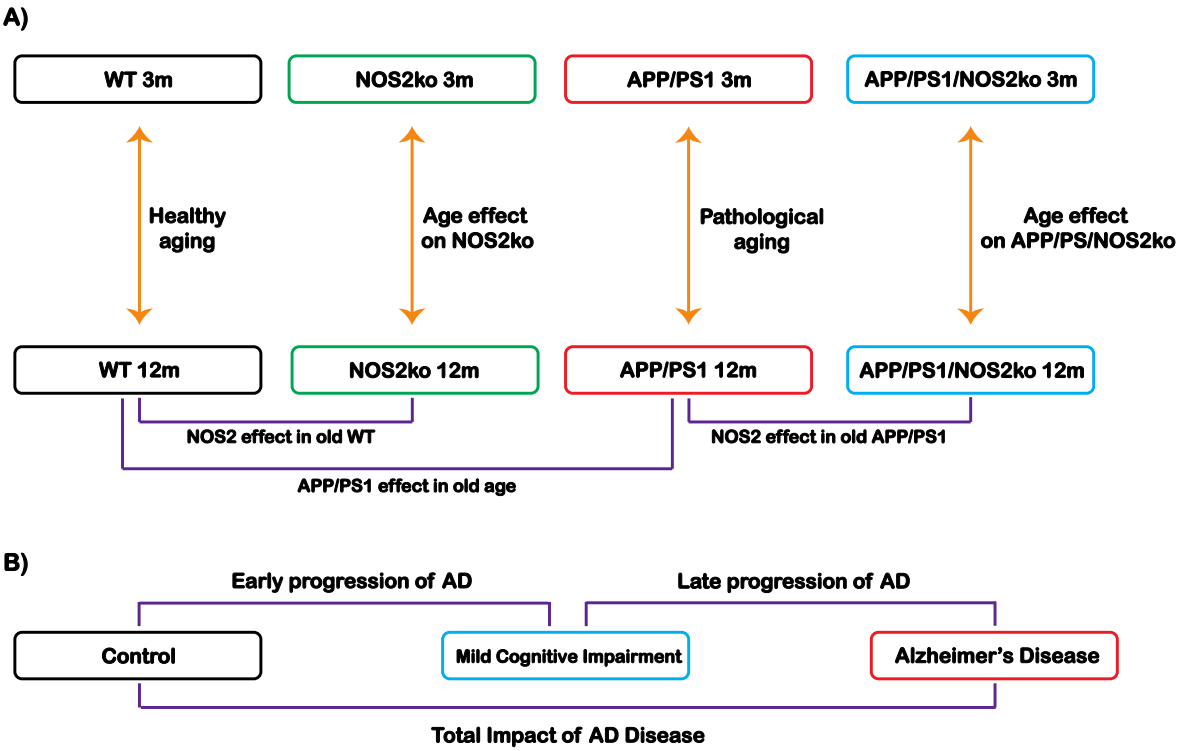

Figure 4. Overview of the experimental groups used in murine and human samples. A) SNO-proteins/peptides from murine synaptosomes were examined using a chain of comparisons to identify the age-dependent, APP/PS1-dependent and NOS2-dependent effects. The experimental groups (n = 12 mice/group) were 3-month and 12-month-old wild type (WT), NOS2ko (NOS2 knockout mice or NOS2 -/-), APP/PS1 (transgenic mice carrying the human amyloid precursor protein and presenilin1 gene) and APP/PS1/NOS2-/- (transgenic mice carrying the human amyloid precursor protein, presenilin1 gene crossed with NOS2ko). B) SNO-proteomes from human synaptosomes (n = 20 human samples/group) were examined using the comparison of disease stage.

This thesis provides information about:

- Method optimization of quantitative proteomics on synaptosomal samples
- The efficiency of the iodoTMT^{TM} protocol when applied to the analysis of synaptosomal samples
- Technical variances of the method as well as the comparability of findings with previous published results in the field.
- Characterization of NOS2-dependent S-nitrosylation on synaptic proteins
- New potential biomarker candidates of neuroinflammation in early AD stage

2. Material and methods

2.1. Materials

REAGENT or RESOURCE	SOURCE	IDENTIFIER
Antibodies		
Rabbit anti-glutamate receptor 1 (GluR1)	Merck KGaA, Darmstadt, Germany	Cat# ab1504, RRID: AB_2113602
Mouse anti-lamin B1	Proteintech Group Inc., Chicago, USA	Cat# 66095-1-Ig, RRID: AB_11232208
Rabbit anti-NMDA receptor 2B (NMDAR2B)	Merck KGaA, Darmstadt, Germany	Cat# ab1557p, RRID: AB_11214394
Mouse anti post-synaptic density (PSD95)	Thermo Fisher, Scientific, Waltham, USA	Cat# MA1-046, RRID: AB_2092361
Rabbit anti-synaptophysin	Abcam Inc., Cambridge, UK	Cat# ab52636, RRID: AB_882786
Mouse anti-tubulin	Thermo Fisher, Scientific, Waltham, USA	Cat# 62204, RRID: AB_1965960
Chemicals		
4-(2-Aminoethyl)benzenesulfonyl fluoride hydrochloride (AEBSF)	Sigma Aldrich Co. LLC., Munich, Germany	Cat# A8456
1.4-Dithiothreit (DTT)	Carl Roth GmbH &Co. KG, Karlsruhe, Germany	Cat# 6908
4X Protein Sample Loading Buffer	LI-COR Inc., Lincoln, Nebraska, USA	Cat# P/N 928-40004
Aceton	Sigma Aldrich Co. LLC., Munich, Germany	Cat# 650501-1L-M
C18 Spin Columns	Thermo Fisher, Scientific, Waltham, USA	Cat# 89870

Dimethylformide (DMF)	Thermo Fisher, Scientific, Waltham, USA	Cat# TS-20673
Dimethyl sulfoxide (DMSO)	Applichem GmbH, Darmstadt, Germany	Cat# A1584
Ethylene diamine tetraacetic acid (EDTA)	Thermo Fisher, Scientific, Waltham, USA	Cat# 15575020
Ethylene glycol tetraacetic acid (EGTA)	Carl Roth GmbH &Co. KG, Karlsruhe, Germany	Cat# 3054
Formic Acid (FA)	Sigma-Aldrich Chemie, Munich, Germany	Cat# 06473-100ML
HENS buffer	Thermo Fisher, Scientific, Waltham, USA	Cat# 90106
Hydroxylamine	Thermo Fisher, Scientific, Waltham, USA	Cat# 90115
Immobilized Anti-TMT™ Resin	Thermo Fisher, Scientific, Waltham, USA	Cat# 90076
Iodoacetamide (IAM)	Sigma Aldrich Co. LLC., Munich, Germany	Cat# A3221-10VL
LC/MS grade acetonitrile (ACN)	Thermo Fisher, Scientific, Waltham, USA	Cat# 51101
LC/MS grade methanol	Thermo Fisher, Scientific, Waltham, USA	Cat# A456-4
Methyl methanethiosulfonate (MMTS)	Thermo Fisher, Scientific, Waltham, USA	Cat# 23011
Nitrocellulose Membranes	Thermo Fisher, Scientific, Waltham, USA	Cat# 88013
Nonidet (NP-40)	United State Biological Inc., Salem, Massachusetts, USA	Cat# N3500
NuPAGE™ 4-12% Bis-Tris Protein Gels	Thermo Fisher, Scientific, Waltham, USA	Cat# NP0321BOX
NuPAGE MES SDS Running Buffer (20X)	Thermo Fisher, Scientific, Waltham, USA	Cat# NP0002
NuPAGE™ Transfer Buffer (20X)	Thermo Fisher, Scientific, Waltham, USA	Cat# NP0006
PageRulerTM Prestained Protein Ladder (10 to 180 kDa)	Thermo Fisher, Scientific, Waltham, USA	Cat# 26616

PBS powder without Ca^{2+}, Mg^{2+}	Biochrome Gmbh, Berlin, Germany	Cat# L 182-01
cOmplete protease inhibitor cocktail	Sigma Aldrich Co. LLC., Munich, Germany	Cat# 04693116001
Sodium ascorbate	Thermo Fisher, Scientific, Waltham, USA	Cat# AC352681000
Sodium chloride (NaCl)	Applichem GmbH, Darmstadt, Germany	Cat# 131659.1214
Sodium deoxycholate (NaDOC)	Sigma Aldrich Co. LLC., Munich, Germany	Cat# D6750
Sodium Dodecyl Sulfate (SDS)	MP Biomedicals	Cat# 04811030
Sodium fluoride (NaF)	Carl Roth GmbH &Co. KG, Karlsruhe, Germany	Cat# P756
Sodium orthovanadate (Na_3VO_4)	Sigma Aldrich Co. LLC., Munich, Germany	Cat# S6508
Sodium pyrophosphate dibasic ($Na_2H_2P_2O_7$)	Sigma Aldrich Co. LLC., Munich, Germany	Cat# P8135
Sucrose	Sigma Aldrich Co. LLC., Munich, Germany	Cat# S9378
Tandem mass tag (TMT) Elution Buffer	Thermo Fisher, Scientific, Waltham, USA	Cat# 90104
trifluoroacetic acid (TFA)	Sigma Aldrich Co. LLC., Munich, Germany	Cat# 302031
Tris-Acetat	Sigma Aldrich Co. LLC., Munich, Germany	Cat# T8280
Tris (hydroxymethyl) aminomethane	Carl Roth GmbH &Co. KG, Karlsruhe, Germany	Cat# 9090
Trypsin	Serva Electrophoresis GmbH, Heidelberg, Germany	Cat# 37294
Tween-20	Sigma Aldrich Co. LLC., Munich, Germany	Cat# P9416
Water for HPLC	Sigma Aldrich Co. LLC., Munich, Germany	Cat# 34877
Critical Commercial Assays		
IodoTMT™ sixplex Label	Thermo Fisher, Scientific,	Cat# 90102

Reagent Set	Waltham, USA	
Pierce BCA Protein Assay Kit	Thermo Fisher, Scientific, Waltham, USA	Cat# 23225
Experimental Models: Organisms Strains		
Mouse: BC57/Bl6	The Jackson Laboratory, Bar Harbor, Maine, USA	RRID:IMSR_JAX:000664
Mouse: APP/PS1	The Jackson Laboratory, Bar Harbor, Maine, USA	https://www.jax.org/strain/005864
Mouse: NOS2-/-	The Jackson Laboratory, Bar Harbor, Maine, USA	http://jaxmice.jax.org/strain/002609.html
Mouse: APP/PS1/NOS2-/-	UKB Bonn animal facility (HET3)	N/A

2.2. Brain samples

2.2.1. Mice

Two age groups were chosen to reflect the age effect on AD progression, 3-month and 12-month-old mice. To analyze the genotype effect in aged mice, four age-matched male transgenic animal groups (APP/PS1, NOS2-/-, APP/PS1/NOS2-/- and wild type) were used in this study that all shared the BC57/Bl6 genetic background. As AD models, hemizygous double transgenic mice APP/PS1 expressing a chimeric mouse/human amyloid precursor protein (Swedish mutation) and a human PS1 Δexon 9 mutation (Jankowsky et al., 2001) were studied, using wild type (WT) as controls. NOS2 knockout or NOS2-/- (additional information can be found at http://jaxmice.jax.org/strain/002609.html) and APP/PS1/NOS2-/- mice were used to see the effect of iNOS-derived nitric oxide (inflammation) in wild type control and APP/PS1 background respectively. APP/PS1 +/- and NOS2-/- mice were bred to generate the litters on one of the group (APP/PS1/NOS2-/-) that used in this study. The deletion of inducible nitric oxide synthase in an APP/PS1 background was used as a way to understand better the role of NO (iNOS-derived NO) in altering chronic neurological disease. Mice were maintained under standard conditions at temperature of 22°C and a 12 h/12 h light/dark cycle, housed in groups and given free access to food and water. Mice were anesthetized and transcardially perfused with ice-cold

normal saline shortly prior to synaptosome isolation. The mice numbers were *n* = 20 per experimental group. Whole brain hemispheres without cerebellum and brainstem were used for protein extraction.

2.2.2. Human samples

Ninety frozen post mortem human brain tissues from the cortical area (*n* = 30 healthy control, *n* = 30 mild cognitive impairment/MCI and *n* = 30 Alzheimer's disease/AD) were obtained from Banner Sun Health Research Institute (BSHRI) Brain and Body Donation Program in Sun City, Arizona (Beach et al., 2015). These three human groups were matched with consideration of age (above 65), sex, post mortem interval / PMI (less than 4 hours), MMSE, Braak stage, and ApoE (Table 1). Diagnoses were made based on the National Institute on Aging/Reagan Institute of the Alzheimer Association (NIA-Reagan) Consensus Recommendations for the postmortem diagnosis of AD. Particularly, tissues were evaluated for their ABC scores (Aβ deposit score, Braak neurofibrilliary tangles stage and CERAD neuritic plaque score), illustrating the level of AD neuropathologic change.

Features	**Control**		**MCI**		**AD**	
	Range	**Mean (SD)**	**Range**	**Mean (SD)**	**Range**	**Mean (SD)**
Age (years)	73 – 99	87.4 (8.1)	83 – 99	92.1 (7.2)	66 – 99	84.3 (10.1)
Number of samples	Male	Female	Male	Female	Male	Female
	17: 13		15 : 15		16: 14	
Post-mortem interval/PMI (hour)	1.5 – 3.8	2.8 (0.70)	1.8 – 3.5	2.7 (0.7)	1.5 – 3.5	2.6 (0.6)
MMSE	26 - 30	28.5 (1.4)	21 - 30	26.7 (2.5)	0 - 28	11.9 (9.8)
Braak Stage	1 – 4	2.7 (1.0)	1 - 5	3.2 (1.1)	4 - 6	5.4 (0.7)
ApoE	3/3		3/3		3/4	

Table 1. Characteristics of human brain tissue. Samples were derived from post mortem control, Mild Cognitive Impairment (MCI) and Alzheimer's Disease (AD) cases with PMI maximum 4 hours. Mean age patients with MCI were higher compared to control or AD patients, which generate a significant difference between MCI and AD groups. There was no significant difference in sex or PMI between the groups. For ApoE genotype, the most common genotype is listed. ANOVA or Chi^2 test were used for group comparisons analysis. According to AD pathogenesis and clinic, AD patients

exhibit significantly declined cognitive performance, progressed further in the Braak staging scheme and a higher frequency of ApoE4 alleles.

2.3. Solutions

Recipe 1: Homogenization and gradient buffers for synaptosome isolation (sucrose density gradient)

Buffer solution	Final concentration
Tris acetate	50 mM
Ethylene diamine tetraacetic acid (EDTA)	1 mM
Ethylene glycol tetraacetic acid (EGTA)	1 mM
Sodium pyrophosphate dibasic ($Na_2H_2P_2O_7$)	5 mM
Sodium fluoride (NaF)	5 mM
Sodium orthovanadate (Na_3VO_4)	2 mM
4-(2-Aminoethyl)benzenesulfonyl fluoride hydrochloride (AEBSF)	1 mM
Protein Inhibitor Cocktail (PIC)	0.2% V/V
pH	7.4

Final Buffers	Preparation
Homogenization buffer	0,32 M Sucrose in buffer solution
Gradient buffer 1	1,40 M Sucrose in buffer solution
Gradient buffer 2	1,00 M Sucrose in buffer solution

Recipe 2: Homogenization buffer for whole brain isolation

	Final concentration
Dulbecco's Phosphate Buffered Saline (PBS)	10x
Sodium fluoride (NaF)	5 mM
Sodium pyrophosphate dibasic ($Na_2H_2P_2O_7$)	20 mM
4-(2-Aminoethyl)benzenesulfonyl fluoride hydrochloride (AEBSF)	1 mM
Sodium Dodecyl Sulfate (SDS)	2%

Recipe 3: RIPA lysis buffer (RadioImmunoPrecipitation Assay)

	Final concentration
Tris (hydroxymethyl) aminomethane pH 7.2	50 mM
Sodium chloride (NaCl)	150 mM
Nonidet-P-40 (NP-40)	2 %
Sodium Deoxycholate (NaDOC)	1 %
Sodium Dodecyl Sulfate (SDS)	0.2 %

Recipe 4: Running buffer for western blot

	Final concentration
MES running Buffer (20X)	50 mL
ddH2O	950 mL
Total	1000 mL

Recipe 5: Transfer buffer for western blot

	Final concentration
NuPAGE™ Transfer Buffer (20X)	50 mL
70% ethanol	285 mL
ddH2O	665 mL
Total	1000 mL

Recipe 6: Tris-buffered saline (with Tween 20) TBS (T) for washing the blot membranes and antibody solutions (first and second)

	Final concentration
Tris (hydroxymethyl) aminomethane	20 mM
NaCl	150 mM
Tween 20	0.1%

Receipe 7: Blocking buffer for western blot

	Final concentration
Tris (hydroxymethyl) aminomethane	20 mM
NaCl	150 mM
Tween 20	0.1%
Bovine serum albumin (BSA)	3%

Recipe 8: C18 spin columns activation solution

	Final concentration
LC/MS grade methanol (or ACN)	200 mL
Water for HPLC	200 mL
Total (per sample)	400 mL

Recipe 9: C18 spin columns equilibration and wash solution

	Final concentration
Trifluoroacetic acid (TFA)	0.5%
LC/MS grade acetonitrile (ACN)	5%
Water for HPLC	to 400 mL
Total (per sample)	400 mL

Recipe 10: C18 spin columns sample buffer

	Final concentration
Trifluoroacetic acid (TFA)	2%
LC/MS grade acetonitrile (ACN)	20%
Water for HPLC	adjusted to end volume
Adding	1µL for every 3µL of sample

Recipe 11: C18 spin columns elution solution

	Final concentration
LC/MS grade acetonitrile (ACN)	70%
Water for HPLC	adjusted to end volume
Total (per sample)	40 mL

2.4. Isolation of synaptosomes

Synaptosomes were prepared from fresh mouse and human brains. Approximately 200 mg tissue was used with equal amounts of gray and white matter. Tissues were then homogenized (9 volumes of buffer per tissue weight) in 0.32 M sucrose buffer (50 mM Tris-acetate, 5 mM disodium pyrophosphate, 1 mM EDTA, 1 mM EGTA, 2 mM Na3VO4, 5 mM NaF, 1 mM AEBSF, 1:500 diluted cOmplete protease inhibitor cocktail, pH 7.4). Homogenization was performed manually using 15 up and down strokes using a glass homogenizer with a Teflon pestle (0.1 to 0.15 mm clearance). Nuclei and cellular debris were removed by centrifugation at 800 g for 5 minutes at 4 °C. The collected supernatant was transferred slowly on top of a discontinuous sucrose gradient consisting of 1.0 M and 1.4 M sucrose buffer. MLS-50 swinging bucket rotor (Beckman, Krefeld, Germany) was used to perform gradient centrifugation at 54000 g for 90 minutes at 4 °C. The synaptosomal fraction was collected from the interface between 1.0 M and 1.4 M sucrose layers. The resultant fraction was diluted with 4-fold volume of HPLC-grade water and sedimented at 54000 g for 15 minutes at 4 °C. The supernatant was taken out and the synaptosomal pellet was stored at −80°C immediately.

2.5. BCA protein assay

A commercial BCA protein assay kit (colorimetric based) from Thermo Scientific Pierce™ was used to estimate the protein concentration. The assay procedure was performed as described by the manufacturer. BCA Reagent A (sodium carbonate, sodium bicarbonate, BCA and sodium tartrate in 0.1 M sodium hydroxide) and reagent B (4% cupric sulphate) are stable at room temperature (Thermo Fisher Scientific). Standard working reagent (SWR) was freshly prepared before use by adding 100

volumes of Reagent A with 2 volumes of Reagent B (ratio 50:1). The mix solution color is apple green. Following the standard assay procedure, BSA 2 mg/ml is used as a standard with 5 working standards (1–5 µg). After incubation at 37°C for 30 min, the absorbance was measured at 562 nm against a reagent blank using a microplate reader (Beckman Coulter Co.). The samples concentration was measured with reference to standards.

2.6. Protein detection by western blot

Following the determination of protein concentrations using the BCA Protein Assay kit, the pellets were resuspended in on RIPA buffer (25mM Tris, 150mM NaCl, 1% NP40, 0.5% NaDOC, 0.1% SDS, pH 7.2). 3-month-old WT mice and healthy control human samples (n=3 each) were used for brain tissue homogenates extracted in RIPA buffer. Equal amounts of protein samples (20 µg) were separated by 4-12% NuPAGE (Invitrogen) using MES buffer and transferred to the nitrocellulose membranes.

Membranes were blocked for 1 hour at room temperature (RT) in 3% BSA in TBS containing 0.01% Tween 20 (TBS-T), followed by incubation at 4°C overnight with primary antibodies in TBS-T (Table 2). After washing with TBS-T, the membranes were incubated in the appropriate dye labeled secondary antibodies (Li-Cor Biosciences) in 3% BSA on TBS-T for 1 hour. Immunolabeled proteins were imaged using Odyssey Infrared Scanner (Li-Cor Biosciences).

Target (protein)	Host	Concentration	Manufacturer
Glutamate receptor 1 (GluR1)	Rabbit	1:1000	Millipore, ab1504
Lamin B1	Mouse	1:500	Proteintech, 66095-1-Ig
NMDA receptor 2B (NMDAR2B)	Rabbit	1:1000	Millipore, ab1557p
Post-synaptic density (PSD95)	Mouse	1:2000	Thermo Fisher Scientific, MA1-064
Synaptophysin	Rabbit	1:1000	Abcam, ab52636

Tubulin	Mouse	1:2000	Thermo Fisher Scientific, 62204

Table 2. Immunoblot analysis of synaptosomal proteins. Synaptosomes and whole brain tissue homogenate of 3-month-old wild type mice and healthy control human samples were analyzed by western blot. The pre- and post-synaptic protein markers were evaluated consists of synaptophysin, NMDAR2B, GluR1 and PSD95. Lamin B1 was used as nuclear marker and alpha tubulin as a loading control.

2.7. Electron microscope

The synaptosome samples were fixed at 4 h at 4°C in modified Karnovsky's fixative (2.5% glutaraldehyde in 0.1 M cacodylate buffer + 2% paraformaldehyde +4 mM $CaCl_2$, pH 7.35). After the sample had been washed in 0.1 M cacodylate buffer for 2 h, it was post-fixed in 1% OsO_4 in cacodylate buffer containing 15 mg per mL potassium ferrocyanide for 1 h at 20°C in the dark. The post-fixed sample was then washed for 5 min to remove unreacted OsO_4, dehydrated gradually in ethanol (two changes 50% ethanol, two changes 70% ethanol, two changes 95% ethanol, four changes 100% ethanol) and embedded in Epon 812 that was left to polymerize at 60°C for 3.5 d. Finally, it was post-stained with 5% uranylacetate for 30 min and lead citrate for 7 min.

2.8. Internal standard

An internal standard was used as a quality control measure for all sixplex analyses. It was also used to identify data that do not meet quality criteria. For this purpose, Pearson correlation coefficient was done across all internal standards on both mouse and human samples. It measures the linear correlation between the samples and has a value between +1 (positive correlation) and -1 (negative correlation). Ideally the Pearson correlation value should be near to +1 on all of the internal standards comparison, which implies that the qualities of the samples are comparable. In this study, the internal standard was pooled from representative equal amounts (50 µg) of all synaptosome samples used in the experiment, aliquoted, and labeled with the iodoTMT^{TM} 126 label of the sixplex. IodoTMT^{TM} 126 was chosen as

the labeling reagent with no specific reason. Internal standard was added at the beginning of the sample work-up and treated equally as other synaptosome samples.

2.9. IodoTMT workflow for synaptosomal proteins

2.9.1. Protein labeling with iodoTMT

Synaptosome pellets were reconstituted in 1 µg $µl^{-1}$ HENS lysis buffer containing 100 mM HEPES (pH 7.8), 1 mM EDTA, 0.1 mM Neocuproine, and 1% SDS from Thermo Fisher Scientific. Equal amount of proteins (50 µg) from each synaptosome sample was individually labeled with iodoTMT sixplex labeling reagent. Followed by digestion, peptides clean up (detergent and salt), enrichment, and MS analysis. MMTS (20 mM final concentration, dissolved in dimethyl formamide) was added to prevent rearrangements of thiol-modifying groups and incubated for 30 min at room temperature with repeated vortexing (protected from light). The MMTS excess was discarded by acetone precipitation stored at -20 °C for 1 h. The pellets were dissolved in 50 µL of HENS buffer and nitrosothiol groups were reduced by 1 µl of 1 M sodium ascorbate (diluted in water). Each sample was directly labeled with 1 µL of iodoTMT labeling reagent (each 0.2 mg iotoTMT reagent was solubilized with 10 µl of LC/MS grade methanol). Allow the reaction to proceed for 1 hour at 37 °C in the dark, then quenched with 0.5 M dithiothreitol (20 mM final concentration) for 15 minutes at 37 °C to remove excess iodoTMT reagents. Six different samples (labeled with iodoTMT™ 126-131) were mixed and alkylated with 10 µl of 0.5 M iodoacetamide in 300 µl of HENS buffer incubated for 1 hour at 37 °C.

2.9.2. Tryptic digestion and peptide desalting

Alkylated samples were then precipitated with acetone precipitation. The precipitate was dissolved in 50 mM ammonium bicarbonate buffer, pH 8 for overnight digestion at 37 °C with trypsin (protein : trypsin ratio = 1:40 w/w). After digestion, the peptides were acidified using 10% trifluoroacetic acid (TFA) to a final concentration of 0.5% and desalted using C18 spin columns (Thermo Fisher Scientific). C18 spin column was prepared for peptides clean up by rinsing the spin column with 200 µl activation solution, repeated twice and followed with equilibration solution (repeated

twice). Sample was then loaded on top of the resin and flow-through was reloaded to ensure complete binding. After washing with wash solution (0.5% TFA in 5% ACN), the elution was done with 70% (v/v) acetonitrile (ACN), dried and dissolved in 100 µL TBS buffer, pH 8.0 (50 mM Tris, 150 M NaCl).

2.9.3. Enrichment of iodoTMT-labeled peptides

For peptide enrichment, the samples were incubated with 30 µl immobilized Anti-TMT™ Resin at room temperature for 2.5 hours with gentle end-over-end rotation. The resin was washed using 100 µl TBS (three times) then subsequently with 100 µl HPLC-grade water (three times). The peptides that bound to the resin were eluted twice with 30 µl TMT elution buffer (Thermo Fisher Scientific). The pooled eluates were dried using vacuum centrifugation and resuspended in 8 µl of 0.1% TFA for nanoHPLC MS/MS analysis.

2.9.4. LC-Mass spectrometry analysis

The solution was injected onto a C18 trap column (100 µm inner diameter, 20 mm length, ReproSil-Pur 120 C18-AQ, Dr. Maisch, Ammerbuch, Germany) packed in-house. Solvent A was 0.1% formic acid (FA), solvent B was 90% ACN, 0.1% FA. The peptides were eluted from trap column onto a C18 analytical column (75 µm inner diameter, 200 mm length, ReproSil-Pur 120 C18-AQ, 1,9 µm, Dr. Maisch, Ammerbuch, Germany). Peptides were separated during a linear gradient from 4% to 35% solvent B within 240 min at a flow rate of 300 nl/min. The nanoHPLC was coupled online to an LTQ Orbitrap Velos mass spectrometer (Thermo Fisher Scientific, Bremen, Germany). Ions between 330 and 1700 m/z were scanned in the Orbitrap detector with a resolution of 30,000 (maximum fill time 400 ms, AGC target 106). The twenty most intense precursor ions with threshold intensity of 5000 were subjected to higher energy collision induced dissociation (HCD). Fragment ions were then analyzed in the Orbitrap. Fragmented peptide ions were omitted from repeated analysis for a period of 15 s.

2.10. Data analysis and protein identification

Data processing and analyses were performed using Proteome Discoverer™ software 2.1.0.81 from Thermo Fisher Scientific. Peptide identification was identified with in-house Mascot server, version 2.5.1 (Matrix Science Ltd, London, UK). MS/MS data (inclusive a-series ions) were matched against mouse / human sequences from SwissProt (release 2015_04). Up to two missed cleavages were allowed for tryptic peptides. Low scoring spectrum matches were re-analyzed with semi tryptic specificity with one missed cleavage. Carbamidomethylation (Cys), acetylation (protein N-terminus), Oxidation (Met), and iodoTMT™ sixplex (on Cys) were included as dynamic modifications. Mascot results from searches against SwissProt were evaluated using percolator algorithm (version 2.05) as implemented in Proteome Discoverer. A posterior error probability of 1% or better was used to identify the resulting peptides. Precursor ion m/z tolerance of 10 ppm and a fragment ion tolerance of 20 mmu were allowed. Due to the experimental design, proteins were reported with at least one matching peptide: In cases that only one site is nitrosylated in a protein, only one labeled peptide can be identified after enrichment.

The biological replicates are combined into one table, which consists of all peptides in the rows and all the groups/conditions of replicates in the columns. The table is filled with intensities. Before applying the statistics, the table is filtered by excluding the peptides that occur only in one or two replicates. The intensities were then log2 transformed, median normalized and compared pairwise between replicates from which the Pearson correlation coefficient is computed for the internal standard (iodoTMT™ 126 labeled). The pooled sample of internal standard was excluded when the Pearson's data was below 0.5 (Hinkle et al., 2003; Mukaka, 2012). After the exclusion, pairwise tests on mice data were performed where each group was compared across age (3-month vs 12-month-old) and genotype. Whilst on human results, pairwise tests were performed where MCI and AD were compared to control patient. To minimize false positive results, the peptides identified in less than 50% of the total biological replicates were omitted (Blonder and Veenstra, 2007; Kuster et al., 2005; Mallick et al., 2007).

The statistical methods used in this study were the combination of Limma, Rank Product and bootstrap analysis. After peptide exclusion, normalized TMT tag reporter

ion intensities were used to calculate fold change using linear model-based (limma) and ranks (RankProd) (Schwammle et al., 2013). Raw intensities were transformed to log2 (fold change) values. P-values were calculated for each peptide and adjusted for multiple testing using Benjamini and Hochberg approach to control false discovery rates. To evaluate if the initial fold change is representative of the population, bootstrap analysis was calculated (Mukherjee et al., 2003b; Wang et al., 2012; Zhang et al., 2016b). Data table (consist of eight conditions for mouse and three for human study) was created with randomly chosen replicates. The bootstrap or random principle is drawing with replacement to generate the null hypothesis to which the actual data were compared (Barbash and Sakmar, 2017). Thus the same replicate can occur more than once in the data table with the same or different conditions. Bootstrapping with 10000 repetitions was used to calculate the confidence interval (CI). The 95% confidence interval of all the 10000 log2 fold changes was calculated for each peptide. The initial calculated log2 fold change was further analyzed to see if the peptide lies within this CI or not. This represents if the initial fold change is a good representation of the population (stated “yes” on the table) or not (“no”).

The criteria for inclusion of a peptide in the mouse groups was the same as that used for human: a protein/peptide was considered significant at a fold-change of more than 1.2-fold (log2 $\pm$ 0.263) and $p < 0.05$ level using adjusted p-values (q-value_limma and/or q-value_RP) or it lays on 95% confidence interval (CI) of bootstrap analysis. Proteins were reported even with one unique peptide due to the experimental design using peptides enrichment. Volcano plots were used to visualize the data; log2 fold change of each SNO-Cys protein was plotted against –log2 adjusted p-value. Increased and decreased SNO proteins were identified in mouse and human synaptosomal samples, which defined as positive and negative fold change ratios in the pairwise group comparison. The identified proteins were annotated using Uniprot/SwissProt database (Bateman et al., 2015) then classified using Panther Gene Ontology (GO) (Thomas et al., 2003) and Gorilla search engine (Eden et al., 2009).

3. Results

3.1. Synaptosome isolations analysis

Various techniques of synaptosome isolation have been established using different centrifugation and buffer reagents, such as sucrose, Ficoll/sucrose or Percoll density gradient centrifugation, all of which result in purifying a crude synaptosome fraction from the contamination (Jaffrey and Snyder, 2001). This study used conventional sucrose density gradient to isolate synaptosomal proteins from mouse and human brain tissues. The yield of the proteins obtained from the purified synaptosomes using sucrose density gradient were scarce but it was comparable between mouse and human samples (3.0 ± 1.0 µg/mg and 2.8 ± 0.8 µg/mg of brain tissue, respectively).

The purity of synaptosome isolations was further confirmed by electron microscopy (Figure 5) and western blot analyses of 3-month-old WT and healthy control human samples using antibodies specific for synaptic and nuclear markers (Figure 6).

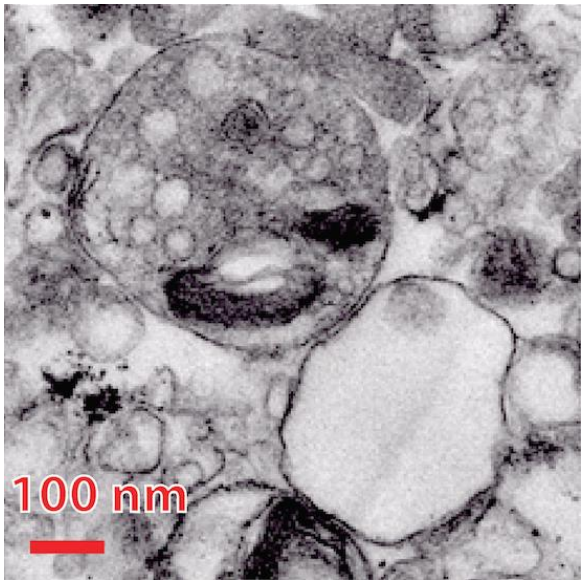

Figure 5. Exemplary image of a synaptosome fraction showing presynaptic terminal including synaptic vesicle and mitochondria, along with postsynaptic membrane. The picture was taken by transmission electron microscopy using a chemical fixation (Sosinsky et al., 2008). Sample taken from the synaptosome isolation of a 3-month-old wild type mouse.

Enrichment of pre- and post-synaptic proteins was determined using western blotting against synaptophysin, NMDAR2B, GluR1 and PSD95 markers in the synaptosomal fraction compared to brain tissue homogenates. In contrast, level of the nuclear marker Lamin B1 was decreased in the synaptosomal fraction. Alpha tubulin was used as loading control.

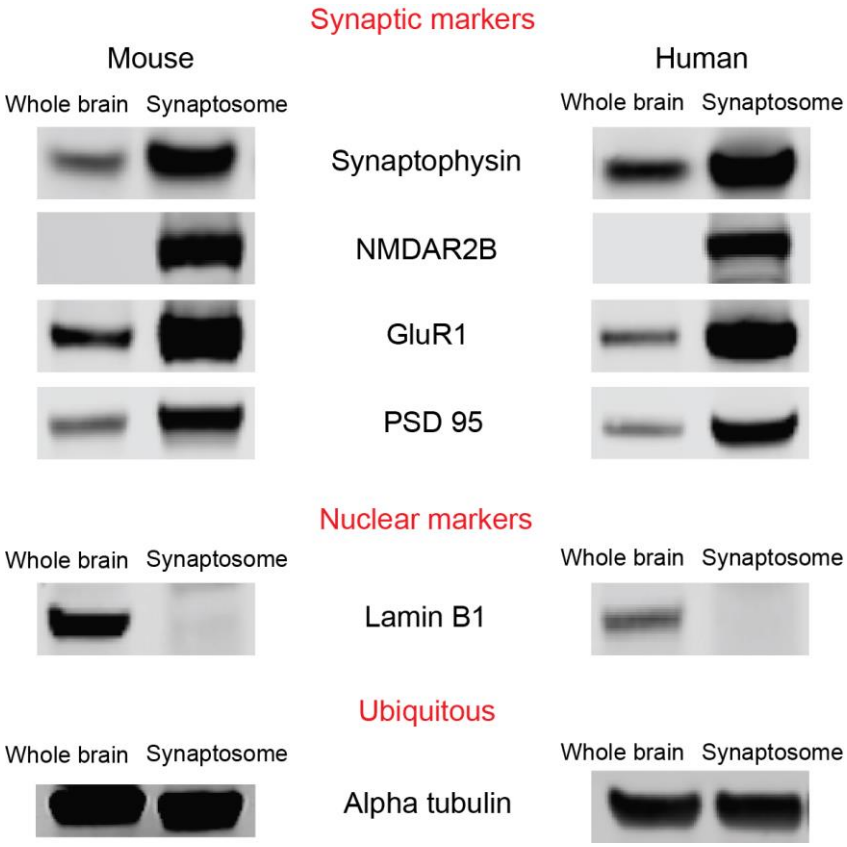

Figure 6. Representative immunoblot analysis of synaptosomal proteins isolated from 3-month-old wild type mouse and healthy control human samples. Compared to the whole brain tissue homogenate, the synaptosomal fraction contained higher levels of synaptophysin (~38 kDa), NMDAR2B (~166 kDa), GluR1 (~100 kDa) and PSD95 (~95 kDa) relative to 20 µg brain tissue homogenates. While the whole brain tissue homogenate showed higher expression of the nuclear marker lamin B1 (~66 kDa). Alpha tubulin was used as a loading control. Equal amounts of protein from whole brain tissue homogenates and synaptosomal fractions were loaded in electrophoresis gels.

3.2. Proteome analysis of synaptosomal proteins

The composition of the SNO-proteome was analyzed using Gene Ontology enRIchment analysis and visuaLiAtion (Gorilla) search engine (Eden et al., 2009) and Uniprot/SwissProt based on the localization classification (Bateman et al., 2015). The Gorilla search engine result (illustrated in Figure 7) indicates enriched GO terms in the cellular components of organelle membrane (GO:0031090), oxidoreductase complex (GO:1990204), cytoplasmic part (GO:0044444), organelle inner membrane (GO:0019866), intracellular organelle (GO:0043229), intracellular membrane bounded organelle (GO:0043231) and components of mitochondrial (GO:0044429; GO:0005739; GO:0031966; GO:0044455; GO:0005743). Definitions of the specific components are available from the Gene Ontology Consortium (http://www.geneontology.org/) database. This result revealed the enrichment of synaptosome components such as cytoplasmic part, cell membrane and mitochondria that are enriched in the presynaptic terminal (Swomley et al., 2014).

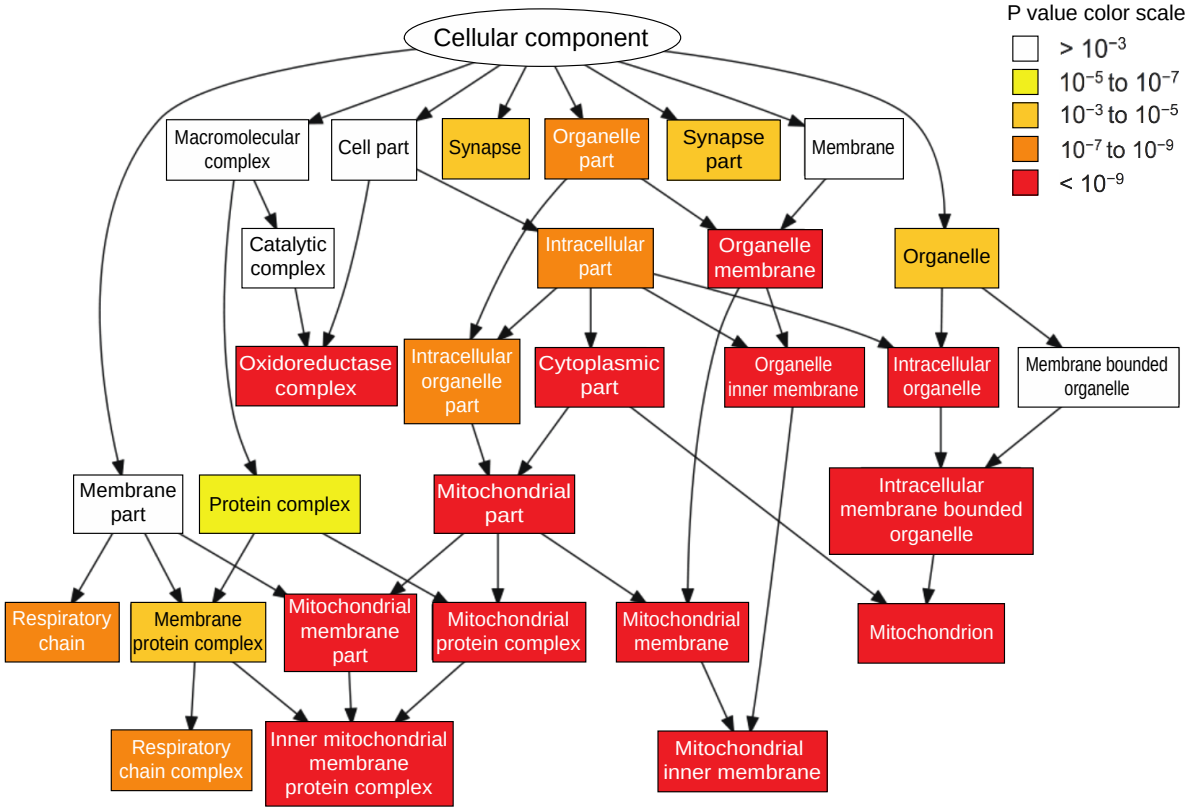

Figure 7. Classification of identified synaptosomal proteins based on cellular localization (Wijasa et al., 2017). Reproduced from “Proteome profiling of s-nitrosylated synaptosomal proteins by isobaric mass tags”, by T. S. Wijasa et al., 2017, Journal of Neuroscience Methods, 291, p. 95-100. Copyright 2017 by Elsevier B. V.

3.3. Method establishment

Proper sample preparation for MS-based analysis is an important step in proteomic workflow, which can influence MS results directly (Gundry et al., 2009). In the initial testing (Table 3), the focus was on three alternative approaches for SNO-quantitation: the widespread used BST, 2D-DIGE with a modified labeling procedure (NitroDIGE) and SNO isobaric mass tags labeling (iodoTMT^{TM}). In the first round of method adaptation, the degree of biotinylation (representing *S*-nitrosylation) in the BST was determined by anti-biotin immunoblotting, streptavidin pull-down followed by immunoblotting and MS based identification of biotinylated peptides. Although BST is frequently used, this method has a relatively low-throughput and the biotinylated peptides hinder the localization of the SNO-Cys modification sites (Qu *et al.*, 2014a). Approximately 4193 unique peptides were identified representing 509 proteins of which approx. 6% were biotinylated on cysteines after the enrichment step. Additionally, when applying the BST approach for SNO labeling, the quantitation still has to be done with additional labels or label-free. The NitroDIGE approach enables multi-group analysis of protein S-nitrosylation and differentiates changes of modified proteins under various conditions. No difference was found between the 2D-DIGE spots of unlabeled synaptosome sample compared to the CyDye^{TM}-labeled synaptosome sample (quantified by SameSpots). Low endogenous S-nitrosylation proteins may be one of the reasons for this unsuccessful transfer method. Among these, labeling with isobaric mass tags (iodoTMT^{TM} sixplex Thermo Fisher Scientific™, USA) provided the most promising results, both in mice and human brain samples. This protocol has the advantage of using one label for enrichment, identification, and multiplex quantitation of modified proteins/peptides. It enables the identification of endogenous SNO-proteins/pepties without NO donor for nitrosylation. The enriched and identified proteins/peptides were in line with previous reports on synaptosomal proteomics.

Methods	Principles	Advantages (+), drawbacks (-), performance on synaptosome sample
1D electrophoresis (1DE) and immunodetection [rieder]	SNO proteins determined by an anti *S*-nitrosocysteine antibody, with the rationale to identify bands containing SNO proteins for following mass spec-based analysis	+ Straightforward approach + Enrichment possible when combined with Anti-SNO-IP – Poor resolution of proteins – No stable labeling of the SNO site
2D electrophoresis (IP-2DE) and immunodetection [rieder]	anti *S*-nitrosocysteine antibody used to immunoprecipate SNO proteins followed by 2D electrophoresis	+ Resolution improved by 2D-separation of proteins + Enrichment possible when combined with Anti-SNO-IP – No stable labeling of the SNO site • <10 spots detected with up to 150 µg of starting material
NitroDIGE [Qu nitrodige]	Modified biotin switch technique (BST) using fluorescence-tagged CyDye™ thiol reactive agents (labeling of SNO-Cys with CyDye™) in combination with 2D DIGE.	+ Low amount of starting material required (50 µg) + Quantitative label on SNO site + Multiplex (2-plex) – Protein resolution improved over other gel based approaches, but lower compared to MS based techniques + Unsuccessful method transfer: No difference between 2DE spots of unlabeled compared to CyDye™-labeled synaptosome sample (quantified by SameSpots). Low endogenous S-nitrosylation proteins may be one of the reason.
Biotin switch technique (BST) with enrichment [jaffrey]	Blocking of free thiols (by MMTS), reduction of *S*-nitrosothiols (by ascorbate), biotin-labeling of previous SNO site. Enrichment of peptides by biotin affinity purification.	+ Enrichment of SNO proteins + Stable labeling of SNO site + Frequently used method with large number of references – After labeling of SNO site, quantitation has to be done with additional labels or label-free

IodoTMT^{TM} switch labeling (iodoTMT^{TM} sixplex)	Same principle as BST, with four major steps: 1st, free thiols blocking (MMTS), 2nd, reduction of *S*-nitrosothiols (ascorbate), 3rd, iodoTMT labeling 4th, affinity enrichment using anti-TMT^{TM} resin	• Low amount of starting material was sufficient (50 µg) • Quantitative label on SNO site • Multiplex (ICAT: 2-plex; IodoTMT^{TM}: 6-plex) • Successful adaption with minimal amount of optimization • High yield and enrichment of SNO peptides

Table 3. Proteomic methods for SNO protein quantification. Various quantitative methods have been developed, which classified into two categories, gel-based and gel-free MS-based proteomics. This table provides an overview of the different methods tested in this study for their applicability on synaptosome samples.

3.4. Proteome comparisons of synaptosomal proteins

Subcellular localization generated from Uniprot/SwissProt displayed comparable enrichments of common synaptosome components between the unlabeled synaptosome (Figure 8A), the IodoTMT labeled SNO synaptosome (Figure 8B) and published results by Engman et al. (Engmann et al., 2010) on regular peptide N-terminal TMT labeling of synaptosome (Figure 8C). Results in figure 8A and 8B were both acquired from the synaptosome isolation protocol on Heneka's laboratory (chapter 2.3) (Wijasa et al., 2017). The SNO-proteome of synaptosome (iodoTMT-labeled) contained 30% mitochondrial proteins (Fig. 8B). Furthermore, high fractions of cytoplasmic (25%), cell membrane (20%) and synapse-associated proteins (6–8%) were found, which is in alignment with the expected composition of synaptosomes (see discussion). The localization of the identified synaptosomal proteins/peptides between unlabeled, and labeled synaptosome (iodoTMT or TMT) displays similar enrichment results with a majority of cytoplasm 24–28%, mitochondria 24–34%, cell membrane 14–22%, and synapse 6–11%. Small amount of endoplasmic reticulum and nuclear associated proteins were also found, due to similar density as synaptosomes.

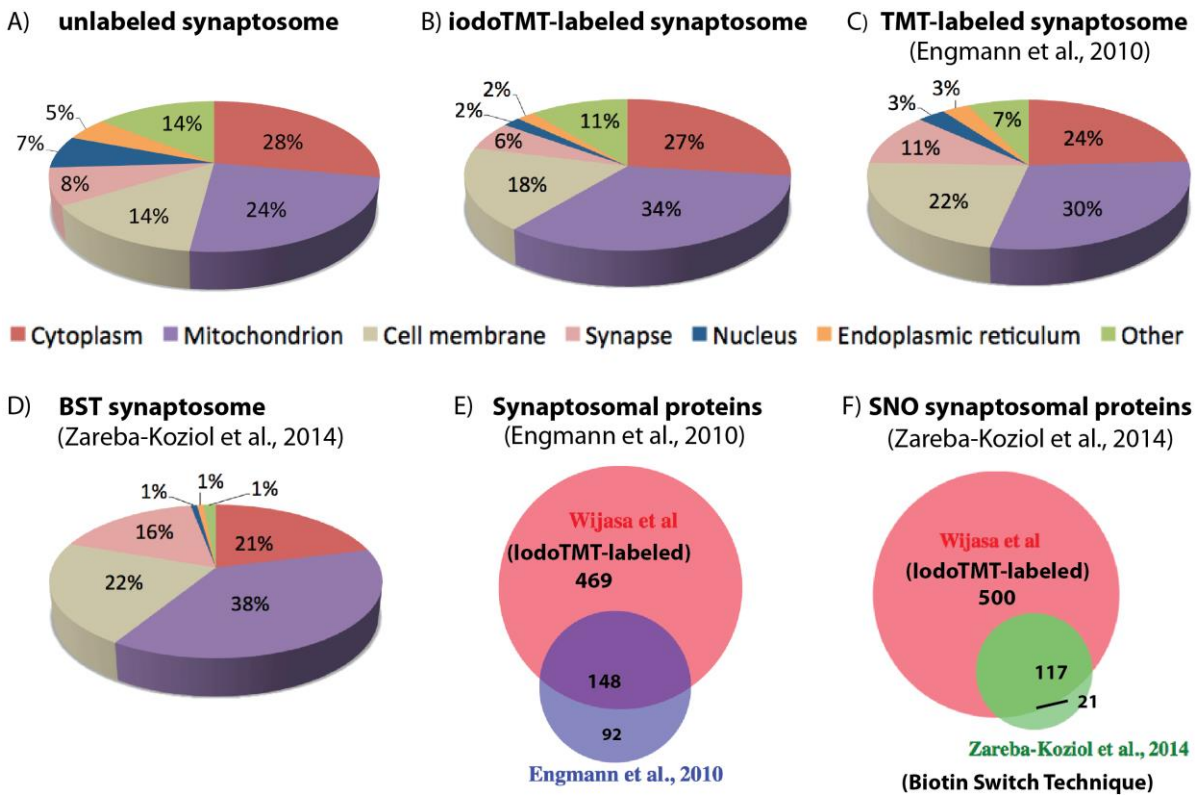

Figure 8. Cellular localization of mouse synaptosome (Wijasa et al., 2017). Reproduced from "Proteome profiling of s-nitrosylated synaptosomal proteins by isobaric mass tags", by T. S. Wijasa et al., 2017, Journal of Neuroscience Methods, 291, p. 95-100. Copyright 2017 by Elsevier B. V.

The subcellular localization analyzed from different variants of synaptosome preparation and labeling combinations was compared. In the murine synaptosome samples, the results using iodoTMT protocol are comparable or higher than those described in published publications on synaptosome samples. As example: BST analysis on SNOSID (SNO side identification) identified 138 SNO proteins (Zareba-Koziol et al., 2014) of which 85% were found overlapping with this study's results (Figure 8F) and 240 proteins were identified using TMT (Tandem Mass Tag) (Figure 8E) both on synaptosome samples. The composition of the detected proteome was consistent with prior publications on the synaptosome proteome, which were labeled with TMT-independent of their modifications (Figure 8C) (Engmann et al., 2010) and with BST on SNOSID (Figure 8D) (Zareba-Koziol et al., 2014). The SNO-proteome of synaptosome contained more than 30% mitochondrial proteins in all labeling

procedures (iodoTMT-labeled, TMT-labeled and Biotin Switch Technique; Figure 8B-D), presumably derived from the large numbers of mitochondria located in synapses.

3.5. IodoTMT and mass spectrometry (MS)-based method performance

The MS-based method using iodoTMT labeling and enrichment was first tested using wild type mouse samples (n = 3) and further extended to human brain samples (n = 2) from donors without CNS disorders. This is done to confirm that the entire procedure performs well in animal and human brain samples. To ensure the consistency and reliability of the analyzed data sets, a comprehensive internal quality control procedure has been implemented. Which is done by analyzing the intensity of reporter ions and calculating the inter-sample variances from the internal standard. The internal standard consisted of all samples used in the experiment; it was pooled, labeled and measured in all runs with iodoTMT126 label reagent. A representative MS/MS spectrum is depicted in Figure 9 showing intense reporter ions and a clear b- and y-series of selected fragment ions.

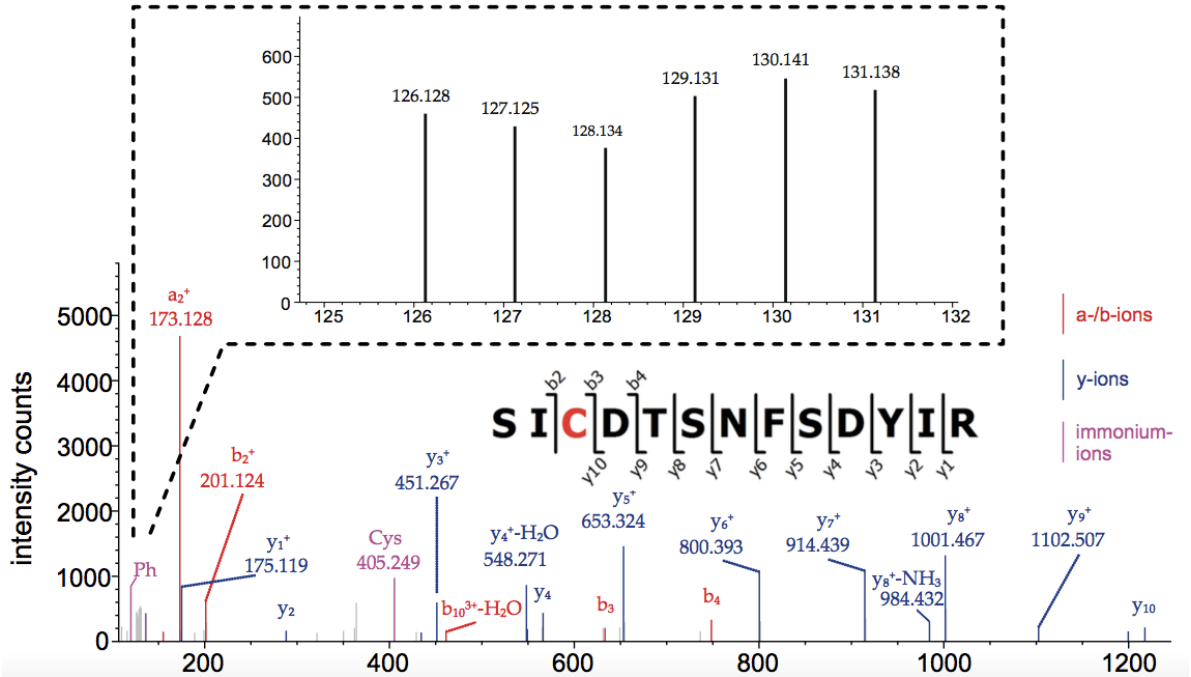

Figure 9. A representative MS/MS spectrum of the iodoTMT-labeled peptide SICDTSNFSDYIR derived from ubiquitin-like modifier-activating enzyme 1, which shows intense reporter ions and b- and y-series of selected fragment ions (Wijasa et

al., 2017). The 6 reporter ion peaks are shown in the enlarged section of the lower mass range. Reproduced from “Proteome profiling of s-nitrosylated synaptosomal proteins by isobaric mass tags”, by T. S. Wijasa et al., 2017, Journal of Neuroscience Methods, 291, p. 95-100. Copyright 2017 by Elsevier B. V.

To analyze the overall method variance including preparative pipetting, sample preparation, digestion, IodoTMT™ labeling, IodoTMT™ enrichment until pooling and analysis of the samples, reporter ion intensities of all identified peptides were compared over all 6 labels (in the same-same-experiment). The average variance between single reporter ion channels and the mean of all channels was 20%. Theoretically, all identified peptides should be linked to a TMT™ label on a previously nitrosylated cysteine. In this study, around 72% of identified peptides contained at least one cysteine, of which 93%-98% were IodoTMT™ labeled. In conclusion, the cysteine-targeted labeling was highly specific, whereas the anti-TMT-antibody-based enrichment and purification approach left around 28% of unlabeled peptides. Unspecific TMT-labeling (<1% of peptides) on the peptide N-terminus (the target of TMT™ protocol) was hardly found. Essentially, the identification of nitrosylated peptides from synaptosome samples was not possible without prior labeling or an enrichment approach.

3.6. Peptides exclusion

For MS quality control, Pearson correlation coefficient was done across all internal standards (iodoTMT™ 126 labeled) on both mouse and human samples. Samples were excluded from further analysis if the Pearson correlation score was below 0.5 or moderate correlation (Figure 10) (Hinkle et al., 2003; Mukaka, 2012). After the exclusion, the study ended up with 60% of the mice samples (n = 12/group from n = 20/group) and 67% of the human samples (n = 20/group from n = 30/group), which were then used for further analysis.

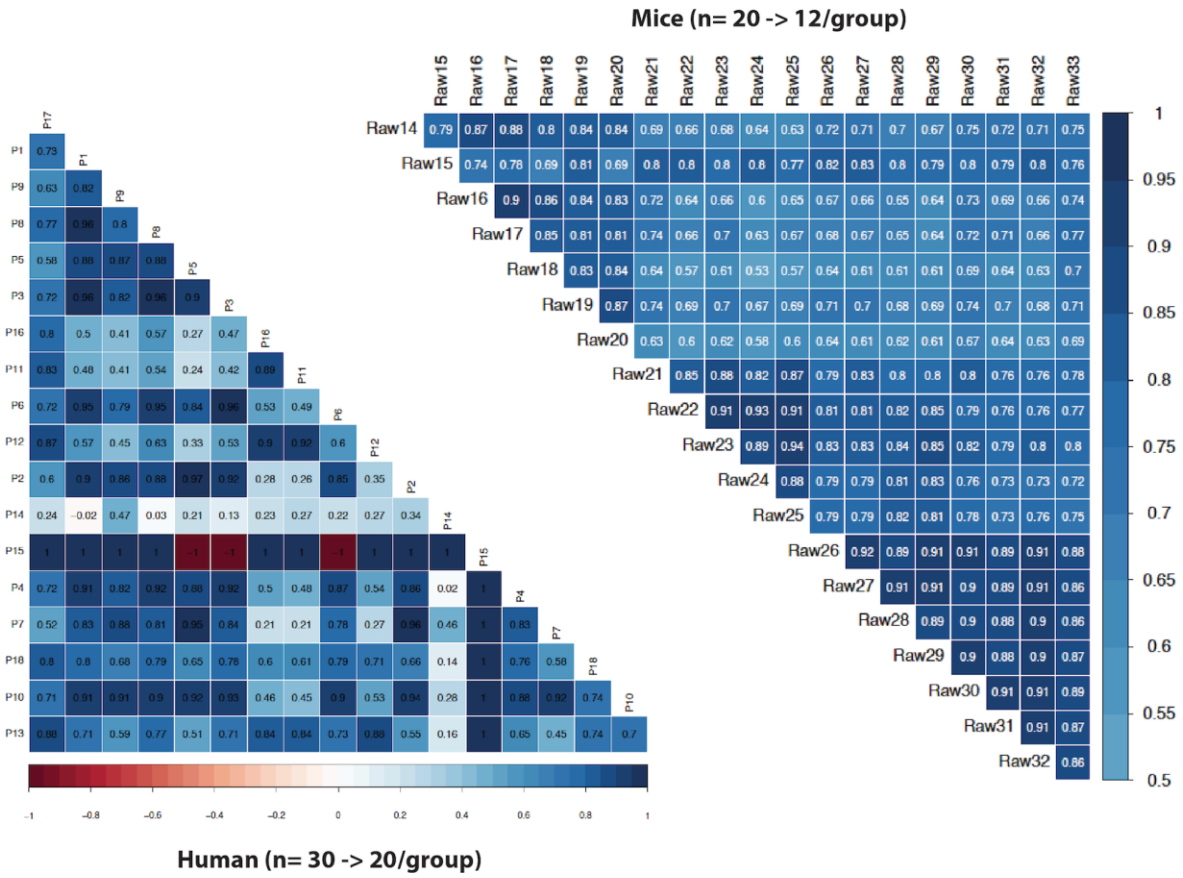

Figure 10. Pearson correlation coefficient for MS quality control. Pearson correlation coefficient was done for all internal standards which labeled with iodoTMT^{TM} 126 on both mouse and human samples. The peptides were excluded from further analysis if Pearson correlation score was below 0.5. The study end up with n=12 mice/group and n=20 human/group after exclusion.

3.7. Statistical analysis of quantitative proteomics data

Increased and decreased SNO proteins/peptides were identified in mouse and human synaptosomal samples. The fold-change threshold was set to 1.2-fold and above based on the value frequently used in data analysis of iodoTMT (Chang et al., 2016; Wojdyla et al., 2016; Yao et al., 2015). The total number of identified synapto-SNO peptides or proteins based on pairwise groups comparison are shown in table 4, 5 and 6. Statistical analysis and magnitude of the response (fold change) were adopted to select meaningful proteins from total identified proteins. The fold change values in human samples were not as high as in mouse samples. Generally, the total numbers of increased SNO proteins/peptides in pairwise group comparisons were higher using bootstrap analysis compared to Limma and RankProduct.

Age effect	WT 12m vs 3m		NOS2-/- 12m vs 3m		APP/PS1 12m vs 3m		APP/PS1/NOS2-/- 12m vs 3m	
	Increased	Decreased	Increased	Decreased	Increased	Decreased	Increased	Decreased
Total peptides	423	401	411	377	406	373	367	425
Total proteins	251	231	243	234	244	220	231	263
Total peptides (n > 50%)	372	363	369	328	363	341	326	373
Total proteins (n > 50%)	222	213	222	209	220	209	207	237
Total peptides (n>50%)[#], fold change ≥ 1.2 fold	176	150	75	30	130	142	68	51
Total proteins (n>50%)[#], fold change ≥ 1.2 fold	101	87	53	22	87	78	58	45
Significant proteins (Limma and RankProduct Vs. Bootstrap)	68 / 94	67 / 61	3 / 53	5 / 20	18 / 87	25 / 78	0 / 58	1 / 44

Table 4. Overview of synapto-SNO peptides at pairwise comparison of mice across age (12-month vs 3-month-old mice). The reproducibility among replicates was set to > 50% to minimize false positive results. Hash sign ([#]) represents significant peptides/proteins with fold change ≥ 1.2 fold (log2 ± 0.263) and adjusted p-value < 0.05 (Limma or RankProduct) (Schwammle et al., 2013) or it lays on 95% Confidence Interval of bootstrap analysis) (Efron and Tibshirani, 1993).

12-month-old mice (Genotype effect)	APP/PS1 - WT		APP/PS1 – APP/PS1/NOS2-/-		WT – NOS2-/-	
	Increased	Decreased	Increased	Decreased	Increased	Decreased
Total peptides	373	429	425	391	433	419
Total proteins	252	271	263	252	258	259
Total peptides (n > 50%)	320	374	370	344	376	365
Total proteins (n > 50%)	224	241	236	231	225	235
Total peptides (n>50%)[#], fold change ≥ 1.2 fold	53	35	49	49	21	89

Total proteins (n>50%)[#], fold change ≥ 1.2 fold	51	34	45	41	20	70
Significant proteins (Limma and RankProduct Vs. Bootstrap)	1 / 51	0 / 34	0 / 45	0 / 41	1 / 20	1 / 70

Table 5. Overview of synapto-SNO peptides at pairwise comparison of 12-month-old mice across genotype. The reproducibility among replicates was set to > 50% to minimize false positive results. Asterisks ([#]) represents significant peptides/proteins with fold change ≥ 1.2 fold (log2 ± 0.263) and adjusted p-value < 0.05 (Limma or RankProduct) (Schwammle et al., 2013) or it lays on 95% Confidence Interval of bootstrap analysis) (Efron and Tibshirani, 1993).

	MCI - Control		**AD – MCI**		**AD - Control**	
	Increased	**Decreased**	**Increased**	**Decreased**	**Increased**	**Decreased**
Total peptides	430	439	462	451	446	423
Total proteins	313	324	330	318	314	298
Total peptides (n > 50%)	203	165	189	188	220	170
Total proteins (n > 50%)	163	126	145	146	166	130
Total peptides (n>50%)[#], fold change ≥ 1.2 fold	1	1	20	10	9	2
Total proteins (n>50%)[#], fold change ≥ 1.2 fold	1	1	16	9	9	2
Significant proteins (Limma and RankProduct Vs. Bootstrap)	0 / 1	0 / 1	2 / 15	4 / 9	0 / 9	0 / 2

Table 6. Overview of synapto-SNO peptides at pairwise comparison of human samples during disease development. The reproducibility among replicates was set to > 50% to minimize false positive results. Hash sign ([#]) represents significant peptides/proteins with fold change ≥ 1.2 fold (log2 ± 0.263) and adjusted p-value < 0.05 (Limma or RankProduct) (Schwammle et al., 2013) or it lays on 95% Confidence Interval of bootstrap analysis) (Efron and Tibshirani, 1993).

3.8. Synapto-SNO proteins analyses

Around 2252 unique peptides were identified in murine synaptosomes representing 1064 proteins, of which 33% were identified nitrosylated for the first time. While in human synaptosomes, 2134 unique peptides were identified representing 1097 proteins, of which 69% were identified nitrosylated for the first time (compared to the SNO database). Whilst the known published data on the SNO database lists 2651 peptides (represent 1348 proteins) on murine and 1250 peptides (represent 717 proteins) on human S-nitrosylated proteome (Lee et al., 2012b)

Since neuroinflammation is thought to represent one of the important factors for AD pathogenesis, NOS2 gene was hypothesized to play an important role. The aim was to identify the NOS2-dependent SNO proteins in AD and related mouse models. In mouse data, multiple group-wise comparisons were performed to determine the effect of aging on each genotype group (12-month old compared to young 3-month-old mice throughout all genotypes) and the effect of the genotype on 12-month-old mice. In human data, multiple group-wise comparisons were performed by comparing the AD disease progression (control to MCI, MCI to AD and control to AD). There is no overlap between up- and down-regulated peptides in all multiple group-wise comparisons on mouse and human data. Among the spectrum of regulated proteins, only those with an increase of nitrosylation might be correlated to inflammation-associated activation of NOS2 (see discussion), which were defined by having a positive FC ≥ +1.2-fold.

3.8.1. Age and genotype effects on S-nitrosylation of synaptic proteins in mouse brain.

To globally visualize the data, log2 fold change of each SNO-Cys protein was plotted against –log2 adjusted p-value in a volcano plot. The volcano plots in figure 11 show synapto-SNO proteins with replicate numbers > 50%, which were altered due to the age effect of each genotype. To identify protein levels changes that related to physiological aging, wild type 12-month-old mice were compared to 3-month-old mice (Figure 11A). After assigning the statistical analysis and setting the magnitude of the response to 1.2-fold or higher (log2 ± 0.263) for candidate proteins, a total of 101 SNO proteins were found to be significantly increased ($P < 0.05$ or it lays on 95% CI

of bootstrap analysis and with FC ≥ 1.2-fold) and 87 SNO proteins decreased. Similarly, the comparison of old and young APP/PS1 mice was performed to investigate pathological aging (Figure 11C). This yielded 87 increased SNO proteins and 78 SNO proteins that were decreased. In order to know which of these SNO proteins were differentially regulated during aging in a NOS2-dependent manner, the same analysis was repeated to compare the synapto-SNO proteome between old and young mice of NOS2-/- and APP/PS1/NOS2-/- background (Figure 11B, D). The age comparison of NOS2-/- mice, yielded 53 SNO proteins that were increased significantly and 22 SNO proteins that were decreased. While in the APP/PS1/NOS2-/- mice, 58 SNO proteins were significantly increased and 45 SNO proteins were decreased.

The candidate proteins were shown in different colors. The red points indicate significant proteins with p-value < 0.05 (Limma or RankProduct) (Schwammle et al., 2013), within 95% Confidence Interval of bootstrap analysis (Efron and Tibshirani, 1993) and have a fold change of ≥ 1.2 fold (log2 ± 0.263). The green points specify significant proteins calculated using the p-value from Limma and RankProduct and have a fold change of ≥ 1.2 fold. The blue points show proteins within 95% Confidence Interval of bootstrap analysis and have a fold change of ≥ 1.2 fold (log2 ± 0.263). While the gray points indicate proteins without any differences (p-value > 0.05, not within 95% Confidence Interval of bootstrap analysis and have a fold change of < 1.2 fold). Candidate proteins were chosen from red, green and blue points.

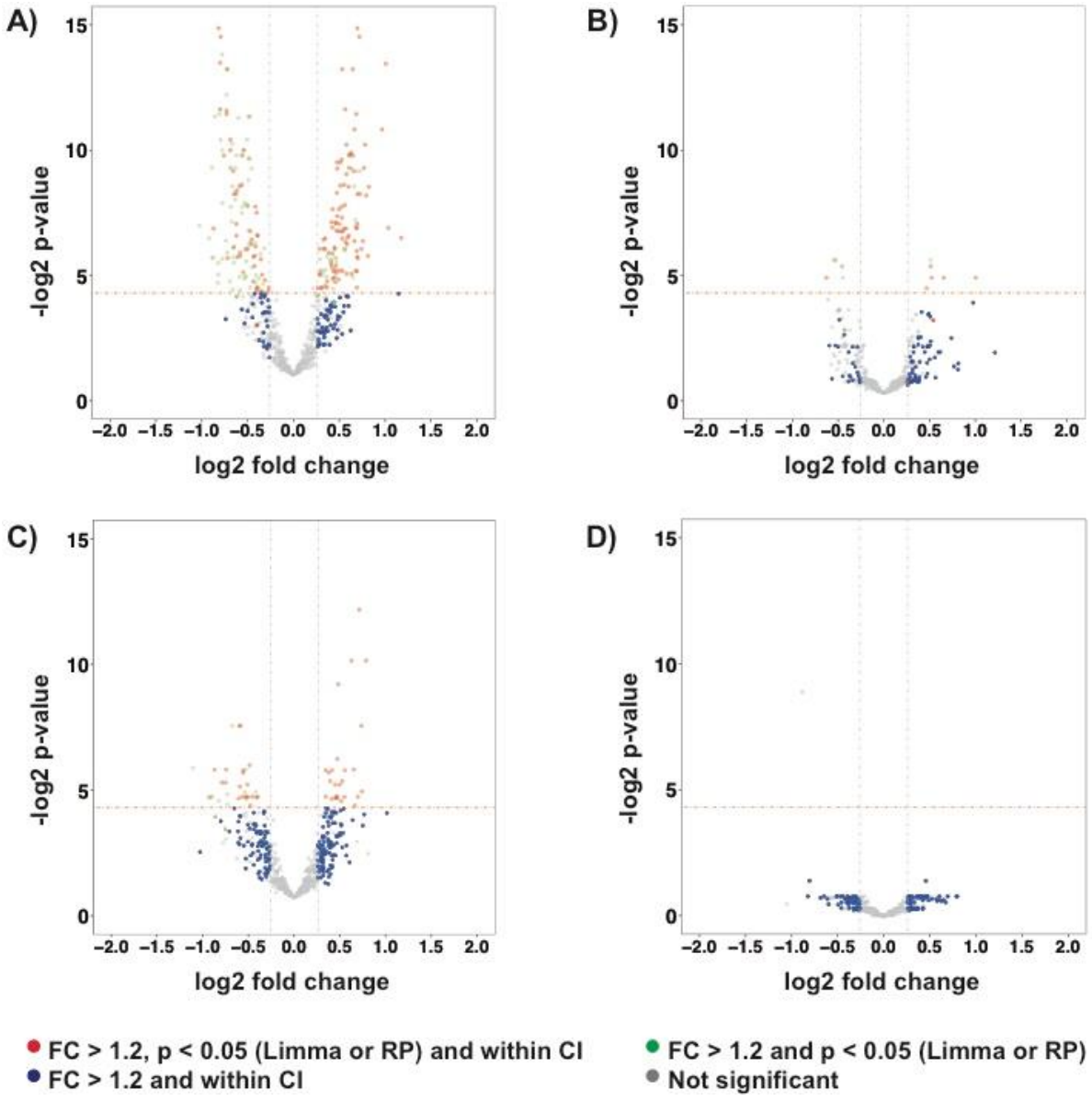

Figure 11. Volcano plot of synaptosome proteome displaying age effect on protein levels for each genotype. Negative log2 p-values (adjusted) were plotted against log2 protein fold change. Increased protein levels were shown on the positive x-axis, and decreased levels were shown on the negative x-axis. The red points show candidates with p-value < 0.05 (Limma or RankProduct) (Schwammle et al., 2013), within 95% Confidence Interval of bootstrap analysis (Efron and Tibshirani, 1993) and have a fold change of ≥ 1.2 fold (log2 ± 0.263). The green points show candidates with p-value < 0.05, not within 95% confidence interval of bootstrap analysis and have a fold change of ≥ 1.2 fold (log2 ± 0.263). The blue points show candidates with p-value > 0.05, within 95% confidence interval of bootstrap analysis and have a fold change of ≥ 1.2 fold (log2 ± 0.263). The gray points show candidates with p-value > 0.05, not within

95% confidence interval of bootstrap analysis and have a fold change of < 1.2 fold (log2 ± 0.263). The experimental groups were 3-month and 12-month-old wild type (WT), NOS2-/- (NOS2 knockout mice), APP/PS1 (transgenic mice carrying the human APP and presenilin1 gene) and APP/PS1/NOS2-/- (transgenic mice carrying the human APP, presenilin1 gene and are NOS2 knockout mice). (A) Aged WT with replicates > 50%. (B) Aged NOS2-/- with replicates > 50%. (C) Aged APP/PS1 with replicates > 50%. (D) Aged APP/PS1/NOS2-/- with replicates > 50%.

To identify the effect of NOS2 gene deletion on WT control and APP/PS1 of 12-month-old mice (genotype effect), three pairwise group comparisons were made. Figure 12 shows the volcano plots of S-nitrosylation on synaptosomal proteins with replicate numbers > 50%, which were altered due to the genotype effect of 12-month-old mice. The statistical analysis and magnitude of the response (1.2-fold or higher; log2 ± 0.263) were assigned for significant proteins. 20 SNO proteins were found elevated in WT compared to NOS2-/- samples, 45 SNO proteins on APP/PS1 compared to APP/PS1/NOS2-/- samples and 51 SNO proteins on APP/PS1 compared to WT samples. Aligned with 70 SNO proteins that were significantly decreased in WT compared to NOS2-/- samples, 41 SNO proteins on APP/PS1 compared to APP/PS1/NOS2-/- samples, 34 SNO proteins on APP/PS1 compared to WT samples.

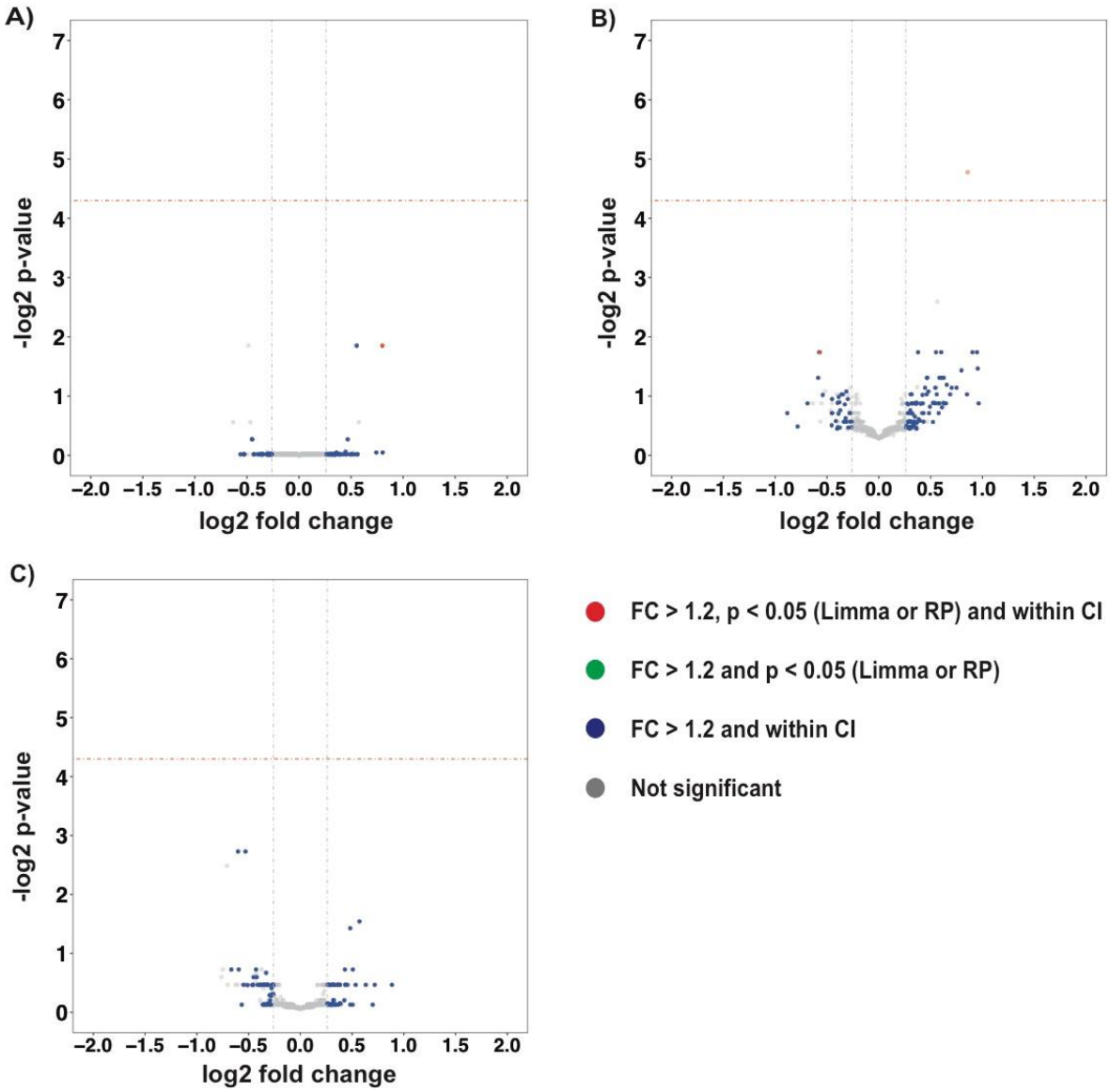

Figure 12. Volcano plot of synaptosome proteome displaying the genotype effect on protein levels in the 12-month-old group. Negative log2 p-values (adjusted) were plotted against log2 protein fold change. Increased protein levels are shown on the positive x-axis, and decreased levels are shown on the negative x-axis. The red points show candidates with p-value < 0.05 (Limma or RankProduct) (Schwammle et al., 2013), within 95% Confidence Interval of bootstrap analysis (Efron and Tibshirani, 1993) and have a fold change of ≥ 1.2 fold (log2 ± 0.263). The green points show candidates with p-value < 0.05, not within 95% confidence interval of bootstrap analysis and have a fold change of ≥ 1.2 fold (log2 ± 0.263). The blue points show candidates with p-value > 0.05, within 95% confidence interval of bootstrap analysis and have a fold change of ≥ 1.2 fold (log2 ± 0.263). The gray points show candidates with p-value > 0.05, not within 95% confidence interval of bootstrap analysis and have

a fold change of < 1.2 fold (log2 ± 0.263). The experimental groups were 12-month-old wild type (WT), NOS2-/-, APP/PS1 and APP/PS1/NOS2-/-. (A) APP/PS1 – WT (12 months old) with replicates > 50%. (B) WT – NOS2-/- (12 months old) with replicates > 50%. (C) APP/PS1 – APP/PS1/NOS2-/- (12 months old) with replicates > 50%.

To visualize the influence of age, Venn diagrams were made to identify the SNO proteins that were differentially regulated only in 12-month-old APP/PS1 mice in a NOS2-dependent manner. The age effect on WT animals was set as a control, showing an increase of S-nitrosylated proteins during physiological aging. In contrast, the age-mediated effect in APP/PS1 mice was taken as a pathological aging, assuming a further increase of S-nitrosylation upon cerebral deposition of Aβ. Venn diagrams for the age comparison showed 17 NOS2-dependent SNO proteins that significantly increased only in aged APP/PS1 mice (Figure 13A). On the genotype comparison in old mice, there were 6 overlap SNO proteins that increased in APP/PS1 vs APP/PS1/NOS2-/- and APP/PS1 vs WT mice. Five of these SNO proteins were modified by NO in response to cerebral amyloidosis (Figure 13B). The results further revealed four overlapping proteins when corrected for age- and genotype-dependent effects: N-myc downstream-regulated gene 2 protein (DRG2), NADH:ubiquinone oxidoreductase Subunit AB1 (NDUFAB1), excitatory amino acid transporter 1 (SLC1A3), and Inactive hydroxysteroid dehydrogenase-like protein 1 (HSDL1) (Figure 13C). The list of NOS2-dependent SNO proteins that were upregulated by aging and / or APP/PS1 genotype is shown in table 7.

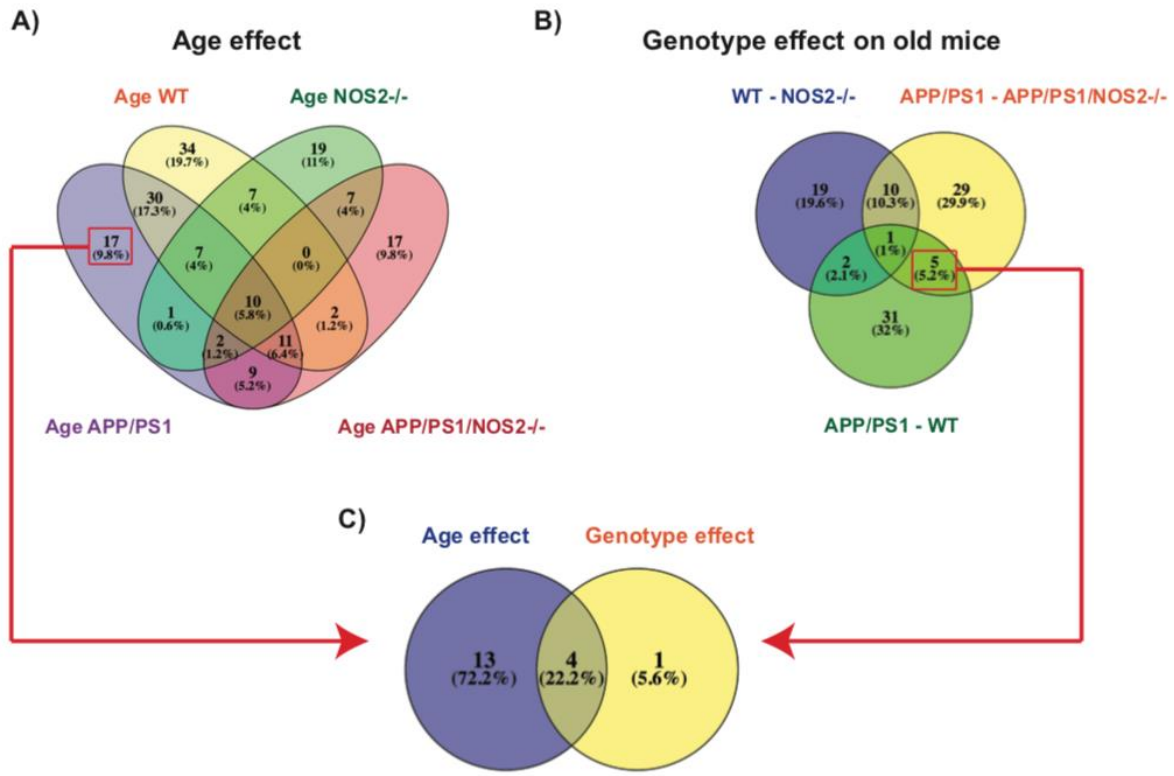

Figure 13. Venn diagram of synaptosomal proteome in mouse brain. (A) The diagrams show the S-nitrosylation proteins that were increased in age comparison. Age effect was determined comparing 12- and 3-month-old mice of all genotypes. Seventeen NOS2-dependent S-nitrosylation proteins were highly expressed in pathologic aging. (B) The diagrams show S-nitrosylation proteins that were increased when the different genotypes were compared in old mice. Five NOS2-dependent S-nitrosylation proteins were increased in aged APP/PS1 mice. (C) The overlap results in increased NOS2-dependent S-nitrosylation proteins from age (17 proteins) and genotype effects (5 proteins) in APP/PS1 mice. There were four overlapping proteins between age and genotype comparison, NDRG2, NDUFAB1, SLC1A3, and HSDL1. Wild type (WT), NOS2-/-, APP/PS1 and APP/PS1/NOS2-/-.

In comparison, twenty SNO proteins were found to be decreased exclusively on the age comparison (12- vs 3-month-old) of the APP/PS1 groups (Figure 14A). On the genotype comparison in old mice, there were 7 overlap SNO proteins that decreased in both analyses, APP/PS1 vs APP/PS1/NOS2-/- and APP/PS1 vs WT mice. Of which 6 SNO proteins were decreased due to the effect of APP/PS1 on WT

and NOS2-/- mice (Figure 14B). The results showed no overlapping proteins from age and genotype effects (Figure 14C).

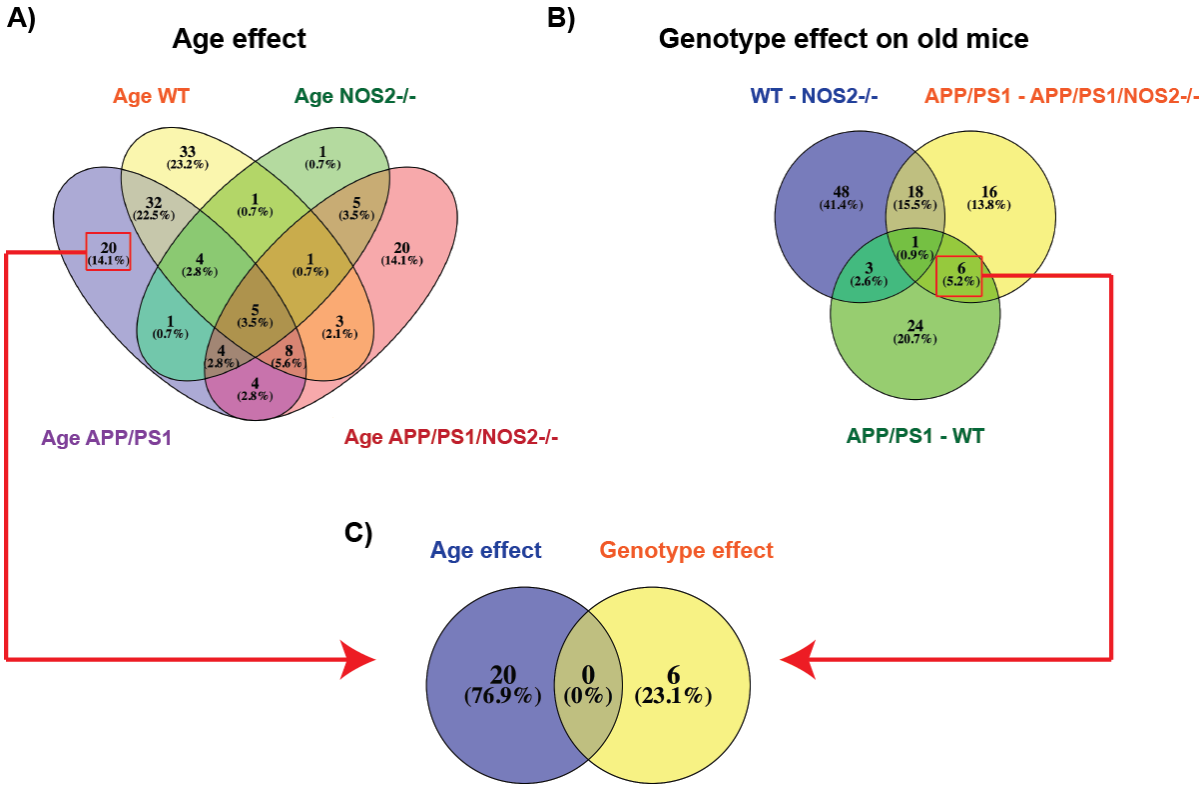

Figure 14. Venn diagram of synaptosomal proteome in mouse brain. (A) The diagrams show the S-nitrosylation proteins that were decreased in age comparison of mice samples. Age effect was determined by comparing 12- and 3-month-old mice in all genotypes. Twenty NOS2-dependent S-nitrosylation proteins were decreased in pathologic aging. (B) The diagrams show S-nitrosylation proteins that were decreased when the different genotypes were compared in old mice. 6 NOS2-dependent S-nitrosylation proteins were decreased in aged APP/PS1 mice. (C) There was no overlap in decreased NOS2-dependent S-nitrosylation proteins from age and genotype effects in APP/PS1 mice. Wild type (WT), NOS2-/-, APP/PS1 and APP/PS1/NOS2-/- .

The functional classification of synaptosomal S-nitrosylated proteins that differentially regulated by age and genotype effects in mouse brain

The selected significant proteins were chosen for further analysis. Table 7 consists of 17 NOS2-dependent S-nitrosylation proteins that increased in 12-month vs 3-month-old APP/PS1 mice (age effect) and 5 proteins that were increased in 12-month-old APP/PS1 mice (genotype effect), as shown in figure 13. Table 8 consists of 20 NOS2-dependent S-nitrosylation proteins that decreased in age comparison of APP/PS1 mice (age effect) and 6 proteins that were decreased in 12-month-old APP/PS1 mice (genotype effect), as shown in figure 14. To further understand the role of NOS2 in the selected proteins, all differentially regulated proteins (increased and decreased) were analyzed using Uniprot/SwissProt database and Panther GO database (http://pantherdb.org) “PANTHER version 13.1 Released 2017-04” at $P < 0.05$ (Figure 15) (Thomas et al., 2003) according to their biological process and molecular function.

Protein Name	Swiss-Prot ID	Gene	Peptide Sequence	SNO Pos. (aa)	Factor	Fold Change	Bootstrap 95% CI	p-value Limma	p-value RP
Elongation factor 2	P58252	EEF2	STLTDSLV**C**K	41	Aging	1.2	yes	0.25	0.52
Heme oxygenase 2	O70252	HMOX2	GTLGGSN**C**PFQTTVAVLR	281[#]	Aging	1.2	yes	0.35	0.34
Succinate dehydrogenase [ubiquinone] flavoprotein subunit, mitochondria	Q8K2B3	SDHA	AAFGLSEAGFNTA**C**LTK	89	Aging	1.2	yes	0.19	0.38
Excitatory amino acid transporter 1	P56564	SLC1A3	**C**LEENNGVDKR	375[#]	Aging	1.2	yes	0.25	0.37
					APP/PS1 - WT	1.2	yes	0.99	0.73
					APP/PS1 - ANO	1.3	yes	0.72	0.45
Phospholipid phosphohydrolase 3	Q99JY8	PLPP3	GFY**C**NDESIK	68[#]	Aging	1.3	yes	0.18	0.35
Zinc transporter 3	P97441	SLC30A3	LEGMAFHH**C**HK	55[#]	Aging	1.3	yes	0.30	0.46
CLIP-associating protein 2	Q8BRT1	CLASP2	SLLVAGAAQYD**C**FFQHLR	135[#]	Aging	1.3	yes	0.40	0.58
Succinyl-CoA ligase [ADP-forming] subunit beta, mitochondrial	Q9Z2I9	SUCLA2	I**C**NQVLV**C**ER	152 or 158	Aging	1.3	yes	0.06	0.38
Acyl carrier protein, mitochondrial	Q9CR21	NDUFAB1	LM**C**PQEIVDYIADK	140	Aging	1.4	yes	0.19	0.59
					APP/PS1 - WT	1.2	yes	0.99	0.73
					APP/PS1 - ANO	1.2	yes	0.91	0.69
Acyl carrier protein, mitochondrial	Q9CR21	NDUFAB1	LM**C**PQEIVDYIADKK	140	Aging	1.3	yes	0.29	0.54
Sodium/potassium-transporting ATPase subunit alpha-3	Q6PIC6	ATP1A3	SSHTWVALSHIAGL**C**NR	418	Aging	1.3	yes	0.41	0.27

Inactive hydroxysteroid dehydrogenase-like protein 1	Q8BTX9	HSDL1	**C**PWLAPSPR	265[#]	Aging	1.3	yes	0.18	0.34
					APP/PS1 - WT	1.2	yes	0.99	0.73
					APP/PS1 - ANO	1.4	yes	0.72	0.45
Succinyl-CoA:3-ketoacid coenzyme A transferase 1, mitochondrial	Q9D0K2	OXCT1	STG**C**DFAVSPN	504	Aging	1.3	yes	0.13	0.22
Receptor-type tyrosine-protein phosphatase alpha	P18052	PTPRA	TGTF**C**ALSTVLER	770[#]	Aging	1.4	yes	0.19	0.48
NFU1 iron-sulfur cluster scaffold homolog, mitochondrial	Q9QZ23	NFU1	LQGS**C**TS**C**PSSIITLK	210 or 213[#]	Aging	1.4	yes	0.05	0.38
Protein NDRG2	Q9QYG0	NDRG2	**C**PVMLVVGDQAPHEDA VVE**C**NSK	255 and 274	Aging	1.5	yes	0.23	0.38
					APP/PS1 - WT	1.3	yes	0.99	0.73
					APP/PS1 - ANO	1.2	yes	0.91	0.74
AP-2 complex subunit beta	Q9DBG3	AP2B1	E**C**HLNADTVSSK	857	Aging	1.7	yes	0.08	0.42
Pyruvate carboxylase, mitochondrial	Q05920	PC	FLYE**C**PWR	622	Aging	1.7	yes	0.03	0.03
Alcohol dehydrogenase class-3	P28474	ADH5	F**C**LNPK	103	APP/PS1 - WT	1.4	yes	0.99	0.73
					APP/PS1 - ANO	1.6	yes	0.72	0.69

Table 7. List of NOS2-dependent synapto-S-nitrosylation proteins increased by aging and / or APP/PS1 genotype. Positions of the SNO site refer to the canonic Swiss-Prot sequences. “Factor” describes the comparison by which the respective protein was identified, either based on aging or APP/PS1 genotype (NOS2-dependent). Proteins were selected based on statistical significance (either adjusted p-value < 0.05 (Limma or RankProduct) (Schwammle et al., 2013) or it lays on 95% confidence interval of bootstrap analysis) (Efron and Tibshirani, 1993), the magnitude of the response to 1.2 fold or higher (log2 ± 0.263), and the reproducibility among replicates (>50%). Hash sign ([#]) represents proteins which have not been reported in previous nitrosylation studies (Lee et al., 2012b).

Protein Name	Swiss-Prot ID	Gene	Peptide Sequence	SNO Pos. (aa)	Factor	Fold Change	Bootstrap 95% CI	p-value Limma	p-value RP
Alpha-internexin	P46660	INA	SFGSEHYL**C**SASSYR	10	Aging	2.0	yes	0.17	0.44
Spectrin beta chain, non-erythrocytic 1	Q62261	SPTBN1	VAHMEF**C**YQEL**C**QLAAER	619 and 624	Aging	1.7	no	0.09	0.05
Myosin-10	Q61879	MYH10	ADF**C**IIHYAGK	576	Aging	1.6	yes	0.05	0.37
Apoptosis-inducing factor 1, mitochondrial	Q9Z0X1	AIFM1	SNIWVAGDAA**C**FYDIK	440	Aging	1.4	yes	0.27	0.51
Tyrosine-protein phosphatase non-receptor type substrate 1	P97797	SIRPA	VI**C**EVAHITLDR	229	Aging	1.4	yes	0.09	0.23
Neuronal growth regulator 1	Q80Z24	NEGR1	**C**EGAGVPPPAFEWYK	239	Aging	1.4	yes	0.05	0.37
Mitochondrial import receptor subunit TOM40 homolog	Q9QYA2	TOMM40	FL**C**GFGLTIG	354	Aging	1.4	yes	0.25	0.19
Cell adhesion molecule 3	Q99N28	CADM3	LLLH**C**EGR	252	Aging	1.3	yes	0.10	0.38
Peptidyl-prolyl cis-trans isomerase FKBP1A	P26883	FKBP1A	RGQT**C**VVHYTGMLEDGK	23	Aging	1.3	yes	0.31	0.41
AP-2 complex subunit alpha-2	P17427	AP2A2	FHL**C**SVPTR	532	Aging	1.3	yes	0.10	0.26
Cell adhesion molecule 2	Q8BLQ9	CADM2	SSPVMEGDLMQLT**C**K	146	Aging	1.3	yes	0.10	0.22
Intercellular adhesion molecule 5	Q60625	ICAM5	MVTIS**C**WAGAR	344	Aging	1.3	yes	0.13	0.41
			SWTWPEGPEQTLH**C**EAR	431		1.2	yes	0.34	0.47
			LFS**C**EVDGKPEPR	595		1.2	yes	0.21	0.26
AP-2 complex subunit alpha-1	P17426	AP2A1	FHL**C**SVATR	533	Aging	1.3	yes	0.14	0.28
NADH dehydrogenase [ubiquinone] 1 alpha subcomplex subunit 9, mitochondrial	Q9DC69	NDUFA9	**C**DVYDIMHLR	86	Aging	1.2	yes	0.31	0.51

Neuronal-specific septin-3	Q9Z1S5	SEPT3	VH**CC**LYFISPTGH	173 or 174	Aging	1.2	yes	0.18	0.23
Guanine nucleotide-binding protein G(I)/G(S)/G(T) subunit beta-1	P62874	GNB1	ELAGHTGYLS**CC**R	148 or 149	Aging	1.2	yes	0.10	0.35
Aminopeptidase B	Q8VCT3	RNPEP	GY**C**FVSYLAH	419	Aging	1.2	yes	0.29	0.53
Guanine nucleotide-binding protein subunit beta-5	P62881	GNB5	YYPSGDAFASGSDDAT**C**R	305	Aging	1.2	yes	0.21	0.46
Protein SOGA3	Q6NZL0	SOGA3	**C**QLQFVK	525	Aging	1.2	yes	0.28	0.36
UPF0554 protein C2orf43 homolog	Q8BVA5	LDAH	TDGW**C**PVK	275	Aging	1.2	yes	0.25	0.59
Pyruvate dehydrogenase E1 component subunit beta, mitochondrial	Q9D051	PDHB	EGIE**C**EVINLR	263	APP/PS1 - WT	1.2	yes	0.99	0.74
					APP/PS1 - ANO	1.6	yes	0.60	0.61
Clathrin heavy chain 1	Q68FD5	CLTC	HSSLAG**C**QIINYR	151	APP/PS1 - WT	1.4	yes	0.83	0.73
			MEGNAEESTLF**C**F	217	APP/PS1 - WT	1.2	yes	0.99	0.73
					APP/PS1 - ANO	1.3	yes	0.72	0.68
			YESLEL**C**R	436	APP/PS1 - ANO	1.4	yes	0.15	0.23
Fascin	Q61553	FSCN1	NASCYFDIEWCDR	334	APP/PS1 - WT	1.4	yes	0.99	0.78
					APP/PS1 - ANO	1.4	yes	0.73	0.68
Synaptotagmin-1	P46096	SYT1	LGDICFSLR	277	APP/PS1 - WT	1.2	yes	0.99	0.73
					APP/PS1 - ANO	1.3	yes	0.60	0.66
ATP synthase subunit epsilon, mitochondrial	P56382	ATP5E	FSQICAK	19	APP/PS1 - WT	1.3	yes	0.99	0.74
					APP/PS1 - ANO	1.3	yes	0.73	0.80
Glyoxalase domain-containing protein 4	Q9CPV4	GLOD4	ALLGYADNQCK	182	APP/PS1 - WT	1.2	yes	0.99	0.73
			HEEFEEGCK	41	APP/PS1 - ANO	1.3	yes	0.72	0.51

Table 8. List of NOS2-dependent synapto-S-nitrosylation proteins that decreased by aging and / or APP/PS1 genotype. Positions of

the SNO site refer to the canonic Swiss-Prot sequences. “Factor” describes the comparison by which the protein was identified, either based on aging or APP/PS1 genotype (NOS2-dependent). Proteins were selected based on the statistical significance (either adjusted p-value < 0.05 (Limma or RankProduct) (Schwammle et al., 2013) or it lays on 95% confidence interval of bootstrap analysis) (Efron and Tibshirani, 1993), the magnitude of the response to 1.2 fold or higher (log2 ± 0.263), and the reproducibility among replicates (>50%). Hash sign (#) represents proteins which have not been reported in previous nitrosylation studies (Lee et al., 2012b).

The analysis of the involved biological processes of the 18 NOS2-dependent SNO proteins (Table 7) that increased by age and genotype comparisons revealed a contribution to the following mechanisms/pathways: metabolic processes (34.4%), cellular processes (28.1%), biological regulation (12.5%), response to stimulus (12.5%), localization (9.4%), and multicellular organismal processes (3.1%). However, the biological process of 26 decreased NOS2-dependent SNO proteins (table 8) includes more variances such as cellular process (27.5%), localization (22.5%), cellular component organization or biogenesis (12.5%), metabolic process (12.5%), developmental process (5%), multicellular organismal process (7.5%), biological regulation (5%), immune system process (2.5%), biological adhesion (2.5%) and locomotion (2.5%). Metabolic process and cellular processes were two of the highest percentage within the biological process category.

Next, the classification was done for all of the differentially regulated SNO proteins from age- and genotype-dependent manner on their molecular function. The increased proteins on both comparisons were classified into: catalytic activity (57.2%), binding (14.3%), transporter activity (14.3%), translation regulator activity (7.1%) and structural molecule activity (7.1%). Additionnally the molecular function of the 26 SNO proteins that decreased was involved in: catalytic activity (46.6%), binding (40%), transporter activity (6.7%) and structural molecule activity (6.7%).

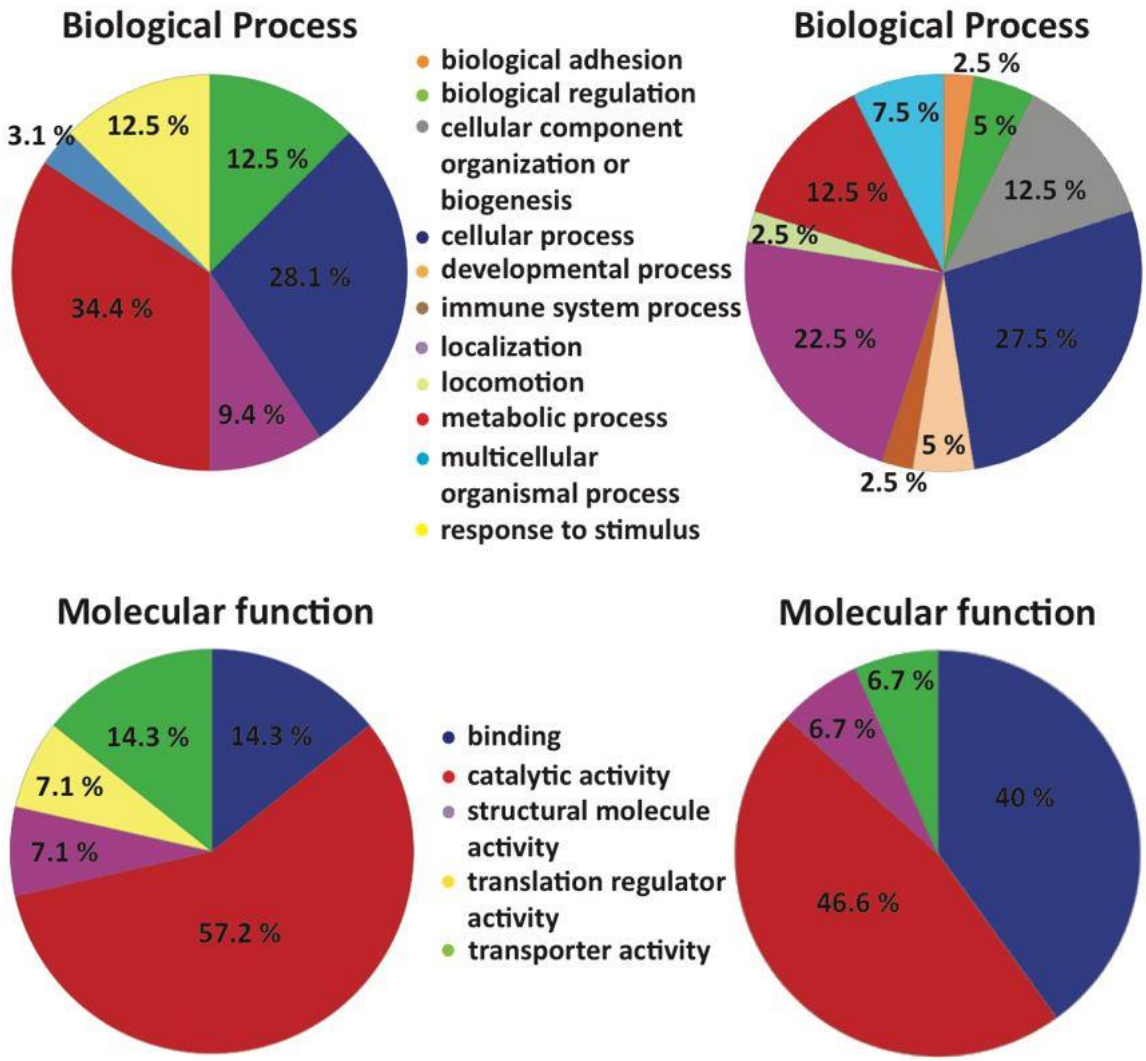

Figure 15. Pie chart showing the functional classification of increased and decreased synaptosomal SNO proteins in both age- and genotype-dependent manner of mouse samples. The iodoTMT identified changes in the synaptosomal proteome were characterized using gene ontology (GO) analysis. Functional categories were based on the annotations of GO using the PANTHER classification system for the categories of biological process and molecular function.

3.8.2. Synaptosomal S-nitrosylated Proteins in AD.

Pairwise comparisons of protein regulation were performed between samples from AD, MCI and healthy controls (Table 1). The pairwise comparisons were done based on the AD stage and healthy control status. Volcano plots on figure 16 show S-nitrosylation proteins with replicate numbers > 50% that were differentially regulated in AD disease progression (control to MCI, MCI to AD or control to AD).

The candidate proteins in figure 16 were shown in different colors. The most substantial candidates will be from red points, which indicate candidates with p-value < 0.05 (Limma or RankProduct) (Schwammle et al., 2013), within 95% confidence iInterval of bootstrap analysis (Efron and Tibshirani, 1993) and have a fold change of ≥ 1.2 fold (log2 ± 0.263). The green points indicate candidates with p-value < 0.05, not within 95% confidence interval of bootstrap analysis and have a fold change of ≥ 1.2 fold (log2 ± 0.263). The blue points indicate candidates with p-value > 0.05, within 95% confidence interval of bootstrap analysis and have a fold change of ≥ 1.2 fold (log2 ± 0.263). While the gray points indicate candidates with p-value > 0.05, not within 95% confidence interval of bootstrap analysis and have a fold change of < 1.2 fold (log2 ± 0.263). Selected proteins for further analysis were chosen from red, green and blue points.

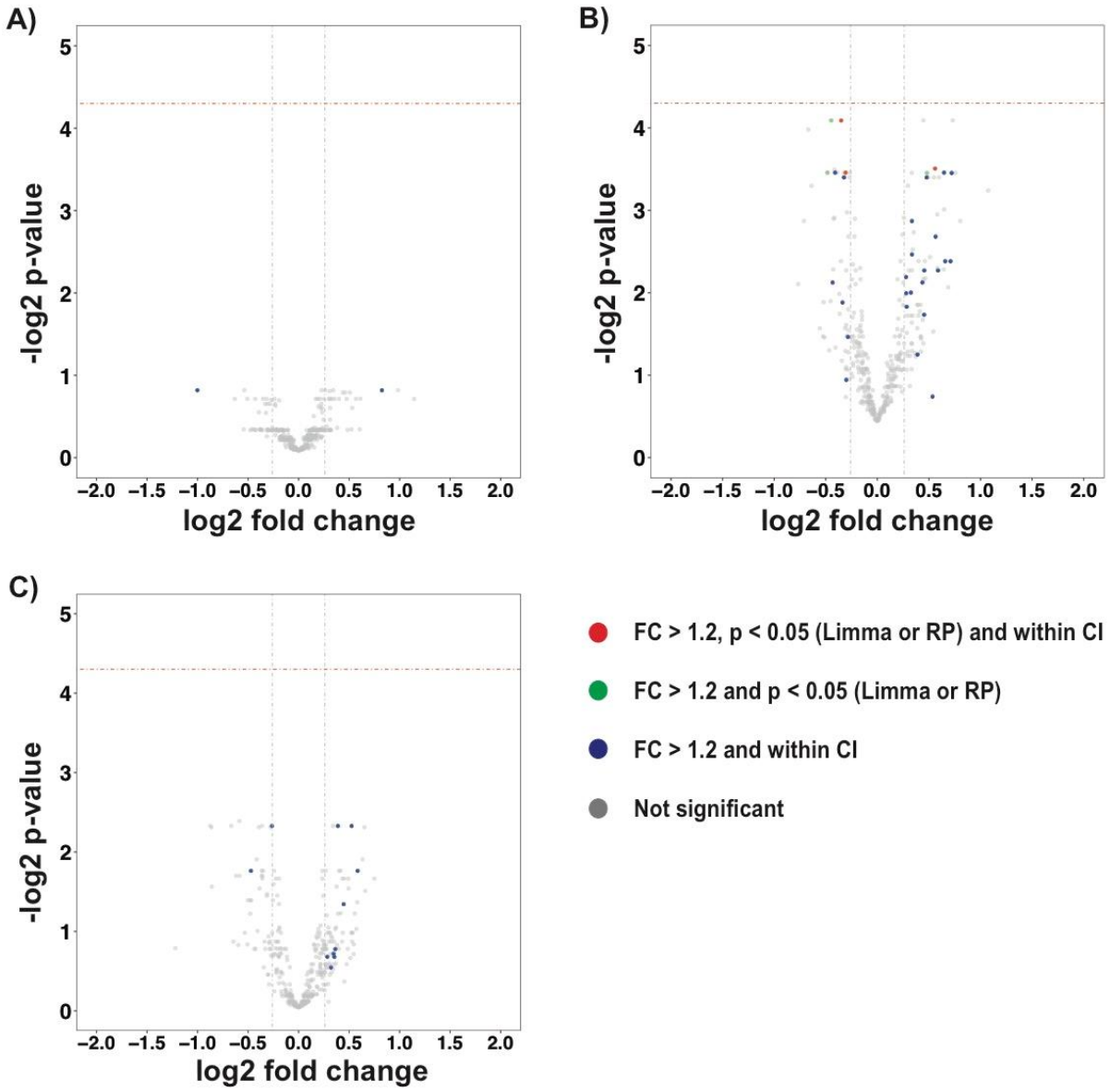

Figure 16. Volcano plot of synaptosome proteome displaying S-nitrosylation proteins from the human samples that were increased during AD disease progression. (A) MCI-Control. (B) AD-MCI. (C) AD-Control. Negative log2 p-values (adjusted) were plotted against log2 protein fold change. Increased protein levels were shown on the positive x-axis, and decreased levels were shown on the negative x-axis. The red points show candidates with p-value < 0.05 (Limma or RankProduct) (Schwammle et al., 2013), within 95% confidence interval of bootstrap analysis (Efron and Tibshirani, 1993) and have a fold change of ≥ 1.2 fold (log2 ± 0.263). The green points show candidates with p-value < 0.05, not within 95% confidence interval of bootstrap analysis and have a fold change of ≥ 1.2 fold (log2 ± 0.263). The blue points show candidates with p-value > 0.05, within 95% confidence interval of bootstrap analysis and have a fold

change of ≥ 1.2 fold (log2 ± 0.263). The gray points show candidates with p-value > 0.05, not within 95% confidence interval of bootstrap analysis and have a fold change of < 1.2 fold (log2 ± 0.263).

Applying the same reproducibility among replicates (>50%), statistical analysis (either adjusted p-value < 0.05 (Schwammle et al., 2013) or it lays on 95% confidence interval of bootstrap analysis (Efron and Tibshirani, 1993) and the magnitude of the response (FC 1.2-fold or higher) for human candidates as for mouse group proteins/peptides, only 1 SNO proteins was found elevated in MCI compared to control samples, 16 SNO proteins were increased on AD compared to MCI, and 9 SNO proteins were increased on AD compared to control (Figure 17A). No protein/peptide was found to be overlap in regulation between all three pairwise comparisons. Myelin-oligodendrocyte glycoprotein (MOG), glutathione s-transferase Mu 3 (GSTM3) and four and a half LIM domains protein 1 (FHL1) were found increased in two pairwise comparison groups (AD vs MCI and AD vs Control). In parallel, 1 SNO proteins was decreased in MCI compared to control samples, 9 SNO proteins were decreased on AD compared to MCI, and 2 SNO proteins were decreased on AD compared to control. No overlap proteins/peptides were found between three pairwise comparison groups (Figure 17B).

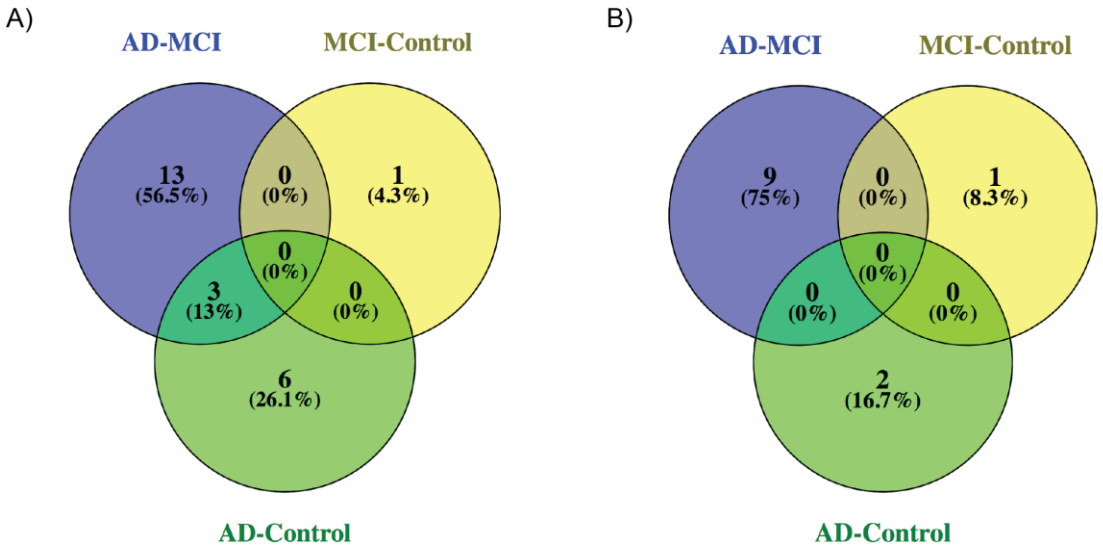

Figure 17. Venn diagram of synaptosomal proteome in human brain. Proteins were selected based on the statistical significance (either adjusted p-value < 0.05

(Schwammle et al., 2013) or it lays on 95% confidence interval of bootstrap analysis (Efron and Tibshirani, 1993) and the reproducibility among replicates (>50%). A) The venn diagrams show S-nitrosylation proteins that were increased during AD disease progression (MCI-Control; AD-MCI; AD-Control) with the magnitude of the response to 1.2-fold or higher (log2 ± 0.263). MOG, GSTM3 and FHL1 were the proteins with fold change values of 1.2-fold or higher (log2 ± 0.263) in two pairwise comparison groups (AD vs MCI and AD vs Control). B) The venn diagrams show S-nitrosylation proteins that were decreased during AD disease progression (MCI-Control; AD-MCI; AD-Control) with the magnitude of the response to 1.2-fold or higher (log2 ± 0.263). There is no overlap between pairwise comparison groups.

The functional classification of synaptosomal S-nitrosylated proteins that differentially regulated by AD stage in human brain

Table 9 provides the list of twenty-three NOS2-dependent S-nitrosylation proteins, which were significantly increased during AD disease progression. While table 10 consists of twelve NOS2-dependent S-nitrosylation proteins, which were significantly decreased in AD disease progression. The selected increased or decreased proteins were then classified using Uniprot/SwissProt database and Panther GO database (http://pantherdb.org) “PANTHER version 13.1 Released 2017-04” at $P < 0.05$ (Figure 18) (Thomas et al., 2003) according to their biological process and molecular function.

Protein Name	Swiss-Prot ID	Gene	Peptide Sequence	SNO Pos. (aa)	Factor	Fold Change	Bootstrap 95% CI	p-value Limma	p-value RP
Four and a half LIM domains protein 1	Q13642	FHL1	FWHDT**C**FR	65#	AD - MCI	1.4	no	0.09	0.05
					AD - Control	1.4	yes	0.20	0.30
Glutathione S-transferase Mu 3	P21266	GSTM3	S**C**ESSMVLGYWDIR	3	AD - MCI	1.4	yes	0.23	0.13
					AD - Control	1.4	yes	0.40	0.55
Myelin-oligodendrocyte glycoprotein	Q16653	MOG	FSDEGGFT**C**FF	127#	AD - MCI	1.3	yes	0.42	0.45
			ALVGDEVELP**C**R	53#	AD - Control	1.2	yes	0.68	0.58
Neurocan core protein	O14594	NCAN	YQ**C**NEGFAQHHVATIR	1244#	MCI - Control	1.8	yes	0.57	0.63
Ankyrin-2	Q01484	ANK2	FWLID**C**R	1304#	AD – MCI	1.6	yes	0.09	0.15
Brain-specific angiogenesis inhibitor 1-associated protein 2	Q9UQB8	BAIAP2	F**C**FLVEK	195#	AD – MCI	1.4	yes	0.21	0.30
Calcium/calmodulin-dependent protein kinase type II subunit gamma	Q13555	CAMK2G	WLNVHYH**C**SGAPAAPL	549#	AD – MCI	1.6	yes	0.09	0.35
2',3'-cyclic-nucleotide 3'-phosphodiesterase	P09543	CNP	RPPGVLH**C**TTK	252#	AD – MCI	1.6	yes	0.19	0.18
			LDEDLAAY**C**R	111#		1.4	yes	0.30	0.22
Cysteine and glycine-rich protein 1	P21291	CSRP1	TVYFAEEVQ**C**EGNSFHK	25	AD – MCI	1.5	yes	0.09	0.00
			S**C**FL**C**MVCK	34 and 37		1.3	yes	0.18	0.30
Band 4,1-like protein 1	Q9H4G0	EPB41L1	DYFGLTF**C**DADSQK	143#	AD – MCI	1.2	yes	0.22	0.36
Glucose-6-phosphate isomerase	P06744	GPI	MIP**C**DFLIPVQTQHPIR	404	AD – MCI	1.4	yes	0.60	0.39
Hyaluronan and proteoglycan link protein 2	Q9GZV7	HAPLN2	LTLSEAHAA**C**R	265#	AD – MCI	1.6	yes	0.19	0.13
Kelch repeat and BTB domain-containing protein 11	O94819	KBTBD11	GDAAVY**C**FHAAAGEWR	329#	AD – MCI	1.3	yes	0.14	0.26
	P62937	PPIA	IIPGFM**C**QGGDFTR	62#	AD – MCI	1.3	yes	0.25	0.19

Peptidyl-prolyl cis-trans isomerase A			KITIAD**C**GQLE	161[#]		1.2	yes	0.25	0.16
26S proteasome non-ATPase regulatory subunit 6	Q15008	PSMD6	QYLFSLYE**C**R	266[#]	AD – MCI	1.2	yes	0.28	0.32
Prostaglandin E synthase 3	Q15185	PTGES3	HLNEIDLFH**C**IDPNDSK	58	AD – MCI	1.4	yes	0.09	0.27
Versican core protein	P13611	VCAN	NGFDQ**C**DYGWLSDASVR	294[#]	AD – MCI	1.5	yes	0.21	0.32
			FDAY**C**FKPK	345[#]		1.5	yes	0.16	0.22
CD44 antigen	P16070	CD44	ALSIGFET**C**R	77[#]	AD – Control	1.5	yes	0.29	0.30
Actin, cytoplasmic 1	P60709	ACTB	DDDIAALVVDNGSGM**C**K	17	AD – Control	1.3	yes	0.20	0.22
Choline transporter-like protein 2	Q8IWA5	SLC44A2	**C**QFAFYGGESGYHR	427[#]	AD – Control	1.3	yes	0.58	0.50
Myelin proteolipid protein	P60201	PLP1	V**C**GSNLLSI**C**K	220 and 228[#]	AD – Control	1.3	yes	0.62	0.58
Cathepsin B	P07858	CTSB	DQGS**C**GS**C**WAFGAVEAI SDR	105 and 108	AD - Control	1.3	yes	0.61	0.51
Aspartate aminotransferase, cytoplasmic	P17174	GOT1	TDD**C**HPWVLPVVK	70	AD - Control	1.2	yes	0.62	0.55

Table 9. List of twenty-three NOS2-dependent synapto-SNO proteins that were increased during AD disease progression in human samples. Positions of the SNO site refer to the canonic Swiss-Prot sequences. “Factor” describes the comparison in which the protein was identified based on the disease progression. Proteins were selected based on the statistical significance (either adjusted p-value < 0.05 (Limma or RankProduct) (Schwammle et al., 2013) or it lays on 95% confidence interval of bootstrap analysis) (Efron and Tibshirani, 1993), the magnitude of the response to 1.2 fold or higher (log2 ± 0.263), and the reproducibility among replicates (>50%). Hash sign ([#]) represents proteins which have not been reported in previous nitrosylation studies (Lee et al., 2012b).

Protein Name	Swiss-Prot ID	Gene	Peptide Sequence	SNO Pos. (aa)	Factor	Fold Change	Bootstrap 95% CI	p-value Limma	p-value RP
Neurofilament light polypeptide	P07196	NEFL	TLEIEA**C**R	322#	MCI - Control	2.0	yes	0.57	0.64
Aconitate hydratase, mitochondrial	Q99798	ACO2	DLGGIVLANA**C**GP**C**IGQW DR	448 and 451	AD - MCI	1.2	yes	0.36	0.41
60 kDa heat shock protein, mitochondrial	P10809	HSPD1	AAVEEGIVLGGG**C**ALLR	442	AD – MCI	1.3	yes	0.09	0.15
Isoleucine--tRNA ligase, mitochondrial	Q9NSE4	IARS2	RPYW**C**ISR	521#	AD – MCI	1.3	yes	0.23	0.17
Malate dehydrogenase, mitochondrial	P40926	MDH2	SQETE**C**TYFSTPLLLGK	285	AD – MCI	1.3	yes	0.27	0.33
Neuronal cell adhesion molecule	Q92823	NRCAM	AAPYWITAPQNLVLSPGE DGTLI**C**R	382#	AD - MCI	1.2	yes	0.52	0.40
Pyruvate dehydrogenase E1 component subunit alpha, somatic form, mitochondrial	P08559	PDHA1	LP**C**IFI**C**ENNR	218 and 222#	AD – MCI	1.2	yes	0.09	0.01
			VDGMDIL**C**VR	261#	AD – MCI	1.3	yes	0.06	0.01
Plexin-A1	Q9UIW2	PLXNA1	FE**C**GW**C**VAER	828 and 831#	AD – MCI	1.4	no	0.06	0.01
Mitochondrial-processing peptidase subunit beta	O75439	PMPCB	FHFGDSL**C**THK	265#	AD – MCI	1.4	no	0.09	0.01
Mitochondrial glutamate carrier 1	Q9H936	SLC25A22	VYTSMSD**C**LIK	52#	AD – MCI	1.3	yes	0.09	0.08
Rabphilin-3A (Exophilin-1)	Q9Y2J0	RPH3A	KNFNI**C**LER	515#	AD - Control	1.4	yes	0.29	0.31
NADH dehydrogenase [ubiquinone] 1 alpha subcomplex subunit 8	P51970	NDUFA8	**C**ALDFFR	66#	AD - Control	1.2	yes	0.20	0.22

Table 10. List of twelve NOS2-dependent SNO proteins that were decreased during AD disease progression in human synaptosome samples. Positions of the SNO site refer to the canonic Swiss-Prot sequences. “Factor” describes the comparison in which the protein was identified based on disease progression. Proteins were selected based on the statistical significance (either adjusted p-value < 0.05 (Limma or RankProduct) (Schwammle et al., 2013) or it lays on 95% confidence interval of bootstrap analysis) (Efron and Tibshirani, 1993), the magnitude of the response to 1.2 fold or higher (log2 ± 0.263), and the reproducibility among replicates (>50%). Hash sign (#) represents proteins which have not been reported in previous nitrosylation studies (Lee et al., 2012b).

In the analysis of the human samples, the biological process of 23 NOS2-dependent SNO proteins, which were increased by AD disease progression increased SNO proteins (Table 9) includes biological regulation (8.3%), cellular component organization or biogenesis (13.9%), cellular process (27.8%), developmental process (11%), Immune system process (5.6%), localization (2.8%), metabolic process (13.9%), multicellular organismal process (13.9%), and response to stimulus (2.8%). While the biological process of decreased NOS2-dependent SNO proteins (Table 10) consist of more variances such as metabolic process (29.1%), cellular process (25%), localization (12.4%), cellular component organization or biogenesis (8.3%), developmental process (4.2%), multicellular organismal process (4.2%), biological regulation (4.2%), biological adhesion (4.2%), locomotion (4.2%) and response to stimulus (4.2%). Metabolic process and cellular processes were also two of the highest percentage from the biological process category.

Next, the classification was done for all of the differentially regulated SNO proteins in human samples with respect to their molecular function. The increased proteins were classified into: catalytic activity (30.7%), binding (23.1%), structural molecule activity (23.1%), receptor activity (7.7%), signal transducer activity (7.7%) and transporter activity (7.7%). While the molecular function of 12 SNO proteins that decreased in human samples was involved in catalytic activity (50%), binding (20%), transporter activity (10%) and receptor activity (10%) and signal transducer activity (10%).

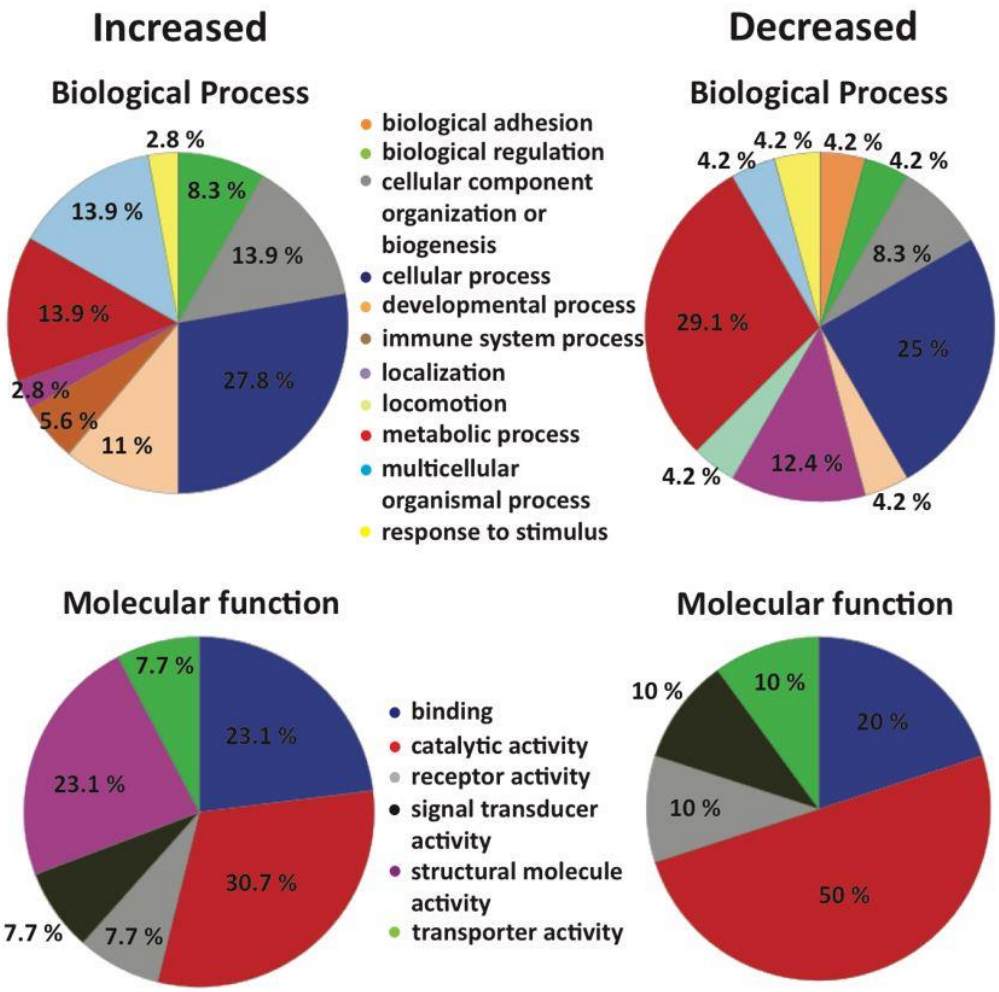

Figure 18. Pie chart showing the functional classification of increased and decreased synaptosomal SNO proteins in human samples. The iodoTMT identified changes in the synaptosomal proteome were characterized using gene ontology (GO) analysis. Functional categories were based on the annotations of GO using the PANTHER Classification System for the categories of Biological process and molecular function.

To see test whether there is a correlation between mouse and human data sets, a direct comparison of mouse and human SNO proteins was performed. Selected candidate proteins (increased or decreased) from the murine synaptosome samples were matched with human candidate proteins. Proteins from table 7 were compared to table 9 and proteins list in table 8 to table 10. This study did not reveal any overlap of increased or decreased SNO proteins (or peptides) between murine and human data sets.

4. Discussion

4.1. Overview of the study

The aim of this study is to identify new biomarker candidates for neuroinflammation in progression to MCI and AD. To achieve this, proteomic analysis was implemented using the iodoTMT enrichment procedure and coupled with HPLC-MS/MS, to identify synaptosomal s-nitrosylated proteins or peptides that are modified in a NOS2-dependent manner in murine and human samples.

Detailed descriptions of the methodological workflow are given in figure 19, from sample generation to protein/peptide identification and quantitation using an isobaric tag labeling procedure and nanoHPLC-MS/MS. In general, synaptosome isolation was done by sucrose density gradient followed by labeling and enrichment procedure using the iodoTMT method, along with mass spectrometry analysis.

For the analysis of s-nitrosylation of proteins and peptides, pairwise comparisons were calculated to test the effect of: (1) age on each genotype and (2) APP/PS1+/- and NOS2-/- at different ages. While in human analysis, pairwise comparisons were created to investigate changes along AD progression by comparing brain samples derived from patients with a diagnosis of AD compared to MCI and aged-matched healthy individuals.

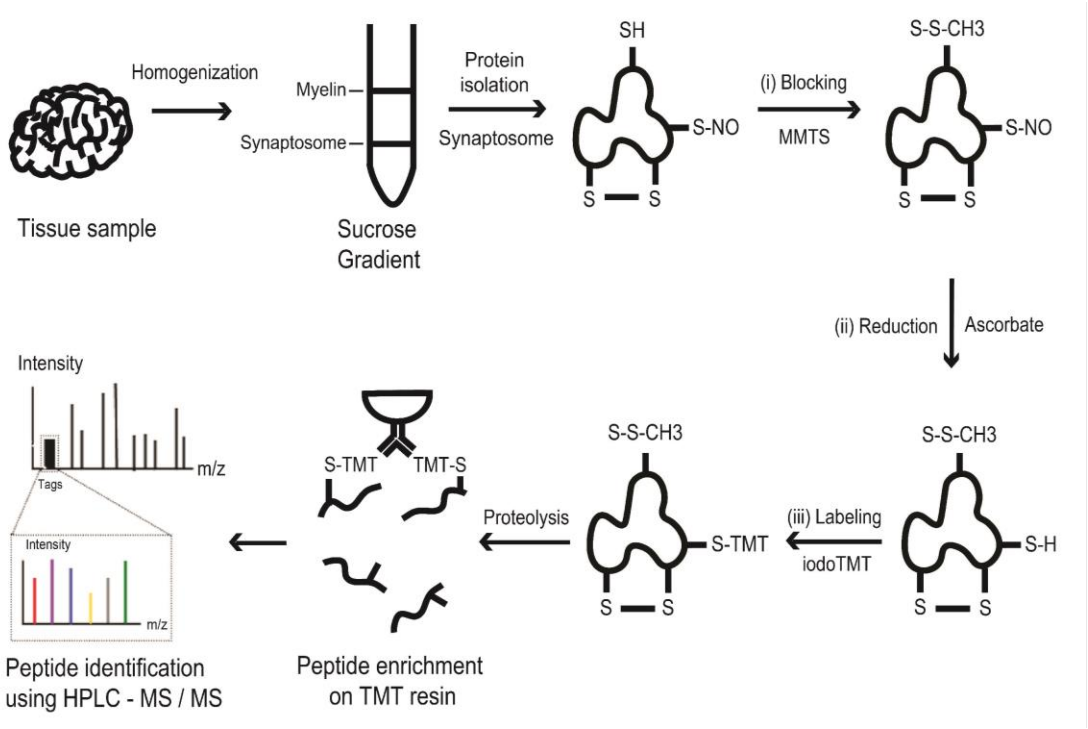

Figure 19. Schematic image of the isobaric tag labeling procedure (Wijasa et al., 2017). Reproduced from “Proteome profiling of s-nitrosylated synaptosomal proteins by isobaric mass tags”, by T. S. Wijasa et al., 2017, Journal of Neuroscience Methods, 291, p. 95-100. Copyright 2017 by Elsevier B. V.

4.2. Synaptosome proteomic

Density-gradient centrifugation techniques are used for synaptosome preparation. These are similar to the isolation of other subcellular fractions containing relatively pure cellular organelles such as the differential centrifugation of sucrose (Gray and Whittaker, 1962; Whittaker et al., 1964), Percoll (Nagy and Delgado-Escuata, 1984) or Ficoll/sucrose (Booth and Clark, 1978). All techniques include steps to purify crude synaptosomal fractions from their contaminants such as nuclei etc. The exact reagents used for the formation of the density gradient and for buffering may differ from lab to lab however, depending on specific applications or personal preferences. As an example, the protocol used by the Henekalab (sucrose density gradient) is described for routine preparation of synaptosomes from fresh human or mouse brain tissue. The purity of the isolated synaptosomes can be analyzed

biochemically with enzymatic markers or estimated by morphological means using electron microscopy. Sucrose density gradient is easy to adapt and does not require specialized tools. It is also evenly applicable for both murine and postmortem human tissue.

Comprehensive studies on the synaptic proteome have been performed in the past (Bai and Witzmann, 2007; Chang et al., 2013; Engmann et al., 2010; Zareba-Koziol et al., 2014). There are various technical approaches used in proteomics for SNO protein quantification such as gel-based, mass spec-based, stable-isotopic labels, or label-free; each has its own unique advantages and deficiencies. Therefore, the suitability of a chosen technique can affect the outcome of a study and experimental design must therefore be done with great care.

4.3. Experimental design

To prevent protein degradation when in isolated form, harvested murine brains were stored immediately in liquid nitrogen and afterwards put at −80°C for longer storage. Sample handling was performed at −4°C. Human brain samples were obtained with maximum PMI of 4 hours from Banner Sun Health Research Institute (BSHRI) Brain and Body Donation Program in Sun City, Arizona, based on the NIA-Reagan Criteria for the Postmortem Diagnosis of AD.

To achieve an optimal result, a combination of fractionation (liquid chromatography) and protein enrichment (iodoTMT labeling) was used on an MS-based method. In HPLC-MS-based proteomics, complex mixtures of proteins are enzymatically cleaved into peptides and subsequently analyzed by mass spectrometry, this is also called bottom-up proteomics (Zhang et al., 2013). Processed proteomic data sets contain thousands of data points, each consisting of peptide MS/MS spectra and m/z values, which consist of amino acid sequence information. Peptide identification is carried out by comparing observed tandem mass spectra from peptide fragmentation with theoretical spectra from a protein database. Peptides can be uniquely matched to a single

protein or shared by more than one protein. Nevertheless, because of post-translational modification, all peptides referring to the same protein will not exhibit the same behavior.

The iodoTMT approach gave an extensive amount of identified proteins acquired from a low amount of starting material (as low as 50 µg of protein from synaptosome lysate) – an important notion for disease-related studies that frequently have to deal with limited amounts of primary material such as synaptosome proteins. Though only cysteine-containing proteins were analyzed, more than a thousand proteins were identified by HPLC-MS/MS. In comparison to prior published studies, the total number of identified SNO proteins was equal or higher (Engmann et al., 2010; Zareba-Koziol et al., 2014). The approach used in this study is able to identify low abundant endogenous levels of SNO proteins without prior induction of nitrosylation by NO donor treatment. Furthermore, it is easy to adapt for human and murine samples.

Mouse data analysis was done to evaluate age- and genotype-mediated effects. It has been shown previously that aging is highly influential in neurodegenerative diseases such as AD (Rizza et al., 2018; Wyss-Coray, 2016; Zareba-Koziol et al., 2014)(Rizza et al., 2018; Wyss-Coray, 2016; Zareba-Koziol et al., 2014). Being a non-modifiable factor of cognitive decline and AD (Spaan, 2016), aging influences the increase or decrease of SNO protein levels. To identify the differences in SNO protein levels, 12-month old mice were compared to 3-month-old mice in all four mice genotypes. The age effect of WT animals was set as a control, showing an increase of S-nitrosylated proteins during physiological aging. The age-mediated effect detected in APP/PS1 mice interpreted as pathological aging, assuming a further increase of S-nitrosylation upon cerebral deposition of Aβ. Additionally, to identify NOS2-dependent SNO proteins modifications during aging, the same statistical analysis was repeated by comparing the SNO proteome of old and young mice of NOS2-/- and APP/PS1/NOS2-/- background. The present study showed that age contributes to differentially regulated levels of nitrosylated proteins in all four genotypes mice. It also showed that physiological aging itself may contribute to the increase and decrease of nitrosylated proteins.

As for the genotype effect in old mice, WT was compared to NOS2-/- in order to identify the effect of NOS2 gene deletion in WT animals. APP/PS1 mice were compared to APP/PS1/NOS2-/- to identify the effect of NOS2 gene deletion on the APP/PS1 background. Furthermore, APP/PS1 was compared to WT to identify the effect of APP/PS1 vs WT control. The SNO proteins that were differentially regulated in mouse and human samples were then used for GO analysis to identify the biological process and molecular function (both increased and decreased proteins). Beyond our expectation, the volcano plot for APP/PS1 vs WT control is quite flat compared to WT vs NOS2-/- and APP/PS1 vs APP/PS1/NOS2-/- mice. Comparing the significant SNO proteins/peptides of APP/PS1 vs WT control on age- and genotype-comparisons, age appears to have more influence in AD mouse model rather than genotype. To maximize the results, this study combined the data from age- and genotype-comparisons. In an ideal result, the significant NOS2-dependent proteins identified in age-mediated effects would overlap 100% with the genotype-mediated effects. When the two are compared however, the number of overlapping proteins was found to be low in increased proteins (see fig. 13c) and none in decreased proteins (see fig. 14c). This is potentially caused by missing values as peptides can be present in a sample but at a concentration below the detection limit of the mass spectrometer. Alternatively, a peptide can be present in a sample at a level above the detection limit but fail to be identified due to technical issues with sample processing or preparation. As such future studies may find more overlapping proteins.

4.4. Statistical analysis of quantitative proteomics data

One of the problems of quantitative analyses in proteomics is multiple non-identical data sets due to missing values (Nilsson et al., 2010; Schwammle et al., 2013). In order to perform optimal statistical analysis, the combination of Limma, RankProduct and bootstrap analysis was utilized. Limma and bootstrap analysis have been used before for quantitative proteomics to detect fold differences in complex samples (Gamazon et al., 2018; Jeannin et al., 2018; Mateus et al., 2018) and also in the isobaric labeling approach to identify PTM

proteins (Zhang et al., 2016a). While Schwammle et al. has recommended the combined use of Limma and RankProduct, which is suitable for large quantitative data sets with missing values from mass spectrometry experiments (Schwammle et al., 2013).

Limma and RankProduct are well-established methods for statistical analysis of large data sets with missing values and are reliable to maintain the correct estimation of type I error (false positive) (Mukherjee et al., 2003; Schwammle et al., 2013). While the bootstrap method provides a more accurate family wise error rate (FWER) (probability of making false discovery or type 1 error) and introduces fewer false negatives (type 2 errors) than standard methods (e.g., Bonferroni's correction) for multiple comparison analyses (Dudoit et al., 2004; Forrest et al., 2005; Søgaard et al., 2014). Their combined use is complementary and yields high detection numbers of regulated features (du Prel et al., 2009).

From the initial analyses, despite having high fold change, not all peptides passed the p-value cutoff of < 0.05 using Limma and RankProduct. This indicates that tests will classify a peptide/protein as non-significant, though it lies within the 95% bootstrap confidence interval. Bootstrap analysis generated a higher number of significant peptides/proteins compared to Limma and RankProduct. It is necessary however to evaluate both p-value and fold change when selecting candidate proteins/peptides. Thus, a non-significant protein with high fold change and within the confidence interval was considered as an interesting candidate.

Furthermore, to assure the quality of the results, exclusion criteria were used to select candidate proteins/peptides. This involved the exclusion of peptides that occur only one or two replicates, that had a Pearson correlation score of 0.5 (moderate correlation) on the internal standard and peptides detected in less than 50% of the whole sample set. After applying the statistical analysis, increased or decreased SNO proteins/peptides were identified in mouse and human synaptosomal samples.

4.5. General analysis of the synapto-SNO proteins

Differential expression of SNO proteins can be caused by changes in protein expression (up or down) before nitrosylation (Hong et al., 2009; Papuc´ et al., 2015), changes in NOS2 expression induced by neuroinflammation (only increased) (Chen et al., 2012; Heneka et al., 2015) and other sources of reactive NO species such as oxidative stress due to aging, environmental toxins or lifestyle factors (Ahmad, 1995; Al-Gubory, 2014; Faraco et al., 2014; Nakamura et al., 2013).

Despite the hypothesis that the amount of nitrosylated proteins/peptides would increase in the murine AD model, proteins/peptides with a decreased number of nitrosylated cysteine residues were identified. The decrease of SNO proteins/peptides potentially results from the identification of proteins/peptides that are continuously nitrosylated under physiological conditions but with lower expression in AD related samples (Gould et al., 2013). It may also suggest that expression of the three NOS enzymes, that are capable of generating the NO needed for such modifications, include non-established patterns; i.e. constitutive NOS isoforms (NOS1, NOS3) are expressed when induced and NOS2 is constitutively expressed (Mattila and Thomas, 2014; Nakamura and Lipton, 2016).

In general, the highest percentage of SNO proteins/peptides are involved in metabolic and cellular processes. This result is in line with previous works showing alterations of metabolic pathways in AD, which may exacerbate neurological symptoms (Cai et al., 2012; Kaddurah-Daouk et al., 2013; Trushina et al., 2013). The next highest percentage of biological process classifications is cellular process, this includes regulation of cell growth, cell cycle, cell division, cell communication and cell death. To identify synapto-SNO proteins/peptides that might be associated with inflammation-induced NOS2 activation, the search was then focused on the up-regulated/increased S-nitrosylated proteins/peptides in mouse and human synaptosomal samples.

4.6. S-nitrosylated proteins analysis in mouse synaptosome samples on age and genotype effects

Mouse data was evaluated for age- and genotype-mediated effects. Young (3-month-old) and old mice (12-month-old) were used in the present study to identify age-dependent effects on each genotype. Aging is a complex process that depends on many factors including genetic, epigenetic and environmental factors throughout life. It is the biggest risk factor for cognitive decline and AD and is a non-modifiable factor (Sochocka et al., 2017; Spaan, 2016). Importantly, this study found that SNO proteins/peptides are regulated (up- or down-regulated) during physiological aging (Nakamura et al., 2013).

NOS2-/- mouse data was used to investigate the role of NOS2-derived NO during the inflammatory response observed in AD neuroinflammation (Colton et al., 2006; Fenyk-Melody et al., 1998). Therefore APP/PS1+/- were crossed with NOS2-/- animals. Based on previous SNO-proteome analysis, it was hypothesized that SNO proteins/peptides would decrease in aged APP/PS1 mice carrying a NOS2 gene deletion (Bateman et al., 2015; Colton et al., 2008; Kummer et al., 2012; Wilcock et al., 2008). Along with the increase of SNO proteins/peptides in human AD samples, this would suggest an early synaptic vulnerability for NO-mediated neuroinflammation (Heneka et al., 2015; Seneviratne et al., 2016). The non-overlapping synapto-SNO proteins of APP/PS1 samples were postulated to show NOS2-dependent proteins in the murine AD model.

The overlapping proteins from the mouse study, according to age and genotype effects, included NDRG2, NDUFAB1, SLC1A3, and HSDL1 (figure 13C) and were associated with AD previously (Bateman et al., 2015; Breuer et al., 2013; Kanehisa et al., 2016; Rong et al., 2017; Scott et al., 2002). NDRG2, HSDL1 and ADH5 proteins were associated with pathological aging. NDRG2 is a cytoplasmic protein involved in cell differentiation and mainly expressed in astrocytes in the CNS (Breuer et al., 2013). NDRG2 was found increased in aging APP/PS1 mice (Rong et al., 2017) and in the cortical neurons of late-onset AD brains (mRNA and protein levels) when compared to controls; beyond age or gender effects (Mitchelmore et al., 2004). The NDRG2 gene is

expressed in the cerebral cortex (frontal, temporal, occipital lobes), cerebellum and hippocampus, which is known to be vulnerable to AD pathology (Mitchelmore et al., 2004; Rong et al., 2017). A recent study by Rong et al. showed the relationship between NDRG2 and AD pathology at the molecular level, mainly beta-amyloid accumulation and abnormal tau phosphorylation (Rong et al., 2017). Their study showed changes in NDRG2 might be related to the generation of beta-amyloid. It was also demonstrated that tau phosphorylation was increased in NDRG2 overexpressed cells and decreased in NDRG2 knock-down cells (Rong et al., 2017). Moreover, nitrosylated NDRG2 has been identified previously to be involved in AD pathology (Seneviratne et al., 2016). HSDL1 is a mitochondrial protein that has been shown to mediate immune system processes, cell differentiation, homeostatic processes and system development (Bateman et al., 2015). No known studies have yet directly related HSDL1 to AD or found in nitrosylated form. ADH5 is a mitochondrial protein that is associated with oxidoreductase activity, nitrosylation (Bateman et al., 2015; Breuer et al., 2013) and is differentially expressed in the hippocampus of AD patients (Guebel and Torres, 2016; Zhang et al., 2015).

Interestingly, data retrieved from the KEGG pathway analysis shows NDUFAB1 (subunit complex I of the mitochondrial respiratory chain) and SDHA (subunit complex II of the mitochondrial respiratory chain) are associated with neurodegenerative disease including AD, Parkinson's and Huntington's disease (Breuer et al., 2013; Kanehisa et al., 2016). NDUFAB1 is essential for energy metabolism as it is a subunit from the first enzyme of the mitochondrial respiratory chain (Sharma et al., 2009). Deficiency of complex I is frequently found in various tissues of patients with neurodegenerative disease such as AD (Kim et al., 2001; Wang et al., 2017). NDUFAB1 has been shown to be responsible for oxidative phosphorylation and downregulated in AD patients (Akila Parvathy Dharshini, 2018; Kim et al., 2001). NDUFAB1 reduction may lead to energy metabolism impairment and result in neuronal cell death (apoptosis) (Kim et al., 2001).

While SDHA is essential for the generation of ATP (oxidative phosphorylation) and involved in the nervous system development (Breuer et

al., 2013; Grimm, 2013). Oxidative stress induces the increase of SDHA expression in the brain of AD patients (Bubber et al., 2005; Shi and Gibson, 2011). This study identified both proteins as NOS2-dependent SNO modified proteins that increased during aging in APP/PS1 mice. Nitrosylated NDUFAB1 protein has been reported to be increased in Parkinson's disease samples (mouse and human) (Hsu et al., 2005). Increase level of nitrosylated SDHA was found in the ovine mitochondrial of heart failure compare to control samples (Radcliffe et al., 2017). Though nitrosylated SDHA has been identified before, there are not many articles published in relation to AD. Thus, nitrosylated NDUFAB1 and SDHA may be of interest for mechanistic studies and as potential biomarker candidates.

Other interesting proteins were SLC1A3, SLC30A3 and EEF2, which are synapse-related proteins (Bateman et al., 2015; Breuer et al., 2013). SLC1A3 or also known as Excitatory amino Acid Transporter 1 (EEAT1) plays an important role in chemical transmission and glutamate secretion (Bateman et al., 2015). Recently SLC1A3 has been identified to be nitrosylated in AD (Seneviratne et al., 2016). SLC1A3 is a glutamate transporter that is expressed in astrocytes and microglia (Ong et al., 2013; Scott et al., 2002). Aβ impaired glutamate uptake causes glutamate accumulation in the extrasynaptic spaces, resulting in synaptic dysfunction via posttranslational modifications such as nitrosylation (Nakamura et al., 2013; Tu et al., 2014). SLC30A3 (Zinc transporter 3 or ZnT3) is a synaptic protein that is involved in neuronal zinc transport to the synaptic cleft (Bateman et al., 2015; Cole et al., 1999). SLC30A3 protein has been related to amyloid beta synaptic targeting (Deshpande et al., 2009) and found reduced in the prefrontal cortex of AD patients (Beyer et al., 2009; Kurita et al., 2016) and an AD mouse model (Tg2576 mice) (Lee et al., 2012a). Although previous studies showed a decrease of SLC30A3 levels, this study identified for the first time a significant increase in nitrosylated SLC30A3 during the progression of pathology in the AD mouse model investigated. The elevated proportion of nitrosylated SLC30A3 may be caused by an increased NO level of the protein (nitrosylation process) due to inflammation.

EEF2 is a main regulator for protein synthesis (initiation, elongation, and termination), synaptic plasticity, memory and consolidation (Li et al., 2005; Taha et al., 2013). EEF2 protein level is reduced in frontal cortex of AD brain samples (Garcia-Esparcia et al., 2017; Li et al., 2005) and APP/PS2 transgenic mice (Garcia-Esparcia et al., 2017). Increase phosphorylated EEF2 has been linked to AD pathogenesis (Argüelles et al., 2014; Li et al., 2005) and is considered a potential AD biomarker (Henriques et al., 2016). EEF2 phosphorylation prevents it from binding to the ribosome (inactivation), thus decreasing the rate of peptide elongation and protein synthesis (Argüelles et al., 2014). Increased nitrosylated EEF2 has been identified in the synaptosomes of APP transgenic mice compared to wild type (Zareba-Koziol et al., 2014). Our study shows that NOS2-dependent nitrosylated EEF2 is increased in aged APP/PS2 transgenic mice compared to young. Identical peptide sequence (STLTDSLV**C**K) was found, which is in line with the result from Zareba-Koziol et al.

4.7. S-nitrosylated proteins analysis in human synaptosome samples

Although no overlap protein/peptide was found in all three pairwise comparisons of human samples, three synapto-SNO proteins (MOG, FHL1 and GSTM3) were found overlapping during AD disease progression (AD vs MCI and AD vs Control). MOG and FHL2 proteins were identified as nitrosylated for the first time. MOG was identified both in human and mouse results (12-month-old APP/PS1 compared to 12-month-old APP/PS1/NOS2-/- mice). MOG is a component in the central nervous system myelin, which is expressed at the oligodendrocyte plasma membrane and outer surface of the myelin sheath (Bateman et al., 2015; Brunner et al., 1989). Increased MOG has been shown as one of the early biomarkers for memory loss in AD using serum samples (Papuc´ et al., 2015) and CSF of AD patients, which indicates altered immune system activity (Maetzler et al., 2011). It has also been used as a biomarker for multiple sclerosis diagnosis (Olsen et al., 2016). MOG can prevent axonal regeneration and trigger demyelinating autoimmunity through T cell-mediated autoimmune response (Ohtani et al., 2011; Podbielska et al., 2013).

FHL1 is a truncated form of complement factor H and mainly expressed in the cardiac and skeletal muscle (Hellwage et al., 1997; Lee et al., 1998). FHL1 gene mutation results in various chronic myopathies including rigid spine syndrome (RSS), scapuloperoneal (SP) and Emery-Dreifuss muscular dystrophy, which are characterized by an increased accumulation of aggregated proteins and vacuoles with misfolded proteins (Sabatelli et al., 2014). FHL1 protein plays a role in inflammatory reactions by enhancing the phagocytosis of Aβ (Hellwage et al., 1997). Increased expression of FHL1 was found in AD brain homogenates (Strohmeyer et al., 2002). GSTM3 belongs to the glutathione S-transferase (GST) superfamily and acts as a protective enzyme from oxidative stress (Tchaikovskaya et al., 2005). Oxidative stress is increased in the aging brain and appears to contribute to AD pathogenesis (Huang et al., 2016). GSTM3 staining was observed at sites of Aβ deposition, neurofibrillary tangles and in microglia of AD brains (Hong et al., 2009; Maes et al., 2010; Tchaikovskaya et al., 2005) and was also found to be nitrosylated before (Lee et al., 2012b).

Further interesting proteins that were found to be nitrosylated for the first time include PLP1, CAMKI2G, PPIA and CD44. PLP1 (or myelin proteolipid protein) is a major myelin protein of the CNS, which is also involved in inflammatory responses and synaptic transmission (Bateman et al., 2015). In AD frontal cortex samples, the MAG:PLP1 ratio (myelin associated glycoprotein to proteolipid protein 1 ratio) was significantly reduced (Thomas et al., 2015). The MAG:PLP1 ratio was used as an indicator for oxygenation to estimate possible hypoperfussion in AD (Miners et al., 2016). Calcium/calmodulin-dependent protein kinase type II subunit gamma (CAMK2G) is known to have an important role for nervous system development, memory formation and synaptic plasticity (Bateman et al., 2015). CAMK2 is found to be dysregulated in AD cases, and may directly contribute to synaptic degeneration and memory deficits (Ghosh and Giese, 2015). PPIA (peptidyl-prolyl cis-trans isomerase A, also known as CyPA or Cyclophilin A) is a secreted protein from monocytes (Nigro et al., 2013) that determines protein folding and trafficking (Bateman et al., 2015). The secretion of protein PPIA is increased during aging (Li et al., 2011), inflammation (Nigro et al., 2013) and AD (Bell et al., 2012). CD44 is a

cell surface glycoprotein protein that is broadly expressed on immune cells (membranes of B cells, monocytes and mature T cells) and may act as an adhesion molecule for astrocyte (Akiyama et al., 1993; Wak and Saunders, 2006). It is involved in the regulation of synaptic plasticity, neuronal development, neurodegeneration (AD, Parkinson, multiple sclerosis) and immune responses (Bateman et al., 2015; Dzwonek and Wilczynski, 2015; Wak and Saunders, 2006). CD44 expression is induced by the pro-inflammatory cytokine TNF (tumor necrosis factor) and is upregulated on T cells during an immune response (Baaten et al., 2010). The level of CD44 expression is elevated in astrocytes and lymphocytes of AD patients (Akiyama et al., 1993; Dzwonek and Wilczynski, 2015; Mossello et al., 2011). Increased CD44 expression was also observed in the substantia nigra of human Parkinson brains and in astrocytes of Parkinson's mouse model (Neal et al., 2018). Furthermore, CD44 expression is increased in the brains and spinal cords of EAE (experimental autoimmune encephalomyelitis) mouse model of multiple sclerosis (Guan et al., 2011).

4.8. Variance of protein expression in murine and human samples

In an ideal situation, the candidate protein/peptide should be able to characterize the disease with 100% sensitivity and 100% specificity. However in reality, identifying such protein biomarkers has proven to be very difficult. Utilizing the approach from this study, the number of significant SNO proteins/peptides found in human synaptosomes was lower compared to those derived from murine tissue. Human brain tissue samples are difficult for differential proteomics, e.g. due to variable post mortem intervals and preanalytical sample handling (before brain banking). The result of the present study could be influenced by both technical and biological differences.

Technically, murine brain samples can be processed immediately after euthanizing the animal, which is not possible for human brain samples. Moreover, murine brain samples were cooled immediately by perfusion using cold saline solution. Previous studies have shown that controlled cold temperature can lower the activity of nitric oxide synthases in murine and

human samples, as this was demonstrated particularly for NOS2 (Hodges et al., 2006; Venturini et al., 1999). In contrast, there was a post mortem interval for human samples of up to 4 h. Loss of proteins (or nitrosylation of proteins) due to degradation during the postmortem period may have limited the yield of SNO proteins/peptides in human samples (Zareba-Koziol et al., 2014). In order to resolve this, a rapid autopsy program for AD patients, designed to analyze labile PTM within a four-hour post mortem interval is needed (i.e. Rapid Autopsy Program of the University Kentucky Alzheimer's Disease Research Center, UKADRC) (Schmitt et al., 2012). The post-mortem interval and small amounts of biopsy tissue available for the human study, compromise equal comparative measurements with mice samples.

Furthermore, synaptosomes from mouse brains could be prepared without freeze-thaw cycles, whereas human brain samples were acquired as frozen material from a biobank, which did not prepare its specimen specifically for this type of analysis. Potentially, the SNO proteome could be further preserved using appropriate inhibitors or chemical stabilizers in addition to cooling and protease inhibitors, when added instantly during preservation. Such substances have not found widespread use yet, despite some studies reporting use of such inhibitors already (Foster et al., 2012; Koo et al., 2016).

Biologically, mouse genetic backgrounds and environmental factors were planned and controlled, while human factors are heterogeneous and cannot be completely controlled. Lifestyle, disease states, environmental factors, age and genetic variation can also influence the physiological condition of human brains (Rescigno et al., 2017; Tripathy et al., 2011).

4.9. Challenges and limitations of this study

A few challenges and limitations were encountered in this study. Though highly efficient, the whole workflow consists of multiple steps (such as blocking, labeling, enrichment, cleaning, digestion) that are time-consuming and may contribute to inter-run variances. When analyzing reporter ion intensities from the same to same-experiment through all identified peptides (all 6 labels), there was an average variance of 20% between single reporter ion channels and the mean of all channels, which were evaluated through all of the identified peptides. This score shows the method variance was within this range. Variance can be introduced at different stages of analysis, which includes manual preparative pipetting, sample preparation, digestion, IodoTMT™ labeling and enrichment until pooling and analysis of the samples.

To control the variables in this quantitative study, it is best to set up an internal standard, which contains pooled and aliquoted proteins of all representative samples. The internal standard should be added at an early stage of each preparation batch and treated as one of the sixplex samples on each LC- MC-run. This allows to manage any technical errors or inconsistencies that may interfere with quantitation. Although this internal standard cannot diminish inter-run-variances, it could be used for quality control purposes. An internal standard was used throughout the experiment; it was labeled and measured in all runs with iodoTMT126 label reagent. It was expected that this sample would show high correlation between the different raw-files using Pearson correlation coefficient (Figure 10). Variation could be due to the stability of the iodoTMT labeling reagent after reconstitution, which found to be limited to 1 week when stored at -20 °C (Wijasa et al., 2017). Therefore, it is recommended to perform all labeling steps for a study within this time frame.

A further limitation arises from the way of labeling and enrichment. Due to fact that only modified peptides are identified and quantified, the procedure generally depends on MS/MS-based information implied from a single peptide ion. Accordingly, protein identifications are only valid when originated from unique (protein-specific) modified peptides. If the identified peptides are not

unique, protein classes or multiple proteins have to be treated as a potential origin of the peptide.

Another challenge is the statistical analysis. Proteomic detection experiments depend on quantitation at the MS/MS level but iodoTMT is known to undergo ratio compression (Bantscheff et al., 2007; Savitski et al., 2011) and hence will show smaller effects. As a result, the p-values will be higher, and the corrected p-values also increase, which lets less proteins/peptides pass the corrected thresholds (Pascovici et al., 2016). Despite having elevated the fold change, few of the proteins/peptides in this study did not pass the p-value cutoff. This suggests a peptide/protein be classified as non-significant by Limma and RankProduct analyses, though it lies in the 95% bootstrap confidence interval. Instead of focusing only on p-value to indicate the degree of confidence in a statistical conclusion, this study used both the p-value and the confidence interval. The p-values generated during hypothesis testing are dependent on the effect size (i.e. the difference between groups compared) meaning larger differences yield lower p-values (Pascovici et al., 2016).

P-value alone does not inform the size or direction of a difference between different groups, while confidence interval does (Bland and Peacock, 2002). P-value is considered clearer than confidence interval due to its rapid decision (yes-or-no) to decide if a value is statistically significant or not (du Prel et al., 2009). However, this “diagnosis on sight” can lead to misinterpretation, as it can lead to clinical decisions that only based on statistics. Confidence interval gives an estimated range of values, which is likely to contain population of interest (Morey et al., 2016). The confident interval is less inclined to misinterpretation and more informative than the p-value (Wood, 2005).

4.10. Conclusion

In general, investigating S-nitrosylation of proteins/peptides prooved to be difficult due to S-nitrosothiol stability and the low abundance of SNO proteins/peptides (without NO donor treatment for s-nitrosylation). The low amount of synaptosomal material further complicated this work. This study does however provide a list of potential synaptosomal AD biomarker candidates of aberrant S-nitrosylation. For validation of the findings, each selected nitrosylated protein/peptide can be tested by targeted analysis to compare AD, MCI and control non-AD subjects. The results implicate that these candidate proteins/peptides could be beneficial as both early diagnostics and outcome measures; which needs to be confirmed in larger studies using CSF samples.

There are numerous biomarker methods for AD discovery and identification, however there is no single biomarker for AD that can fulfill all the criteria for an ideal biomarker. Definite limitations such as sample handling and lack of method standardization exist for almost all current approaches. Next to this limitation, the application of a combination of biomarkers may be necessary to obtain an accurate and reliable identification of preclinical AD. Therefore, a combination of imaging, biochemical, genetic and cognitive assessments may be essential to achieve the best option for an AD biomarker.

Protocols (supplement)

1. BCA protein assay

1.1. Working solution (Thermo Scientific)

Columns in well plate	4	6	8	12
Stock A (clear white solution)	6.6 mL	10 mL	13 mL	20 mL
Stock B (clear blue solution)	0.14 mL	0.2 mL	0.26 mL	0.4 mL

1.2. BSA standard is prepared from 2mg/ml (vial), diluted with distilled water

1.3. 96 well plate (in duplo, example: 1-2 and 3-4)

	1	2	3	4	…	12
A	25 µl WR	25 µl WR	2.5 µl sample 1	2.5 µl sample 1		
B	25 µl ampuwa / 0	25 µl ampuwa / 0	2.5 µl sample 2	2.5 µl sample 2		
C	25 µl BSA 62.5 µg/mL	25 µl BSA 62.5 µg/mL	2.5 µl sample 3	2.5 µl sample 3		
D	25 µl BSA 125 µg/mL	25 µl BSA 125 µg/mL	2.5 µl sample 4	2.5 µl sample 4		
E	25 µl BSA 250 µg/mL	25 µl BSA 250 µg/mL	2.5 µl sample 5	2.5 µl sample 5		
F	25 µl BSA 500 µg/mL	25 µl BSA 500 µg/mL	2.5 µl sample 6	2.5 µl sample 6		
G	25 µl BSA 1000 µg/mL	25 µl BSA 1000 µg/mL	2.5 µl sample 7	2.5 µl sample 7		
H	25 µl BSA 2000 µg/mL	25 µl BSA 2000 µg/mL	2.5 µl sample 8	2.5 µl sample 8		

1.4. Add 200 µl of working solution to each well (A-H to 1-4)

1.5. Incubate for 30 min to 1 hour (with lid on) at 37 °C -> color will change from clear green to clear purple)

1.6. Read the absorbance at 562 nm against a reagent blank using a microplate reader (Beckman Coulter Co.). The samples concentration was measured with reference to standards.

2. Whole brain tissue homogenization
    2.1. Add 1 ml/ 150 mg tissue (wet weight) homogenization buffer + protease inhibitors.
    2.2. Homogenize tissue using Precellys 24 tissue homogenizer (Bertin technology) at 5500 rpm speed for 20 seconds.
    2.3. Aliquot in 200 µl fractions (H fraction)
    2.4. If it is needed, use one aliquot for RNA extraction, mix it with 1600µl Trizol
    2.5. Lyse 200 µl with an equal volume of RIPA buffer.
    2.6. Sonicate for 15 s, 80% duty, 12% power.
    2.7. Incubate for 30 min on ice.
    2.8. Centrifuge at 100000 g for 30 min in ultra centrifuge (TLA-55) at 4 °C
    2.9. Save supernatant (R fraction) and pellet (F fraction) in – 80 °C

LIST OF PUBLICATIONS

Publications

"S-nitrososynatosome analysis in Alzheimer's disease and transgenic mouse models" (In preparation, first author)

Ardura-Fabregat A, Boddeke EWGM, Boza-Serrano A, Brioschi S, Castro-Gomez S, Ceyzériat K, Dansokho C, Dierkes T, Gelders G, Heneka MT, Hoeijmakers L, Hoffmann A, Iaccarino L, Jahnert S, Kuhbandner K, Landreth G, Lonnemann N, Löschmann PA, McManus RM, Paulus A, Reemst K, Sanchez-Caro JM, Tiberi A, Van der Perren A, Vautheny A, Venegas C, Webers A, Weydt P, Wijasa TS, Xiang X, Yang Y.
"Targeting Neuroinflammation to Treat Alzheimer's Disease"
CNS Drugs. 2017 Dec 19. doi.org/10.1007/2Fs40263-017-0483-3

Wijasa TS, Sylvester M, Brocke-Ahmadinejad N, Kummer MP, Brosseron F, Gieselmann V, Heneka MT.
"Proteome profiling of s-nitrosylated synaptosomal proteins by isobaric mass tags"
J Neurosci Methods. 2017 Aug 5. pii: S0165-0270(17)30287-X.
doi:10.1016/j.jneumeth.2017.08.005

Poster presentations

"Detection of nitrosative changes of the synaptosome as biomarkers of neuroinflamation in Alzheimer's disease". The 2016 Alzheimer's Disease Congress.

"Nitro-Proteomics to discover synaptosomal biomarkers of neuroinflammation in Alzheimer´s disease". DZNE Bonn Science Retreat, Nov 2015.

"Nitrosylation and nitration of synaptosomal proteins in Alzheimer's disease"
EMBL Symposium Mechanisms of Neurodegeneration, June 2015

"Nitro-Proteomics to discover synaptosomal biomarkers of neuroinflammation in Alzheimer´s disease". Venusberg meeting on Neuroinflammation, May 2015

"Nitro-Proteomics to discover synaptosomal biomarkers of neuroinflammation in Alzheimer´s disease".
DZNE Bonn clinical meeting, Dec 2014

"Nitro-Proteomics to discover synaptosomal biomarkers of neuroinflammation in Alzheimer´s disease". Alzheimer's Association International Conference (AAIC), July 2014

"Nitro-Proteomics to discover synaptosomal biomarkers of neuroinflammation in Alzheimer´s disease". Cluster Science Days (ImmunoSensation, Bonn cluster of excellence), November 2014

Acknowledgement:

This work was funded by the German Center for Neurodegenerative Diseases (DZNE e.V.) within the Helmholtz Association, by the German Research Council (DFG, Klinische Forscherguppe 177, TP4), the Institute of Biochemistry and Molecular Biology at the Rheinische Friedrich-Wilhelms University, European Union's Seventh Framework Programme (FP7/2007-2013) under grant agreement n° HEALTH-F2-2011-278850 (INMiND) and the EU-IMI program n° 115568 (AETIONOMY). Michael T. Heneka is a member of the Cluster of Excellence “Immunosensation”.

The Banner Sun Health Research Institute Brain and Body Donation Program is supported by the National Institute of Neurological Disorders and Stroke, U24 NS072026 National Brain and Tissue Resource for Parkinson’s Disease and Related Disorders; National Institute on Aging, P30 AG19610 Arizona Alzheimer’s Disease Core Center; Arizona Department of Health Services, Arizona Alzheimer’s Consortium; Arizona Biomedical Research Commission, Arizona Parkinson's Disease Consortium; Michael J. Fox Foundation for Parkinson’s Research.

Recognitions:

Firstly, I would like to thank my Heavenly Father for His grace, benefaction and for giving me the determination to pursue my dreams.

I acknowledge with extreme gratitude the professional supervision from Prof. Dr. Michael Heneka. Thank you for giving me this amazing opportunity and providing me all the necessary resources for this project. Prof. Dr. Thomas Klockgether, for believing in my research and financing the BIOMARKAPD project. Special thanks to Dr. Frederic Brosseron, for the helpful suggestions throughout my PhD study and patience in answering all of my questions. I also want to give my sincere acknowledgment to Prof. Dr. Volkmar Gieselmann, Dr. Mark Sylvester and Dr. Nahal Ahmadinejad, for their collaboration and full support on the proteomic analysis. I would like to thank the members of my dissertation committee for your time, guidance and feedback.

Also, thanks to Ana Vieira-Saecker, Angelika Griep, Francesco Santarelli and Stephanie Schwartz for helping me with my experiments. Dr. Ildiko Racz, for the time in reviewing my articles and thesis. Dr. Sach Mukherjee, for helping me with the statistic questions. To Ms. Anke Krämer and Ms. Heike Schmitz, thank you for the administrative assistance.

This journey would not have been possible without the support of my family. I am especially grateful to my late mother, father, my aunt Wijanti and late uncle Bert who supported me in every way. I always knew that you believed in me and wanted the best for me. Without your love and support, I wouldn't be in my position now. Thanks to my big brother and sister in law for supporting me whenever I am down. You were always there to support me mentally.

I owe thanks to two very special people. My husband Paul, for his continued and unfailing love, support and understanding, all of which made the completion of this thesis possible. You were always there for me at the times I thought it impossible to continue. And my baby boy, Xavier, whose smile always brightens my day. You are mommy's little miracle. Words can never describe how grateful I am to have both of you. I consider myself the luckiest in the world

to have such a lovely and caring family, standing beside me with their love and unconditional support.

My heart felt regards go to my mother in law and father in law, for their love and moral support. Thank you for taking care of Xavier while I was finishing my articles and thesis.

Finally, my humble thanks for everyone who I failed to mention, that helped me (mentally and physically) complete this study. This dissertation would not have been possible without you. May God reward your kindness.

I dedicate this thesis to my late mother, who has been my constant source of inspiration, and to my late uncle Bert, who always had faith in me. Mommy, uncle Bert, this is for you.

References:

Ahmad, S. (1995). Oxidative stress from environmental pollutants. Arch Insect Biochem Physiol. *29*, 135–157.

Akila Parvathy Dharshini, S. (2018). Exploring the selective vulnerability in Alzheimer disease using tissue specific variant analysis. Genomics.

Akiyama, H., Tooyama, I., Kawamata, T., Ikeda, K., and McGeer, P.L. (1993). Morphological diversities of CD44 positive astrocytes in the cerebral cortex of normal subjects and patients with Alzheimer's disease. Brain Res *632*, 249–259.

Al-Gubory, K.H. (2014). Environmental pollutants and lifestyle factors induce oxidative stress and poor prenatal development. Reprod Biomed Online *29*, 17–31.

Anand, P., and Stamler, J.S. (2012). Enzymatic mechanisms regulating protein S-nitrosylation: implications in health and disease. J. Mol. Med. Berl. Ger. *90*, 233–244.

Argüelles, S., Camandola, S., Cutler, R.G., Ayala, A., and Mattson, M.P. (2014). Elongation factor 2-diphthamide is critical for translation of two IRES-dependent protein targets, XIAP and FGF2, under oxidative stress conditions. Free Radic. Biol. Med. *67*, 131–138.

Baaten, B.J.G., Li, C.-R., and Bradley, L.M. (2010). Multifaceted regulation of T cells by CD44. Commun Integr Biol. *3*, 508–512.

Bai, F., and Witzmann, F.A. (2007). Synaptosome Proteomics. Subcell Biochem *43*, 77–98.

Bantscheff, M., Schirle, M., Sweetman, G., Rick, J., and Kuster, B. (2007). Quantitative mass spectrometry in proteomics: a critical review. Analytical and Bioanalytical Chemistry *389*, 1017–1031.

Barbash, S., and Sakmar, T.P. (2017). Length-dependent gene misexpression is associated with Alzheimer's disease progression. Scientific Reports *7*, 190.

Bateman, A., Martin, M.J., O'Donovan, C., Magrane, M., Apweiler, R., Alpi, E., Antunes, R., Arganiska, J., Bely, B., Bingley, M., et al. (2015). UniProt: A hub for protein information. Nucleic Acids Res. *43*, D204–D212.

Baumann, B., Woehrer, A., Ricken, G., Augustin, M., Mitter, C., Pircher, M., Kovacs, G.G., and Hitzenberger, C.K. (2017). Visualization of neuritic plaques in Alzheimer's disease by polarization-sensitive optical coherence microscopy. Scientific Reports *7*, 43477.

Beach, T.G., Adler, C.H., Sue, L.I., Serrano, G., Shill, H.A., Walker, D.G., Lue, L., Roher, A.E., Dugger, B.N., Maarouf, C., et al. (2015). Arizona Study of Aging and Neurodegenerative Disorders and Brain and Body Donation Program. Neuropathology *35*, 354–389.

Bell, R.D., Winkler, E.A., Singh, I., Sagare, A.P., Deane, R., Wu, Z., Holtzman, D.M., Betsholtz, C., Armulik, A., Sallstrom, J., et al. (2012). Apolipoprotein E controls cerebrovascular integrity via cyclophilin A. Nature *485*, 512–516.

Benhar, M., Forrester, M.T., and Stamler, J.S. (2009). Protein denitrosylation: enzymatic mechanisms and cellular functions. Nat. Rev. Mol. Cell Biol. *10*, 721–732.

Bertram, L., and Tanzi, R.E. (2005). The genetic epidemiology of neurodegenerative disease. J. Clin. Invest. *115*, 1449–1457.

Beyer, N., Coulson, D.T.., Heggarty, S., Ravid, R., Irvine, G.B., Hellemans, J., and Johnston, J.A. (2009). ZnT3 mRNA levels are reduced in Alzheimer's disease post-mortem brain. Molecular Neurodegeneration *4*, 53.

Bland, M., and Peacock, J. (2002). Interpreting statistics with confidence. The Obstetrician and Gynaecologist *4*, 176–180.

Blonder, J., and Veenstra, T.D. (2007). Computational prediction of proteotypic peptides. Expert Rev Proteomics. Expert Rev Proteomics *4*, 351–354.

Bogdan, C., Rollinghoff, M., and Dienfenbach, A. (2000). Reactive oxygen and reactive nitrogen intermediates in innate and specific immunity. Curr Opin Immunol *12*, 64–76.

Booth, R.F., and Clark, J.B. (1978). A rapid method for the preparation of relatively pure metabolically competent synaptosomes from rat brain. Biochem. J *176*, 365–370.

Boyd-Kimball, D., Castegna, A., Sultana, R., Poon, H.F., Petroze, R., Lynn, B.C., Klein, J.B., and Butterfield, D.A. (2005). Proteomic identification of proteins oxidized by Abeta(1-42) in synaptosomes: implications for Alzheimer's disease. Brain Res. *1044*, 206–215.

Braak, H., and Braak, E. (1991). Neuropathological stageing of Alzheimer-related changes. Acta Neuropathol. (Berl.) *82*, 239–259.

Braak, H., and Del Tredici, K. (2011). The pathological process underlying Alzheimer's disease in individuals under thirty. Acta Neuropathol. (Berl.) *121*, 171–181.

Braak, H., Thal, D.R., Ghebremedhin, E., and Del Tredici, K. (2011). Stages of the Pathologic Process in Alzheimer Disease: Age Categories From 1 to 100 Years. J Neuropathol Exp Neurol. *70*, 960–969.

Breitling, R., Armengaud, P., Amtmann, A., and Herzyk, P. (2004). Rank products: a simple, yet powerful, new method to detect differentially regulated genes in replicated microarray experiments. FEBS *573*, 83–92.

Breuer, K., Foroushani, A.K., Laird, M.R., Chen, C., Sribnaia, A., Lo, R., Winsor, G.L., Hancock, R.E.W., Brinkman, F.S.L., and Lynn, D.J. (2013). InnateDB: systems biology of innate immunity and beyond—recent updates and continuing curation. Nucl. Acids Res. *41*, 1228–1233.

Bruijn, R.F.A.G. De, and Ikram, M.A. (2014). Cardiovascular risk factors and future risk of Alzheimer ' s disease. BMC Med. *12*, 130.

Brunner, C., Lassmann, H., Waehneldt, T., and Matthieu, J.M. (1989). Differential ultrastructural localization of myelin basic pro- tein, myelin/oligodendroglial glycoprotein, and 2′,3′-cyclic nucleotide 3′-phosphodiesterase in the CNS of adult rats. J Neurochem 52 *52*, 296–304.

Bubber, P., Haroutunian, V., Fisch, G., Blass, J.P., and Gibson, G.E. (2005). Mitochondrial abnormalities in Alzheimer brain: Mechanistic implications. Ann. Neurol. *57*, 695–703.

Cai, H., Cong, W., Ji, S., Rothman, S., Maudsley, S., and Martin, B. (2012). Metabolic Dysfunction in Alzheimer's Disease and Related Neurodegenerative Disorders. Curr Alzheimer Res. *9*, 5–17.

Castellani, R.J., Rolston, R.K., and Smith, M.A. (2010). Alzheimer Disease. Dis. Mon. *56*, 484–546.

Chang, A.C.Y., Ong, S.-G., LaGory, E.L., Kraft, P.E., Giaccia, A.J., Wu, J.C., and Blau, H.M. (2016). Telomere shortening and metabolic compromise underlie dystrophic cardiomyopathy. Proc Natl Acad Sci U S A. *113*, 13120–13125.

Chang, R.Y.K., Nouwens, A.S., Dodd, P.R., and Etheridge, N. (2013). The synaptic proteome in Alzheimer's disease. Alzheimers Dement. J. Alzheimers Assoc. *9*, 499–511.

Chen, X., Guan, T., Li, C., Shang, H., Cui, L., Li, X.-M., and Kong, J. (2012). SOD1 aggregation in astrocytes following ischemia/reperfusion injury: a role of NO-mediated S-nitrosylation of protein disulfide isomerase (PDI). J. Neuroinflammation *9*, 237–237.

Chen, Y., Ching, W., Lin, Y., and Chen, Y. (2013). Methods for detection and characterization of protein S-nitrosylation. Methods *62*, 138–150.

Chintamaneni, M., and Bhaskar, M. (2012). Biomarkers in Alzheimer's disease: a review. ISRN Pharmacol. *2012*, 984786–984786.

Choi, Y., Tenneti, L., Le, D.A., Ortiz, J., Bai, G., Chen, H.V., and Lipton, S.A. (2000). Molecular basis of NMDA receptor- coupled ion channel modulation by S-nitrosylation. Nat. Neurosci. *3*, 15–21.

Chow, V.W., Mattson, M.P., Wong, P.C., and Gleichmann, M. (2011). An Overview of APP Processing Enzymes and Products. Neuromolecular Med. *12*, 1–12.

Chung, K.K.K. (2007). Say NO to Neurodegeneration : Role of S -Nitrosylation in Neurodegenerative Disorders. Neurosignals *15*, 307–313.

Clayton, D.A., and Shadel, G.S. (2014). Purification of Mitochondria by Sucrose Step Density Gradient Centrifugation. Cold Spring Harb. Protoc. *2014*, pdb.prot080028.

Cole, T.B., Wenzel, H.J., Kafer, K.E., Schwartzkroin, P.A., and Palmiter, R.D. (1999). Elimination of zinc from synaptic vesicles in the intact mouse brain by disruption of the ZnT3 gene. Proc Natl Acad Sci U S A *96*, 1716–1721.

Colton, C.A., Vitek, M.P., Wink, D.A., Xu, Q., cantillana, V., Previti, M.L., and Nostrand, W.E. (2006). NO synthase 2 (NOS2) deletion promotes multiple pathologies in a mouse model of Alzheimer's disease. Proc. Natl. Acad. Sci. *103*, 12867–12872.

Colton, C.A., Wilcock, D.M., Wink, D.A., Davis, J., Van, W.E., and Vitek, M.P. (2008). The Effects of NOS2 Gene Deletion on Mice Expressing Mutated Human AβPP. J Alzheimer Dis. *15*, 571–587.

Crous-Bou, M., Minguillon, C., Gramunt, N., and Molinuevo, J.L. (2017). Alzheimer's disease prevention: from risk factors to early intervention. Alzheimers Res. Ther. *9*, 71.

Davies, C.A.A., Mann, D.M.A.M., Sumpter, P.Q.Q., and Yates, P.O.O. (1987). A quantitative morphometric analysis of the neuronal and synaptic content of the frontal and temporal cortex in patients with Alzheimer's disease. J Neurol Sci *78*, 151–164.

Dayon, L., and Sanchez, J. (2012). Relative protein quantification by MS/MS using the tandem mass tag technology. Methods Mol. Biol. *893*, 115–127.

Deshpande, A., Kawai, H., Metherate, R., Glabe, C.G., and Busciglio, J. (2009). A role for synaptic zinc in activity-dependent Abeta oligomer formation and accumulation at excitatory synapses. J Neurosci. *29*, 4004–4015.

Dudoit, S., van der Laan, M.J., and Pollard, K.S. (2004). Multiple testing. Part I. Single-step procedures for control of general type I error rates. Stat Appl Genet Mol Biol *3*.

Dzwonek, J., and Wilczynski, G.M. (2015). CD44: molecular interactions, signaling and functions in the nervous system. Front Cell Neurosci. *9*, 175.

Eden, E., Navon, R., Steinfeld, I., Lipson, D., and Yakhini, Z. (2009). GOrilla: a tool for discovery and visualization of enriched GO terms in ranked gene lists. BMC Bioinformatics *10*, 48.

Efron, B., and Tibshirani, R.J. (1993). An introduction to the Bootstrap (Chapman & Hall, New York).

Engmann, O., Campbell, J., Ward, M., Giese, K.P., and Thompson, A.J. (2010). Comparison of a protein-level and peptide-level labeling strategy for quantitative proteomics of synaptosomes using isobaric tags. J. Proteome Res. *9*, 2725–2733.

Europa.eu (2017). New scientific yardstick to help early diagnosis of Alzheimer's disease.

Faraco, G., Wijasa, T.S., Park, L., Moore, J., Anrather, J., and Iadecola, C. (2014). Water deprivation induces neurovascular and cognitive dysfunction through vasopressin-induced oxidative stress. J. Cereb. Blood Flow Metab. Off. J. Int. Soc. Cereb. Blood Flow Metab. *34*, 1–9.

Fenyk-Melody, J.E., Garrison, A.E., Brunnert, S.R., Weidner, J.R., Shen, F., Shelton, B.A., and Mudgett, J.S. (1998). Experimental Autoimmune Encephalomyelitis Is Exacerbated in Mice Lacking the NOS2 Gene. J Immunol *160*, 2940–2946.

Fiandaca, M.S., Mapstone, M.E., Cheema, A.K., and Federoff, H.J. (2014). The critical need for defining preclinical biomarkers in Alzheimer ' s disease. Alzheimers Dement. *10*, S196–S212.

Fillenbaum, G.G., van Belle, G., Morris, J.C., Mohs, R.C., Mirra, S.S., Davis, P.C., Tariot, P.N., Silverman, J.M., Clark, C.M., Welsh-Bohmer, K.A., et al. (2008). CERAD (Consortium to Establish a Registry for Alzheimer's Disease) The first 20 years. Alzheimers Dement. *4*, 96–109.

Finkel, T. (2011). Signal transduction by reactive oxygen species. J. Cell Biol. Cell Biol. *194*, 7–15.

Flicker, C., Ferris, S.H., and Reisberg, B. (1991). Mild cognitive impairment in the elderly: Predictors of dementia . Neurology *41*, 1006.

Forrest, M.S., Lan, Q., Hubbard, A.E., Zhang, L., Vermeulen, R., Zhao, X., Li, G., Wu, Y.-Y., Shen, M., Yin, S., et al. (2005). Discovery of novel biomarkers by microarray analysis of peripheral blood mononuclear cell gene expression in benzene-exposed workers. Environ Health Perspect *113*, 801–807.

Förstermann, U., and Sessa, W.C. (2012). Nitric oxide synthases: Regulation and function. Eur. Heart J. *33*, 829–837.

Forstermann, U., Closs, E.I., Pollock, J.S., Nakane, M., Schwarz, P., Gath, I., and Kleinert, H. (1994). Nitric Oxide Synthase Isozymes Characterization, Purification, Molecular Cloning, and Functions Ulrich. Hypertension *23*, 1121–1131.

Foster, M.W., Yang, Z., Gooden, D.M., Thompson, J.W., Ball, C.H., Turner, M.E., Hou, Y., Pi, J., Moseley, M.A., and Que, L.G. (2012). Proteomic Characterization of the Cellular Response to Nitrosative Stress Mediated by S-Nitrosoglutathione Reductase Inhibition. J. Proteome Res. 2480–2491.

Furukawa, K., Sopher, B.L., Rydel, R., Begley, J.G., Pham, D.G., Martin, G.M., and Mattson, M.P. (1996). Increased Activity-Regulating and Neuroprotective Efficacy of a-Secretase-Derived Secreted Amyloid Precursor Protein Conferred by a C-Terminal Heparin-Binding Domain. J. Neurochem. *67*, 1882–1896.

Galasko, D., and Montine, T. j (2010). Biomarkers of Oxidative Damage and Inflammation in Alzheimer´s Disease. Biomark Med *4*, 27–36.

Gamazon, E.R., Trendowski, M.R., Wen, Y., Wing, C., Delaney, S.M., Huh, W., Wong, S., Cox, N.J., and Dolan, M.E. (2018). Gene and MicroRNA Perturbations of Cellular Response to Pemetrexed Implicate Biological Networks and Enable Imputation of Response in Lung Adenocarcinoma. Scientific Reports *8*, 733.

Garcia-Esparcia, P., Sideris-Lampretsas, G., Hernandez-Ortega, K., Grau-Rivera, O., Sklaviadis, T., Gelpi, E., and Ferrer, I. (2017). Altered mechanisms of protein synthesis in frontal cortex in Alzheimer disease and a mouse model. Am J Neurodegener Dis. *6*, 15–25.

Gendron, T.F., and Petrucelli, L. (2009). The role of tau in neurodegeneration. Mol. Neurodegener. *4*, 13.

Ghosh, A., and Giese, K.P. (2015). Calcium/calmodulin-dependent kinase II and Alzheimer's disease. Mol Brain *8*, 78.

Glass, C.K., Saijo, K., Winner, B., Marchetto, M.C., and Gage, F.H. (2010). Mechanisms Underlying Inflammation in Neurodegeneration. Cell *140*, 918–934.

Gleason, O.C. (2003). Delirium. Am. Fam. Physician *67*, 1027–1034.

Goate, A., Chartier-Harlin, M., Mullan, M., Brown, J., Crawford, F., Fidani, L., Giuffra, L., Haynes, A., Irving, N., James, L., et al. (1991). Segregation of a missense mutation in the amyloid precursor protein gene with familial Alzheimer's disease. Nature *349*, 704–706.

Gould, N., Doulias, P.-T., Tenopoulou, M., Raju, K., and Ischiropoulos, H. (2013). Regulation of protein function and signaling by reversible cysteine S-nitrosylation. J. Biol. Chem. *288*, 26473–26479.

Graeber, M.B., and Möller, H.J. (1998). The case described by Alois Alzheimer in 1911. Eur. Arch. Psychiatry Clin. Neurosci. *248*, 111–122.

Gray, E., and Whittaker, V.P. (1962). The isolation of nerve endings from brain: an electron-microscopic study of cell fragments derived by homogenization and centrifugation. J Anat. *96*, 79–88.

Green, S.J., Scheller, L.F., Marietta, M.A., Seguin, M.C., Klotz, F.W., Slayter, M., Nelson, B.J., and Nacy, C.A. (1994). Nitric Oxide : Cytokine-regulation of nitric oxide in host resistance to intracellular pathogens. Immunol. Lett. *43*, 87–94.

Guan, H., Nagarkatti, P.S., and Nagarkatti, M. (2011). CD44 reciprocally regulates the differentiation of encephalitogenic Th1/Th17 and Th2/Treg cells through epigenetic modulation involving DNA methylation of cytokine gene promoters thereby controlling the development of experimental autoimmune encephalomyelitis. J Immunol *186*, 6955–6964.

Guebel, D.V., and Torres, N.V. (2016). Sexual Dimorphism and Aging in the Human Hyppocampus: Identification, Validation, and Impact of Differentially Expressed Genes by Factorial Microarray and Network Analysis. Front. Aging Neurosci. *8*, 229.

Gundry, R.L., White, M.Y., Murray, C.I., Kane, L.A., Fu, Q., Stanley, B.A., and Van Eyk, J.E. (2009). Preparation of Proteins and Peptides for Mass Spectrometry Analysis in a Bottom-Up Proteomics Workflow. Curr Protoc Mol Biol. *Unit 10.25*.

Habib, S., and Ali, A. (2011). Biochemistry of Nitric Oxide. Indian J. Clin. Biochem. *26*, 3–17.

Hebert, L.E., Weuve, J., Scherr, P.A., and Evans, D.A. (2013). Alzheimer disease in the United States (2010 – 2050) estimated using the 2010 Census. Neurology *80*, 1778–1783.

Hellwage, J., Kuhn, S., and Zipfel, P.F. (1997). The human complement regulatory factor-H-like protein 1, which represents a truncated form of factor H, displays cell-attachment activity. Biochem. J. *326*, 321–327.

Heneka, M.T., and Feinstein, D.L. (2001). Expression and function of inducible nitric oxide synthase in neurons. J. Neuroimmunol. *114*, 8–18.

Heneka, M.T., O'Banion, M.K., Terwel, D., and Kummer, M.P. (2010). Neuroinflammatory processes in Alzheimer's disease. J. Neural Transm. *117*, 919–947.

Heneka, M.T., Kummer, M.P., and Latz, E. (2014). Innate immune activation in neurodegenerative disease. nature reviews immunology *14*, 463–477.

Heneka, M.T., Carson, M.J., Khoury, J. El, Landreth, G.E., Brosseron, F., Feinstein, D.L., Jacobs, A.H., Wyss-Coray, T., Vitorica, J., Ransohoff, R.M., et al. (2015). Neuroinflammation in Alzheimer's disease. Lancet Neurol. *14*, 388–405.

Heneka, M.T., Golenbock, D.T., and Latz, E. (2015b). Innate immunity in Alzheimer's disease. Nat Immunol *16*, 229–236.

Henriques, A.G., Müller, T., Oliveira, J.M., Cova, M., da Cruz e Silva, C.B., and da Cruz e Silva, O.A.B. (2016). Altered protein phosphorylation as a resource for potential AD biomarkers. Sci Rep *6*, 30319.

Hinkle, D., Wiersma, W., and Jurs, S. (2003). Applied Statistics for the Behavioral Sciences (Boston: Houghton Mifflin).

Hippius, H. (2003). The discovery of Alzheimer's disease. Dialogues Clin. Neurosci. *5*, 101–108.

Hodges, G.J., Zhao, K., Kosiba, W.A., and Johnson, J.M. (2006). The involvement of nitric oxide in the cutaneous vasoconstrictor response to local cooling in humans. J Physiol *574*, 849–857.

Hong, G.-S., Heun, R., Jessen, F., Popp, J., Hentschel, F., Kelemen, P., Schulz, A., Maier, W., and Kölsch, H. (2009). Gene variations in GSTM3 are a risk factor for Alzheimer's disease. Neurobiol Aging *30*, 691–696.

Hsu, M., Srinivas, B., Kumar, J., Subramanian, R., and Andersen, J. (2005). Glutathione depletion resulting in selective mitochondrial complexI inhibition in dopaminergic cells is via an NO-mediated pathwaynot involving peroxynitrite: implications for Parkinson's disease. Journal of Neurochemistry *92*, 1091–1103.

Huang, W.-J., Zhang, X., and Chen, W.-W. (2016). Role of oxidative stress in Alzheimer's disease. Biomed Rep. *4*, 519–522.

Hyman, B.T., Phelps, C.H., Beach, T.G., Bigio, E.H., Cairns, N.J., Carrillo, M.C., Dickson, D.W., Duyckaerts, C., Frosch, M.P., Masliah, E., et al. (2012). National institute on aging-Alzheimer's association guidelines for the neuropathologic assessment of Alzheimer's disease: A practical approach. Acta Neuropathol. (Berl.) *8*, 1–13.

Issaq, H.J., Conrads, T.P., Janini, G.M., and Veenstra, T.D. (2002). Methods for fractionation, separation and profiling of proteins and peptides. Electrophoresis *23*, 3048–3061.

Jaffrey, S.R., and Snyder, S.H. (2001). The biotin switch method for the detection of S-nitrosylated proteins. Sci STKE *2001*, pl1.

Jankowsky, J.L., Slunt, H.H., Ratovitski, T., Jenkins, N.A., Copeland, N.G., and Borchelt, D.R. (2001). Co-expression of multiple transgenes in mouse CNS: A comparison of strategies. Biomol. Eng. *17*, 157–165.

Jeannin, P., Chaze, T., Gianetto, Q.G., Matondo, M., Gout, O., Gessain, A., and Afonso, P.V. (2018). Proteomic analysis of plasma extracellular vesicles reveals mitochondrial stress upon HTLV-1 infection. Scientific Reports *8*, 5170.

Jensen, E.C. (2012). The Basics of Western Blotting. Anat. Rec. *295*, 369–371.

Ju, Y., Fu, M., Wu, L., and Yang, G. (2015). Strategies and Tools for Detection of Protein S-Nitrosylation and S-Sulfhydration. Biochem. Anal. Biochem. *4*, 4.

Kaddurah-Daouk, R., Zhu, H., Sharma, S., Bogdanov, M., Rozen, S.G., Matson, W., Oki, N.O., Motsinger-Relf, A.A., Churchill, E., Lei, Z., et al. (2013). Alterations in metabolic pathways and networks in Alzheimer's disease. Transl Psychiatry. *3*, e244.

Kanehisa, M., Sato, Y., Kawashima, M., Furumichi, M., and Tanabe, M. (2016). KEGG as a reference resource for gene and protein annotation. Nucl. Acids Res. *44*, 457–462.

Kim, S.H., Vlkolinsky, R., Caims, N., Fountoulakis, M., and Lubec, G. (2001). The reduction of NADH: Ubiquinone oxidoreductase 24- and 75-kDa subunits in brains of patients with Down syndrome and Alzheimer's disease. Life Sci. *68*, 2741–2750.

Kiss, D.S., Toth, I., Jocsak, G., Sterczer, A., Bartha, T., Frenyo, L. V, and Zsarnovszky, A. (2016). Preparation of purified perikaryal and synaptosomal mitochondrial fractions from relatively small hypothalamic brain samples. MethodsX *3*, 417–429.

Kito, K., and Ito, T. (2008). Mass Spectrometry-Based Approaches Toward Absolute Quantitative Proteomics. Curr. Genomics *9*, 263–274.

Knowles, R.G., and Moncada, S. (1994). Nitric oxide synthases in mammals. Biochem. J. *298*, 249–258.

Koo, S., Spratt, H.M., Soman, K. V, Stafford, S., Gupta, S., Petersen, J.R., Zago, M.P., Kuyumcu-martinez, M.N., Brasier, A.R., Wiktorowicz, J.E., et al. (2016). S-Nitrosylation Proteome Profile of Peripheral Blood Mononuclear Cells in Human Heart Failure. Int. J. Proteomics *2016*, 1–19.

Korolev, I. (2014). Alzheimer's Disease: A Clinical and Basic Science Review. Med. Stud. Res. J. *4*, 24–33.

Kummer, M.P., and Heneka, M.T. (2014). Truncated and modified amyloid-beta species. Alzheimers Res. Ther. *6*, 28.

Kummer, M.P., Hülsmann, C., Hermes, M., Axt, D., and Heneka, M.T. (2012). Nitric oxide decreases the enzymatic activity of insulin degrading enzyme in APP/PS1 mice. J. Neuroimmune Pharmacol. Off. J. Soc. NeuroImmune Pharmacol. *7*, 165–172.

Kurita, H., Okuda, R., Yokoo, K., Inden, M., and Hozumi, I. (2016). Protective roles of SLC30A3 against endoplasmic reticulum stress via ERK1/2 activation. Biochem Biophys Res Commun. *479*, 853–859.

Kuster, B., Schirle, M., Mallick, P., and Aebersold, R. (2005). Scoring proteomes with proteotypic peptide probes. Nat Rev Mol Cell Biol *6*, 577–583.

Laferla, F.M., Green, K.N., and Oddo, S. (2007). Intracellular amyloid-β in Alzheimer's disease. Nat. Rev. Neurosci. *8*, 499–509.

Lee, J.-Y., Cho, E., Seo, J.-W., Hwang, J.J., and Koh, J.-Y. (2012a). Article Navigation Alteration of the Cerebral Zinc Pool in a Mouse Model of Alzheimer Disease. J Neuropathol Exp Neurol. *71*, 211–222.

Lee, S.M., Tsui, S.K., Chan, K.K., Gracia-Barcelo, M., Waye, M.M., Fung, K.P., Liew, C.C., and Lee, C.Y. (1998). Chromosomal mapping, tissue distribution and cDNA sequence of four-and-a-half LIM domain protein 1 (FHL1). gene *216*, 163–170.

Lee, T.Y., Chen, Y.J., Lu, C.T., Ching, W.C., Teng, Y.C., Huang, H. Da, and Chen, Y.J. (2012b). dbSNO: A database of cysteine S-nitrosylation. Bioinformatics *28*, 2293–2295.

Li, J., Xie, H., Yi, M., Lefang, P., Dan, L., Xiang, C., and Jian, D. (2011). Expression of cyclophilin A and CD147 during skin aging. Zhong Nan Da Xue Xue Bao Yi Xue Ban. *36*, 203–211.

Li, X., Alafuzoff, I., Soininen, H., Winblad, B., and Pei, J.-J. (2005). Levels of mTOR and its downstream targets 4E-BP1, eEF2, and eEF2 kinase in relationships with tau in Alzheimer's disease brain. FEBS J. *272*, 4211–4220.

Liu, Y., Qing, H., and Deng, Y. (2014). Biomarkers in Alzheimer ' s Disease Analysis by Mass Spectrometry-Based Proteomics. Int J Mol Sci. 7865–7882.

Maes, O., Schipper, H.M., Chong, G., Chertkow, H.M., and Wang, E. (2010). A GSTM3 polymorphism associated with an etiopathogenetic mechanism in Alzheimer disease. Neurobiol Aging *31*, 34–45.

Maetzler, W., Berg, D., Synofzik, M., Brockmann, K., Godau, J., Melms, A., Gasser, T., Hörnig, S., and Langkamp, M. (2011). Autoantibodies against amyloid and glial-derived antigens are increased in serum and cerebrospinal fluid of Lewy body-associated dementias. J Alzheimers Dis. *26*, 171–179.

Mallick, P., Schirle, M., Chen, S.S., Flory, M.R., Lee, H., Martin, D., Ranish, J., Raught, B., Schmitt, R., Werner, T., et al. (2007). Computational prediction of proteotypic peptides for quantitative proteomics. Nat. Biotechnol *25*, 125–131.

Mangialasche, F., Polidori, M.C., Monastero, R., Ercolani, S., Camarda, C., Cecchetti, R., and Mecocci, P. (2009). Biomarkers of oxidative and nitrosative damage in Alzheimer's disease and mild cognitive impairment. Ageing Res. Rev. *8*, 285–305.

Mannick, J.B., and Schonhoff, C.M. (2002). Nitrosylation: the next phosphorylation? Arch Biochem Biophys *408*, 1–6.

Martínez-ruiz, A., Cadenas, S., and Lamas, S. (2011). Nitric oxide signaling: classical, less classical, and nonclassical mechanisms. Free Radic. Biol. Med. *51*, 17–29.

Mateus, A., Bobonis, J., Kurzawa, N., Stein, F., Helm, D., Hevler, J., Typas, A., and Savitski, M.M. (2018). Thermal proteome profiling in bacteria: probing protein state in vivo. Molecular Systems Biology *14*, e8242.

Mattila, J.T., and Thomas, A.C. (2014). Nitric Oxide Synthase: Non-Canonical Expression Patterns. Front Immunol. *5*, 478.

Mattson, M.P. (1997). Cellular Actions of & 4myloid Precursor Protein and Its Soluble and Fibrillogenic Derivatives. Physiol. Rev. *77*, 1081–1132.

Miners, J.S., Palmer, J.C., and Love, S. (2016). Pathophysiology of Hypoperfusion of the Precuneus in Early Alzheimer's Disease. Brain Pathol. *26*, 533–541.

Mirra, S.S., Heyman, A., McKeel, D., Sumi, S.M., Crain, B.J., Brownlee, L.M., Vogel, F.S., Hughes, J.P., van Belle, G., and Berg, L. (1991). The Consortium to Establish a Registry for Alzheimer's Disease (CERAD). Part II. Standardization of the neuropathologic assessment of Alzheimer's disease. Neurology *41*, 479–486.

Mitchelmore, C., Bu¨chmann-Møller, S., Rask, L., West, M.J., Troncoso, J.C., and Jensen, N. (2004). NDRG2: a novel Alzheimer's disease associated protein. Neurobiol Dis. *16*, 48–58.

Mitulovic, G., and Mechtler, K. (2006). HPLC techniques for proteomics analysis--a short overview of latest developments. Brief Funct Genomic Proteomic *5*, 249–260.

Montine, T.J., Phelps, C.H., Beach, T.G., Bigio, E.H., Cairns, N.J., Dickson, D.W., Duyckaerts, C., Frosch, M.P., Masliah, E., Mirra, S.S., et al. (2012). National institute on aging-Alzheimer's association guidelines for the neuropathologic assessment of Alzheimer's disease: A practical approach. Acta Neuropathol. (Berl.) *123*, 1–11.

Morey, R.D., Hoekstra, R., Rouder, J.N., Lee, M.D., and Wagenmakers, E.-J. (2016). The fallacy of placing confidence in confidence intervals. Psychonomic Bulletin & Review *23*, 103–123.

Mossello, E., Ballini, E., Mello, A.M., Tarantini, F., Simoni, D., Baldasseroni, S., and Marchionni, N. (2011). Biomarkers of Alzheimer's Disease: From Central Nervous System to Periphery? International Journal of Alzheimer's Disease *2011*, *Article ID 342980*, 7 pages.

Mukaka, M. (2012). A guide to appropriate use of Correlation coefficient in medical research. Malawi Med J. *24*, 69–71.

Mukherjee, S.., Sykacek, P., Roberts, S.., and Gurr, S.. (2003). Gene Ranking Using Bootstrapped P-values. Sigkdd Explor. *5*, 14.

Nagy, A., and Delgado-Escuata, A.V. (1984). Rapid preparation of synaptosomes from mammalian brain using nontoxic isoosmotic gradient material (Percoll). J Neurochem. *43*, 1114–1123.

Nakamura, T., and Lipton, S. a (2016). Protein s-nitrosylation as a therapeutic target for neurodegenerative diseases. Sci Trends Pharmacol *37*, 73–84.

Nakamura, T., and Lipton, S.A. (2007). S-Nitrosylation and uncompetitive / fast off-rate (UFO) drug therapy in neurodegenerative disorders of protein misfolding. Cell Death Differ. *14*, 1305–1314.

Nakamura, T., Cho, D.-H., and Lipton, S.A. (2012). Redox regulation of protein misfolding, mitochondrial dysfunction, synaptic damage, and cell death in neurodegenerative diseases. Exp. Neurol *238*, 12–21.

Nakamura, T., Tu, S., Akhtar, M.W., Sunico, C.R., Okamoto, S.-I., and Lipton, S. a (2013). Aberrant protein s-nitrosylation in neurodegenerative diseases. Neuron *78*, 596–614.

Neal, M.L., Boyle, A.M., Budge, K.M., Safadi, F.F., and Richardson, J.R. (2018). The glycoprotein GPNMB attenuates astrocyte inflammatory responses through the CD44 receptor. Journal of Neuroinflammation *15*, 73.

Nesvizhskii, A.I. (2007). Protein Identification by Tandem Mass Spectrometry and Sequence Database Searching. Methods Mol Biol *367*, 87–119.

Nigro, P., Pompilio, G., and Capogrossi, M. (2013). Cyclophilin A: a key player for human disease. Cell Death and Disease *4*, e888.

Nilsson, T., Mann, M., Aebersold, R., Iii, J.R.Y., Bairoch, A., and Bergeron, J.J.M. (2010). Mass spectrometry in high-throughput proteomics : ready for the big time. Nat. Publ. Group *7*, 681–685.

Ohtani, S., Kohyama, K., and Matsumoto, Y. (2011). Autoantibodies recognizing native MOG are closely associated with active demyelination but not with neuroinflammation in chronic EAE. Neuropathology *31*, 101–111.

Olsen, J.A., Kenna, L.A., Tipon, R.C., Spelios, M.G., stecker, M.M., and Akirav, E.M. (2016). A Minimally-invasive Blood-derived Biomarker of Oligodendrocyte Cell-loss in Multiple Sclerosis. EBioMedicine *10*, 227–235.

Ong, S. (2010). Whole proteomes as internal standards in quantitative proteomics. Genome Med. *2*, 49.

Ong, W.Y., Tanaka, K., Dawe, G.S., Ittner, L.M., and Farooqui, A.A. (2013). Slow Excitotoxicity in Alzheimer's Disease. Journal of Alzheimer's Disease *35*, 643–668.

Papuc´, E., Kurys-Denis, E., Krupski, W., Tatara, M., and Rejdak, K. (2015). Can Antibodies Against Glial Derived Antigens be Early Biomarkers of Hippocampal Demyelination and Memory Loss in Alzheimer's Disease? Journal of Alzheimer's Disease *48*, 115–121.

Pascovici, D., Handler, D., Wu, J.X., and Haynes, P.A. (2016). Multiple testing corrections in quantitative proteomics: a useful but blunt tool. proteomics *16*, 2448–2453.

de Paula, V. de J.R., Guimarães, F.M., Diniz, B.S., and Forlenza, O.V. (2009). Neurobiological pathways to Alzheimer's disease: Amyloid-beta, TAU protein or both? Dement Neuropsychol *3*, 188–194.

Petersen, Ronald C. (2009). Early Diagnosis of Alzheimer's Disease: Is MCI Too Late? *6*, 324–330.

Plácido, A.I., Pereira, C.M.F., Duarte, A.I., Candeias, E., Correia, S.C., Santos, R.X., and Carvalho, C. (2014). The role of endoplasmic reticulum in amyloid precursor protein processing and traf fi cking : Implications for Alzheimer ' s disease. Biochim. Biophys. Acta *1842*, 1444–1453.

Podbielska, M., Banik, N.L., Kurowska, E., and Hogan, E.L. (2013). Myelin Recovery in Multiple Sclerosis: The Challenge of Remyelination. Brain Sci. *3*, 1282–1324.

du Prel, J.-B., Hommel, G., Röhrig, B., and Blettner, M. (2009). Confidence Interval or P-Value? Dtsch Arztebl Int *106*, 335–339.

Pursiheimo, A., Vehmas, A.P., Afzal, S., Suomi, T., Chand, T., Strauss, L., Poutanen, M., Rokka, A., Corthals, G.L., and Elo, L.L. (2015). Optimization of Statistical Methods Impact on Quantitative Proteomics Data. J. Proteome Res. *14*, 4118–4126.

Qiu, C., Kivipelto, M., and Von Strauss, E. (2009). Epidemiology of Alzheimer's disease: occurrence, determinants, and strategies toward intervention. Dialogues Clin. Neurosci. *11*, 111–128.

Qu, F., Yang, M., and Rasooly, A. (2016). Dual signal amplification electrochemical biosensor for monitoring the activity and inhibition of the Alzheimer related protease # -secretase (BACE1) Dual signal amplification electrochemical biosensor for monitoring the activity and inhibition of the A. Anal. Chem. *88*, 10559–10565.

Qu, J., Nakamura, T., Cao, G., Holland, E.A., Mckercher, S.R., and Lipton, S.A. (2011). S-Nitrosylation activates Cdk5 and contributes to synaptic spine loss induced by β -amyloid peptide. Proc. Natl. Acad. Sci. *108*, 14330–14335.

Qu, Z., Meng, F., Bomgarden, R.D., Viner, R.I., Li, J., Rogers, J.C., Cheng, J., Greenlief, C.M., Cui, J., Lubahn, D.B., et al. (2014a). Proteomic quantification and site-mapping of S -nitrosylated proteins using isobaric iodoTMT reagents. J. Proteome Res. *13*, 3200–3211.

Qu, Z., Meng, F., Zhou, H., Li, J., Wang, Q., Wei, F., Cheng, J., Greenlief, C.M., Lubahn, D.B., Sun, G.Y., et al. (2014b). NitroDIGE analysis reveals inhibition of protein S-nitrosylation by epigallocatechin gallates in lipopolysaccharide-stimulated microglial cells. J. Neuroinflammation *11*, 17.

Radcliffe, E., Sun, J., Aponte, A., Eisner, D., Murphy, E., and Trafford, A. (2017). Heart failure increases mitochondrial s-nitrosylation. Heart *103*, A1–A162.

Reczek, E.E., James, M.F., and Brems, H. (2006). NO synthase 2 (NOS2) deletion promotes multiple pathologies in a mouse model of Alzheimer's disease. Proc. Natl. Acad. Sci. *103*, 12867–12872.

Ren, R., Dammer, E.B., Wang, G., Seyfried, N.T., and Levey, A.I. (2014). Proteomics of protein post-translational modifications implicated in neurodegeneration. Transl. Neurodegener. *3*, 23.

Rescigno, T., Micolucci, L., Tecce, M.F., and Capasso, A. (2017). Bioactive Nutrients and Nutrigenomics in Age-Related Diseases. molecules *22*.

Rizza, S., Cardaci, S., Montagna, C., Di Giacomo, G., De Zio, D., Bordi, M., Maiani, E., Campello, S., Borreca, A., A. Puca, A., et al. (2018). S-nitrosylation drives cell senescence and aging in mammals by controlling mitochondrial dynamics and mitophagy. PNAS *115*, E3388–E3397.

Rong, X.-F., Sun, Y.-N., Liu, D.-M., Yin, H.-J., Peng, Y., Xu, S.-F., Wang, L., and Wang, X.-L. (2017). The pathological roles of NDRG2 in Alzheimer's disease, a study using animal models and APPwt-overexpressed cells. CNS Nerusci Ther *23*, 667–679.

Sabatelli, P., Castagnaro, S., Tagliavini, F., Chrisam, M., Sardone, F., Demay, L., Richard, P., Santi, S., Maraldi, N.M., Merlini, L., et al. (2014). Aggresome-autophagy involvement in a sarcopenic patient with rigid spine syndrome and a p.C150R mutation in FHL1 gene. Front Aging Neurosci. *6*, 215.

Sakono, M., and Zako, T. (2010). Amyloid oligomers: formation and toxicity of Aβ oligomers. FEBS Journal *277*, 1348–1358.

Sara, S.J. (2009). The locus coeruleus and noradrenergic modulation of cognition. Nature Reviews Neuroscience *10*, 211–223.

Satoh, A., and Lijima, K.M. (2017). Roles of tau pathology in the locus coeruleus (LC) in age-associated pathophysiology and Alzheimer's disease pathogenesis: Potential strategies to protect the LC against agin. Brain Res *pii: S0006-8993*, 30562–0.

Savitski, M.M., Sweetman, G., Askenazi, anor, Marto, J.A., Lang, M., Zinn, N., and Bantscheff, M. (2011). Delayed Fragmentation and Optimized Isolation Width Settings for Improvement of Protein Identification and Accuracy of Isobaric Mass Tag Quantification on Orbitrap-Type Mass Spectrometers. Anal. Chem *83*, 8959–8967.

Sayre, L.M., Perry, G., and Smith, M.A. (2008). Oxidative Stress and Neurotoxicity. Chem. Res. Toxicol. *21*, 172–188.

Scheff, S.W., Neltner, J.H., and Nelson, P.T. (2014). Is synaptic loss a unique hallmark of Alzheimer's disease? Biochem. Pharmacol. *88*, 517–528.

Schmitt, F.A., Nelson, P.T., Abner, E., Scheff, S., Jicha, G.A., Smith, C., Cooper, G., Mendiondo, M., Danner, D.D., Van Eldik, L.J., et al. (2012). University of Kentucky Sanders-Brown healthy brain aging volunteers: donor characteristics, procedures, and neuropathology. Curr. Alzheimer Res. *9*, 724–733.

Schwammle, V., Leon, I.R., and Jensen, O.N. (2013). Assessment and improvement of statistical tools for comparative proteomics analysis of sparse data sets with few experimental replicates. J. Proteome Res. *12*, 3874–3883.

Schwartz, M., Kipnis, J., Rivest, S., and Prat, A. (2013). How Do Immune Cells Support and Shape the Brain in Health, Disease, and Aging? J Neurosci *33*, 17587–17596.

Scott, H., Pow, D.V., Tannenberg, A.E.G., and Dodd, P.R. (2002). Aberrant expression of the glutamate transporter excitatory amino acid transporter 1 (EAAT1) in Alzheimer's disease. J. Neurosci *22*, RC206.

Seneviratne, U., Nott, A., Bhat, V., Ravindra, K.C., Wishnok, J.S., Tsai, L.-H., and Tannenbaum, S.R. (2016). S-nitrosation of proteins relevant to Alzheimer's disease during early stages of neurodegeneration. Proc Natl Acad Sci U S A *113*, 4152–4157.

Sengupta, U., Nilson, A.N., and Kayed, R. (2016). The Role of Amyloid-β Oligomers in Toxicity, Propagation, and Immunotherapy. EBioMedicine *6*, 42–49.

Serrano-pozo, A., Frosch, M.P., Masliah, E., and Hyman, B.T. (2011). Neuropathological Alterations in Alzheimer Disease. Cold Spring Harb. Perspect. Med. *1*, a006189.

Sharma, L.K., Lu, J., and Bai, Y. (2009). Mitochondrial Respiratory Complex I: Structure, Function and Implication in Human Diseases. Curr Med Chem. *16*, 1266–1277.

Shi, Q., and Gibson, G.E. (2011). Up-regulation of the mitochondrial malate dehydrogenase by oxidative stress is mediated by miR-743a. J. Neurochem. *118*, 440–448.

Sochocka, M., Diniz, B.S., and Leszek, J. (2017). Inflammatory Response in the CNS: Friend or Foe? Mol Neurobiol *54*, 8071–8089.

Søgaard, A., Johannsen, A., Plank, B., Hovy, D., and Martinez, H. (2014). What's in a -value in NLP? In Proc. of CoNLL.

Sosinsky, G.E., Crum, J., Jones, Y.Z., Lanman, J., Smarr, B., Martone, M.E., Deerinck, T.J., Johnson, J.E., and Mark, H. (2008). The Combination of Chemical Fixation Procedures with High Pressure Freezing and Freeze Substitution Preserves Highly Labile Tissue Ultrastructure for Electron Tomography Applications. J Struct. Biol. *161*, 359–371.

Spaan, P.E.J. (2016). Cognitive decline in normal aging and early Alzheimer's disease: A continuous or discontinuous transition? A historical review and future research proposal. Cogent Psychology *3*, 1185226.

Sperling, R., Mormino, E., and Johnson, K. (2014). The evolution of preclinical Alzheimer's disease: Implications for prevention trials. Neuron *84*, 608–622.

Sperling, R.A., Aisen, P.S., Beckett, L.A., Bennett, D.A., Craft, S., Fagan, A.M., Iwatsubo, T., Jack, C.R., Kaye, J., Montine, T.J., et al. (2011). Toward defining the preclinical stages of Alzheimer's disease: Recommendations from the National Institute on Aging-Alzheimer's Association workgroups on diagnostic guidelines for Alzheimer's disease. Alzheimers Dement. *7*, 280–292.

Sterka, D.J., and Marriott, I. (2006). Characterization of nucleotide- binding oligomerization domain (NOD) protein expression in primary murine microglia. journal of neuroimmunology *179*, 65–75.

Strohmeyer, R., Ramirez, M., Cole, G.J., Mueller, K., and Rogers, J. (2002). Association of factor H of the alternative pathway of complement with agrin and complement receptor 3 in the Alzheimer's disease brain. J Neuroimmunol. *131*, 135–146.

Swomley, A.M., Förster, S., Keeney, J.T., Triplett, J., Zhang, Z., Sultana, R., and Butterfield, D.A. (2014). Abeta, oxidative stress in Alzheimer disease: Evidence based on proteomics studies. Biochim. Biophys. Acta *1842*, 1248–1257.

Taha, E., Gildish, I., Gal-Ben-Ari, S., and Rosenblum, K. (2013). The role of eEF2 pathway in learning and synaptic plasticity. Neurobiology of Learning and Memory *105*, 100–106.

Takeda, S., Sato, N., Ikimura, K., Nishino, H., Rakugi, H., and Morishita, R. (2013). Increased blood-brain barrier vulnerability to systemic inflammation in an Alzheimer disease mouse model. Neurobiol Aging *34*, 2064–2070.

Tanzi, R.E., and Bertram, L. (2005). Twenty Years of the Alzheimer ' s Disease Amyloid Hypothesis : A Genetic Perspective. Cell *120*, 545–555.

Tchaikovskaya, T., Fraifeld, V., Urphanishvili, T., Andorfer, J.H., Davies, P., and Listowsky, I. (2005). Glutathione S-transferase hGSTM3 and ageing- associated neurodegeneration: relationship to Alzheimer's disease. Mech. Mech Ageing Dev. *126*, 309–315.

Terry, R.D., Masliah, E., Salmon, D.P., Butters, N., Deteresa, R., Hill, R., Hansen, L.A., and Katzman, R. (1991). Physical Basis of Cognitive Alterations in Alzheimer ' s Disease : Synapse loss is the Major Correlate of Cognitive Impairment. Ann Neurol *30*, 572–580.

Thal, D.R., Rub, U., Orantes, M., and Braak, H. (2002). Phases of A beta-deposition in the human brain and its relevance for the development of AD. Neurology *58*, 1791–1800.

Thomas, P.D., Campbell, M.J., Kejariwal, A., Mi, H., Karlak, B., Daverman, R., Diemer, K., Muruganujan, A., and Narechania, A. (2003). PANTHER: A library of protein families and subfamilies indexed by function. Genome Res. *13*, 2129–2141.

Thomas, T., Miners, S., and Love, S. (2015). Post-mortem assessment of hypoperfusion of cerebral cortex in Alzheimer's disease and vascular dementia. Brain *138*, 1059–1069.

Towbin, H., Staehelint, T., and Gordon, J. (1979). Electrophoretictransferofproteinsfrompolyacrylamidegelsto nitrocellulosesheets:Procedureandsomeapplications. Proc. Natl. Acad. Sci. *76*, 4350–4354.

Tripathy, K., Nanda, T., and Sudharani, O.. (2011). The Influence of Environmental and Genetic Factors on Various Disorders and Diseases. J Genet Syndr Gene Ther *S:11*.

Trushina, E., Dutta, T., Persson, X.-M.T., Mielke, M.M., and Petersen, Ronald C. (2013). Identification of Altered Metabolic Pathways in Plasma and CSF in Mild Cognitive Impairment and Alzheimer's Disease Using Metabolomics. PLoS One. *8*, e63644.

Tu, S., Okamoto, S.-I., Lipton, S.A., and Xu, H. (2014). Oligomeric Aβ-induced synaptic dysfunction in Alzheimer's disease. Molecular Neurodegeneration *9*, 48.

Tuli, L., and Ressom, H.W. (2009). LC–MS Based Detection of Differential Protein Expression. J Proteomics Bioinform *2*, 416–438.

Uehara, T., Nakamura, T., Yao, D., Shi, Z., Gu, Z., Ma, Y., Masliah, E., Nomura, Y., and Lipton, S.A. (2006). S-nitrosylated protein-disulphide isomerase links protein misfolding to neurodegeneration. Nature *441*, 513–517.

Venturini, G., Colasanti, M., Fioravanti, E., Bianchini, A., and Ascenzi, P. (1999). Direct Effect of Temperature on the Catalytic Activity of Nitric Oxide Synthases Types I , II , and III. Nitric Oxide *3*, 375–382.

Viaro, F., Nobre, F., and Evora, P.R.B. (2000). Expression of Nitric Oxide Synthases in the Pathophysiology of Cardiovascular Diseases. Arq. Bras. Cardiol. *74*, 4.

Wak, T.W., and Saunders, M.E. (2006). T Cell Activation. In The Immune Response, pp. 373–401.

Wallace, M.N., Geddes, J.G., A, F.D., and Masson, M.R. (1997). Nitric oxide synthase in reactive astrocytes adjacent to beta-amyloid plaques. Exp. Neurol. *144*, 266–272.

Wang, W.-Y., Tan, M.-S., Yu, J., and Tan, L. (2015). Role of pro-inflammatory cytokines released from microglia in Alzheimer's disease. Annals of Translational Medicine *3*, 136.

Wang, X., Anderson, G.A., Smith, R.D., and Dabney, A.R. (2012). A hybrid approach to protein differential expression in mass spectrometry-based proteomics. Bioinformatics *28*, 1586–1591.

Wang, Z., Yan, X., and Zhao, C. (2017). Dynamical differential networks and modules inferring disrupted genes associated with the progression of Alzheimer's disease. Exp Ther Med. *14*, 2969–2975.

Webb-Robertson, B.-J., Wiberg, H.K., Matzke, M.M., Brown, J.N., Mcdermott, J.E., Smith, R.D., Rodland, K.D., Metz, T.O., Joel, G., and Waters, K.M. (2015). Review, Evaluation, and Discussion of the Challenges of Missing Value Imputation for Mass Spectrometry-Based Label-Free Global Proteomics. J Proteome Res *14*, 1993–2001.

Whittaker, B.V.P., Michaelson, I.A., and Kirkland, R.J.A. (1964). The Separation of Synaptic Vesicles from Nerve-Ending Particles (' Synaptosomes '). Biochem. J. *90*, 293–303.

Wijasa, T.S., Sylvester, M., Brocke-Ahmadinejad, N., Kummer, M.P., Brosseron, F., Gieselmann, V., and Heneka, M.T. (2017). Proteome profiling of s-nitrosylated synaptosomal proteins by isobaric mass tags. J. Neurosci. Methods *291*, 95–100.

Wilcock, D.M., Lewis, M.R., Van Nostrand, W.E., Davis, J., Previti, M.L., Gharkholonarehe, N., Vitek, M.P., and Colton, C.A. (2008). Progression of amyloid pathology to Alzheimer's pathology in an APP transgenic mouse model by removal of NOS2. J. Neurosci *28*, 1537–1535.

Wojdyla, K., and Rogowska-Wrzesinska, A. (2015). Differential alkylation-based redox proteomics-Lessons learnt. Redox Biol *6*, 240–252.

Wojdyla, K., Wrzesinski, K., Williamson, J., Fey, S.J., and Rogowska-Wrzesinska, A. (2016). Acetaminophen-induced S-nitrosylation and S-sulfenylation signalling in 3D cultured hepatocarcinoma cell spheroids. Toxicol. Res. *5*, 905–920.

Wood, M. (2005). Bootstrapped Confidence Intervals as an Approach to Statistical Inference. sage publications *8*, 454–470.

Wyss-Coray, T. (2016). Ageing, neurodegeneration and brain rejuvenation. Nature *539*, 180–186.

Wyss-coray, T., and Rogers, J. (2012). Inflammation in Alzheimer Disease — A Brief Review of the Basic Science and Clinical Literature. Cold Spring Harb. Perspect. Biol. *2*, a006346.

Yao, C., Behring, J.B., Shao, D., Sverdlov, A.L., Whelan, S.A., Elezaby, A., Yin, X., Siwik, D.A., Seta, F., Costello, C.E., et al. (2015). Overexpression of Catalase Diminishes Oxidative Cysteine Modifications of Cardiac Proteins. PLoS One *10*, e0144025.

Yao, P.J., Zhu, M., Pyun, E.I., Brooks, A.I., Therianos, S., Meyers, V.E., and Coleman, P.D. (2003). Defects in expression of genes related to synaptic vesicle trafficking in frontal cortex of Alzheimer's disease. Neurobiol. Dis. *12*, 97–109.

Yiannopoulou, K.G., and Papageorgiou, S.G. (2013). Current and future treatments for Alzheimer's disease. Ther. Adv. Neurol. Disord. *6*, 19–33.

Zahid, S., Khan, R., Oellerich, M., Ahmed, N., and Asif, a R. (2014). Differential S-nitrosylation of proteins in Alzheimer's disease. Neuroscience *256*, 126–136.

Zareba-Koziol, M., Szwajda, A., Dadlez, M., Wyslouch-Cieszynska, A., and Lalowski, M. (2014). Global analysis of S-nitrosylation sites in the wild type (APP) transgenic mouse brain-clues for synaptic pathology. Mol Cell Proteomics *13*, 2288–2305.

Zhang, H., Liu, T., Zhang, Z., Payne, S.H., Zhang, B., Mcdermott, J.E., Zhou, J.-Y., Petyuk, V.A., Chen, L., Ray, D., et al. (2016a). Integrated Proteogenomic Characterization of Human High-Grade Serous Ovarian Cancer. Cell *166*, 1–11.

Zhang, L., Guo, X.Q., Chu, J.F., Zhang, X., Yan, Z.R., and Li, Y.Z. (2015). Potential hippocampal genes and pathways involved in Alzheimer's disease: a bioinformatic analysis. Genet. Mol. Res. *14*, 7218–7232.

Zhang, W., Sun, J., Cao, H., Tian, R., Cai, L., Ding, W., and Qian, P.-Y. (2016b). Post-translational modifications are enriched within protein functional groups important to

bacterial adaptation within a deep-sea hydrothermal vent environment. Microbiome *4*, 49.

Zhang, Y., Fonslow, B.R., Shan, B., Baek, M.-C., and Yates III, J.R. (2013). Protein Analysis by Shotgun/Bottom-up Proteomics. Chem. Rev. *113*, 2343–2394.

Zhao, Q., Yu, J., and Tan, L. (2015). S-Nitrosylation in Alzheimer ' s disease. Mol. Neurobiol. *51*, 268–280.